

# Atomic and molecular excitation processes in microwave induced plasmas : a spectroscopic study

**Citation for published version (APA):**

Timmermans, E. A. H. (1999). *Atomic and molecular excitation processes in microwave induced plasmas : a spectroscopic study*. [Phd Thesis 1 (Research TU/e / Graduation TU/e), Applied Physics and Science Education]. Technische Universiteit Eindhoven. <https://doi.org/10.6100/IR526711>

**DOI:**

[10.6100/IR526711](https://doi.org/10.6100/IR526711)

**Document status and date:**

Published: 01/01/1999

**Document Version:**

Publisher's PDF, also known as Version of Record (includes final page, issue and volume numbers)

**Please check the document version of this publication:**

- A submitted manuscript is the version of the article upon submission and before peer-review. There can be important differences between the submitted version and the official published version of record. People interested in the research are advised to contact the author for the final version of the publication, or visit the DOI to the publisher's website.
- The final author version and the galley proof are versions of the publication after peer review.
- The final published version features the final layout of the paper including the volume, issue and page numbers.

[Link to publication](#)

**General rights**

Copyright and moral rights for the publications made accessible in the public portal are retained by the authors and/or other copyright owners and it is a condition of accessing publications that users recognise and abide by the legal requirements associated with these rights.

- Users may download and print one copy of any publication from the public portal for the purpose of private study or research.
- You may not further distribute the material or use it for any profit-making activity or commercial gain
- You may freely distribute the URL identifying the publication in the public portal.

If the publication is distributed under the terms of Article 25fa of the Dutch Copyright Act, indicated by the "Taverne" license above, please follow below link for the End User Agreement:

[www.tue.nl/taverne](http://www.tue.nl/taverne)

**Take down policy**

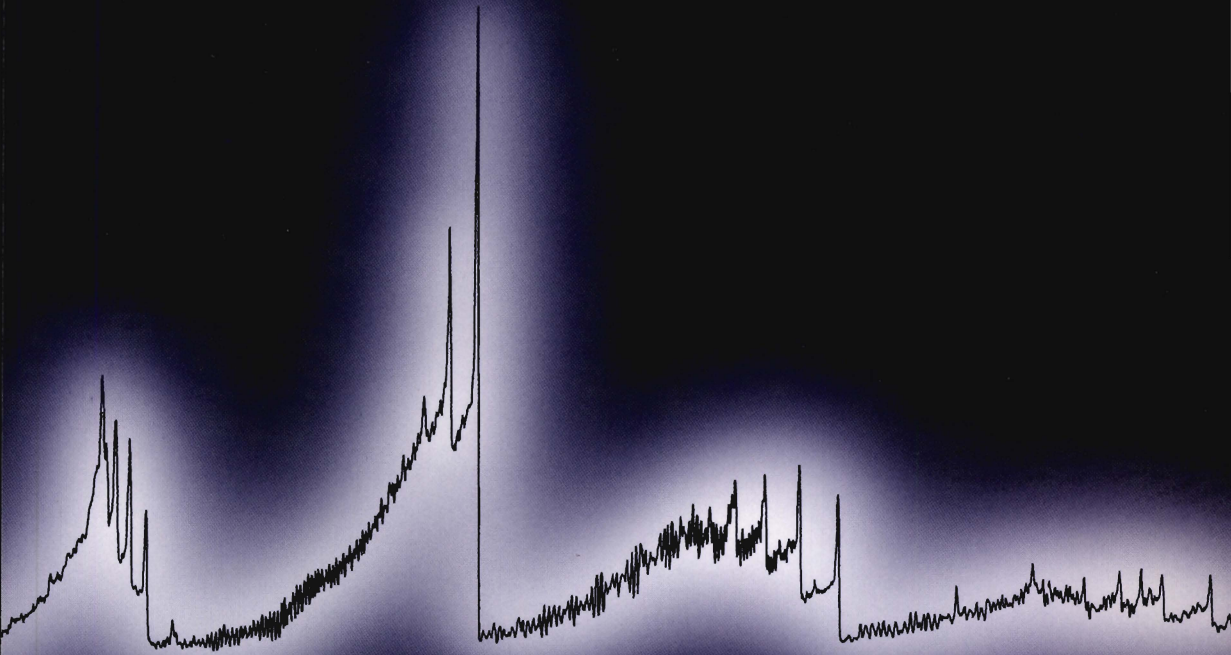
If you believe that this document breaches copyright please contact us at:

[openaccess@tue.nl](mailto:openaccess@tue.nl)

providing details and we will investigate your claim.

**Atomic and Molecular  
Excitation Processes in  
Microwave Induced Plasmas**

*A Spectroscopic Study*



**Eric Timmermans**

# Atomic and Molecular Excitation Processes in Microwave Induced Plasmas

## *A Spectroscopic Study*

### Proefschrift

ter verkrijging van de graad van doctor  
aan de Technische Universiteit Eindhoven,  
op gezag van de Rector Magnificus, prof.dr. M. Rem,  
voor een commissie aangewezen door het College  
voor Promoties in het openbaar te verdedigen op  
dinsdag 19 oktober 1999 om 16.00 uur

door

**Eric Aldegonda Henricus Timmermans**

geboren te Kessel

Dit proefschrift is goedgekeurd door de promotoren:

**prof.dr.ir. D.C. Schram**

en

**prof.dr. J.A.C. Broekaert**

Copromotor:

**dr. J.A.M. van der Mullen**

Het in dit proefschrift gepresenteerde onderzoek is verricht in het kader van een project van **TDO** (Centrum Technologie voor Duurzame Ontwikkeling) getiteld:

*“Robuuste en flexibele apparatuur voor het on-line meten aan afvalverbrandingsprocessen”*

Financiële ondersteuning is verleend door:

- TDO
- STW (“Stichting voor de Technische Wetenschappen”),
- SAI (“Stan Ackermans Instituut”) en
- AVR-Chemie



Drukwerk: Universiteitsdrukkerij Technische Universiteit Eindhoven

CIP-DATA LIBRARY TECHNISCHE UNIVERSITEIT EINDHOVEN

Timmermans, Eric Aldegonda Henricus.

Atomic and Molecular Excitation Processes in Microwave Induced Plasmas *A Spectroscopic Study*

Eric Aldegonda Henricus Timmermans.-

Eindhoven: Eindhoven University of Technology, 1999.-

Thesis.-

With summary in Dutch.-

ISBN 90-386-0887-X

NUGI 812

Trefwoorden: plasma / atomaire-emissiespectroscopie / spectroscopie / plasmadiagnostiek / plasma toortsen

Subject headings: microwave induced plasma / AES / spectroscopy / plasma diagnostics / plasma torches

# Contents

<b>1. General introduction</b>	<b>1</b>
1 Applications of microwave induced plasmas .....	2
2 Field applicators .....	3
3 Spectrochemical analysis .....	7
4 This thesis .....	9
<b>2. Spectrochemical characteristics of microwave induced plasma torches</b>	<b>13</b>
1 Introduction .....	14
2 The TIA and the MPT compared to the ICP.....	15
3 Experimental results .....	17
3.1 General plasma observations.....	17
3.2 Spectroscopic characteristics.....	19
3.3 Emission from the tail flame .....	20
3.4 Detection limits.....	21
3.5 Influence of molecular gases .....	23
4 Conclusions .....	24
<b>3. AES for the on-line monitoring of incineration processes</b>	<b>27</b>
1 Introduction, the aims of combustion gas analysis .....	28
2 Atomic emission spectroscopy (AES) for combustion gas analysis .....	30
3 The experimental setup .....	31
3.1 Introduction.....	31
3.2 The “conventional” ICP as excitation source for molecular gases.....	31
3.3 The “Torche à Injection Axiale” (TIA) .....	34
3.4 The optical set-up .....	36
3.5 Combustion gas sampling .....	37
4 Experimental results .....	39
4.1 General results .....	39
4.2 Observed elements.....	40
4.3 Molecular interference.....	42
4.4 Towards quantitative measurements .....	43
5 Discussion.....	44

<b>4.</b>	<b>The behavior of molecules in microwave induced plasmas studied by optical emission spectroscopy: 1. plasmas at atmospheric pressure</b>	<b>47</b>
1	Introduction .....	48
2	Experiments and instrumentation .....	49
3	Results and discussion.....	54
3.1	Characteristics of argon plasmas produced by the TIA and GS.....	54
3.2	TIA spectra for different molecular analyte gases .....	54
3.3	TIA spectra for different CO <sub>2</sub> flows.....	58
3.4	TIA spectra at different heights in the plasma .....	59
3.5	Plasmas expanding in gases other than air .....	59
3.6	Plasmas produced by the guide-surfatron .....	60
4	Conclusions .....	61
<b>5</b>	<b>The behavior of molecules in microwave induced plasmas studied by optical emission spectroscopy: 2. plasmas at reduced pressure</b>	<b>65</b>
1	Introduction .....	66
2	Experiments and instrumentation .....	67
3	Results and discussion.....	68
3.1	General observations from discharges at reduced pressure .....	68
3.2	Association mechanisms for diatomic molecules.....	71
3.3	Origin of the Swan system emission of the C <sub>2</sub> radical .....	72
3.4	Matrix effects.....	74
3.5	Influence of the pressure.....	75
3.6	Reduced-pressure surfatron discharges for molecular gas analysis.....	77
4	Conclusions .....	79
<b>6.</b>	<b>Excitation balances and transport properties studied by power interruption experiments</b>	<b>83</b>
1	Introduction .....	84
2	Experimental set-up.....	85
2.1	The plasma sources.....	85
2.2	Instrumentation for the power interruption experiments .....	86
3	Theory .....	87
3.1	Different effects of power interruptions.....	87
3.2	Excitation balances .....	89
3.3	Typical ICP responses explained .....	92
4	Experimental results .....	94

4.1	General findings from the power interruption measurements .....	94
4.2	Transport properties derived from responses of different species .....	96
4.3	Influence of molecular gas additives .....	100
4.4	The TIA and the MPT compared .....	101
4.5	Determination of the axial flow velocity .....	102
5	Conclusions .....	104
<b>7.</b>	<b>The behavior of argon <math>4s^3P_2</math> metastables in the TIA studied via diode laser absorption</b>	<b>107</b>
1	Introduction .....	108
2	Theory .....	110
2.1	The principles of absorption measurements .....	110
2.2	Broadening mechanisms .....	114
3	Experimental set-up .....	115
3.1	The microwave-induced argon plasma torch .....	115
3.2	Diode laser absorption measurements .....	115
3.3	Frequency calibration .....	117
4	Experimental results .....	117
4.1	General results .....	117
4.2	Frequency shift .....	118
4.3	Abel inversion .....	120
4.4	The argon ASDF .....	121
4.5	Profile broadening .....	122
4.6	Influence of the gas flow .....	123
4.7	Influence of the power input .....	124
4.8	Quenching by molecular gas additives ( $CO_2$ ) .....	125
5	Conclusions .....	126
<b>8.</b>	<b>General conclusions</b>	<b>129</b>
	<b>Summary</b>	<b>132</b>
	<b>Samenvatting</b>	<b>134</b>
	<b>Dankwoord</b>	<b>136</b>
	<b>Curriculum vitae</b>	<b>137</b>

# 1

## General introduction



## 1. Applications of microwave-induced plasmas

Plasmas nowadays are widely used in many industrial, research or laboratory applications. One category of these plasmas is formed by the so-called Microwave-Induced Plasmas [1] (MIPs), which have in common that they are created and sustained by microwave energy, i.e. electromagnetic radiation in the frequency range of 300 MHz – 10 GHz. A striking feature of MIPs is the wide range of operational conditions that can be applied: dependent on the plasma source, power levels can range from a few Watt up to several hundreds of kilowatts, the discharge pressure might range from less than  $10^{-2}$  Pa up to several times atmospheric pressure, whereas many different discharge gases might be used (both noble and molecular gases). A result of this broad range of operational conditions is that plasmas with widely varying plasma parameters can be created (such as electron density, electron temperature, gas temperature, ionization degree and chemical composition). Moreover, the geometry of the plasmas can be largely influenced. Because practical applications as well as laboratory research usually call for plasmas with specific characteristics and a controllable geometry, MIPs are in many cases preferable to other plasmas.

Some applications of MIPs that have been reported in literature are:

- *Materials processing* [2], such as deposition, etching, cutting, welding, cleaning and surface modification. Examples of deposited layers are amorphous silicon [3] and diamond-like coatings [4]. For processing, low pressure microwave-induced plasmas are often used in combination with Electron Cyclotron Resonance (ECR) in order to create high densities of reactive species [5]. An example of a commercially available MIP source that can be used for processing [6] is the Slot Antenna (SLAN), a ring resonator field applicator producing voluminous low pressure plasmas with diameters up to 66 cm, developed by the group of Prof. Engemann at the University of Wuppertal [7].
- *Waste treatment*, such as detoxification of detrimental gases [8].
- *Ion production*, e.g. for ion bombardment [9].
- The use as *atomization source*, e.g. as N atom source that can be used for nitriding in a remote plasma system [10].
- The use as *light source*. The commercially available Solar1000 lamp (Fusion Lighting) for instance, is a microwave-induced sulfur discharge operated at 2.45 GHz [11].
- The use as *excitation source* in analytical chemistry [12,13].

The plasmas studied in this thesis are of the latter type and can be divided into three categories: free expanding atmospheric plasma torches, surface-wave sustained plasmas and plasmas produced by resonant cavities. The aim of the presented spectroscopic study is to get a better basic understanding of plasmas used as spectrochemical excitation sources, and of the investigated microwave induced plasmas in particular. In section 2 the field applicators that are used for the plasma generation will be discussed. A short introduction into spectrochemical analysis will be given in section 3. Finally, a survey of the remainder of this thesis will be given in section 4.

## 2. Field applicators

Microwave-generators of 2.45 GHz are readily commercially available and as a result the vast majority of MIPs are operated at this frequency. All studied microwave discharges in this thesis are therefore sustained by 2.45 GHz radiation as well. Despite large differences in energy coupling modes, all discharges have in common that the EM energy is mainly absorbed by free electrons, which subsequently transfer energy towards the atoms and molecules via elastic collisions (heavy particle heating) and via inelastic collisions (e.g. excitation, ionization and dissociation). The heavy particles are finally cooled by the cold surrounding gases or the wall of the quartz discharge tube.

Microwave power is usually transferred from the magnetron towards the plasma field applicator via a coaxial line (up to approximately 500 W) or a waveguide system (for higher power levels as well). The dominant propagation mode in coaxial lines is the TEM mode (transverse electromagnetic mode, i.e. both the electrical and magnetic field component in the direction of propagation are zero), which does not have a cut-off frequency. The dimensions of coaxial lines are such that within the specified frequency range no other modes can be excited. By allowing one propagation mode only, maximum control over the EM energy is achieved with respect to the coupling into field applicators, stability and reproducibility. In rectangular waveguides the propagation of the TEM mode is not possible<sup>a</sup>, whereas excitation of the TE mode (transverse electric, i.e. no electrical field component in the direction of propagation) and the TM mode (transverse magnetic, i.e. no magnetic field component in the direction of propagation) is only possible if the frequency of the EM field exceeds a cutoff frequency. For the TE<sub>mn</sub> and the TM<sub>mn</sub> mode, with  $m$  and  $n$  integers ( $\geq 0$ )<sup>b</sup> that follow from the eigenvalues of the Helmholtz equation for the EM field [1], this cutoff frequency  $f_{mn}$  is given by:

$$f_{mn} = \frac{1}{2\sqrt{\epsilon\mu}} \left( \frac{m^2}{a^2} + \frac{n^2}{b^2} \right)^{1/2}, \quad (1)$$

with  $a$  the width and  $b$  and height of the waveguide ( $a > b$ ) and  $\epsilon$  and  $\mu$  the permittivity and permeability of the medium inside the waveguide respectively. For 2.45 GHz radiation in many cases the WR-340 waveguide is used, in which due to its dimensions (86.4×43.2 mm<sup>2</sup>) only the TE<sub>10</sub> mode can be excited ( $f_{10}=1.74$  GHz in air). This mode is depicted in figure 1.

<sup>a</sup> It can easily be shown that TEM waves cannot propagate in a single conductor.

<sup>b</sup> For TE modes it is required that either  $m \neq 0$  or  $n \neq 0$ , whereas for TM modes it is required that both  $m \neq 0$  and  $n \neq 0$ , so that of all TM modes the TM<sub>11</sub> mode has the lowest cut-off frequency (3.90 GHz inside a WR-340 waveguide in air)

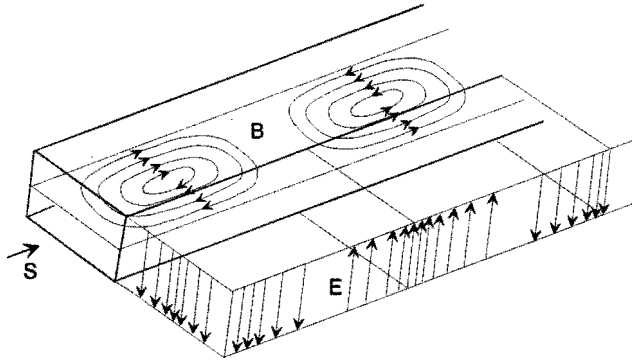
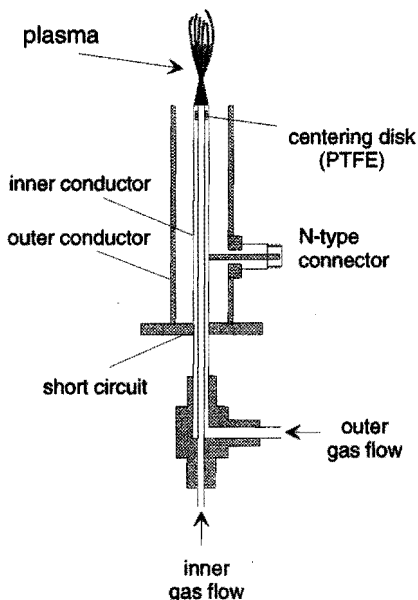


Figure 1. The pattern of the electric field  $E$  and the magnetic field  $B$  of a wave propagating in the  $TE_{10}$  mode (e.g. in a rectangular WR-340 waveguide). The electric field components are perpendicular to the direction of propagation  $\vec{S}$ .

The plasma applicators that are used in this study can be divided into three categories, namely free expanding plasma torches, plasmas produced by resonant cavities and surface wave sustained plasmas:

- Examples of *free expanding atmospheric plasma torches* are the TIA (Torche à Injection Axiale) [14] and the MPT (Microwave Plasma Torch) [15], which is shown in figure 2.



This type of plasma torches basically consists of an energy-input device, matching and tuning devices and an inner and outer conductor (which may be connected through a galvanic contact). The inner conductor usually serves as gas channel as well and is terminated by a nozzle. Dependent on the geometry of the torch and matching and tuning properties, microwave energy can be efficiently coupled in via a coaxial feed line (e.g. for the MPT) or a waveguide system (e.g. for the TIA). This energy propagates in a TEM-like mode and is absorbed by the plasma, constituting a load at the end of the coaxial-like transmission line.

Figure 2. The Microwave Plasma Torch (MPT), which is used for the creation of free expanding atmospheric plasmas.

- Examples of *resonant cavities* are the Beenakker cavity and the Broida-type cavity<sup>c</sup>. Resonator systems represent one of the initial devices used for microwave plasma generation [16]. In these systems a (standing) wave pattern is created and energy is coupled into a discharge tube that is located at a position with high electrical field strength. In figure 3 the Beenakker cavity is shown, which is operated in the  $TM_{010}$  mode [16]. Cylindrical cavities operating in other modes (e.g.  $TE_{011}$ ,  $TE_{111}$  and  $TM_{011}$ ) are reported as well. Plasmas usually can be created at reduced and atmospheric pressure.

The resonance frequency of the  $TM_{010}$  mode in a cylindrical resonator with radius  $R$  is given by [16]:

$$f_{010} = \frac{2.405}{2\pi R \sqrt{\epsilon\mu}}, \quad (2)$$

so that an air-filled cavity is resonant for 2.45 GHz radiation if it has an inner diameter of 94 mm. In practice this diameter is chosen slightly larger to enable the introduction of tuning devices. In order to achieve a high energy density, the (axial) depth of the cavity is kept as small as possible (and should at least be smaller than the diameter in order to avoid mixing with other modes such as the  $TE_{111}$  mode). However, to restrict the disturbing influence of the apertures in the cavity the minimum depth should at least be 1.5 cm.

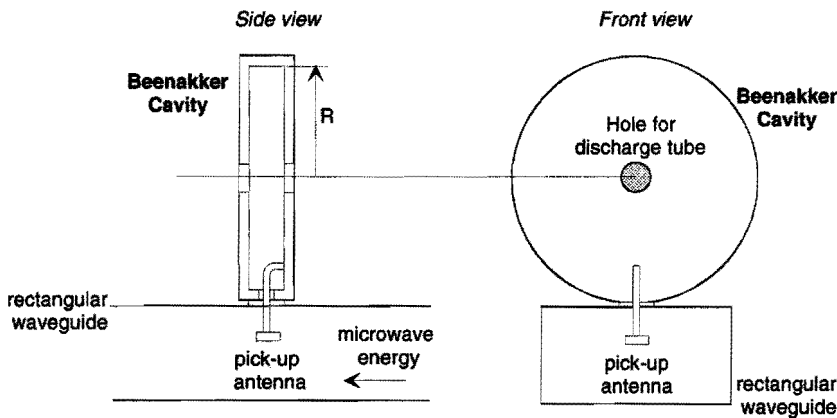


Figure 3. *The Beenakker cavity in detail. Apart from the waveguide-fed Beenakker cavity (like shown in the figure), cavities with a coaxial feed line exist as well. The plasmas is created in a quartz tube and due to the local energy coupling, the active zone of the plasma is largely located within the resonant cavity.*

In figure 4 the reflection of a Beenakker cavity is given as a function of the frequency<sup>d</sup>. It can be seen that the cavity is resonant for a small frequency range only. The narrow bandwidth and deep absorption profile ensure a high quality factor of the cavity, which has the advantage that energy with the resonant frequency can efficiently be coupled into the cavity. A disadvantage of a small bandwidth is that changes in the resonant frequency of a

<sup>c</sup> Not used as plasma source for the experiments presented in this thesis.

<sup>d</sup> Measured at Philips CFT with a vector network analyzer (Rode & Schwartz ZVRE).

tuned cavity, e.g. induced by impedance changes, may severely deteriorate the power absorption. The given reflection profile for instance, is measured from a cavity without quartz tube: The introduction of a discharge tube (without plasma) decreases the resonant frequency by 40 MHz. In order to be able to manipulate the resonance frequency, resonant cavities are usually equipped with one or more tuning stubs.

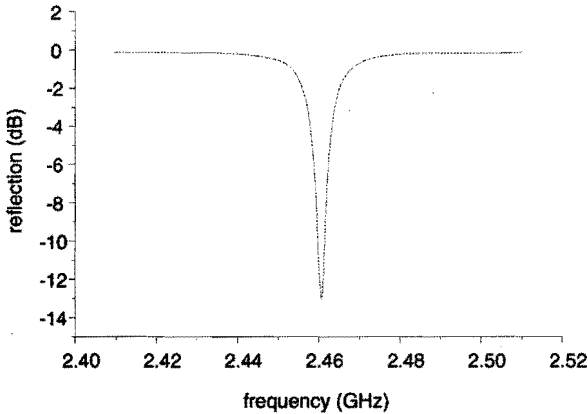


Figure 4.  
The reflection coefficient of a Beenakker cavity as function of the frequency measured with a vector network analyzer. It should be noted that the cavity is resonant for a small frequency range only.

- Examples of *surface-wave sustained plasma sources* are the surfatron, which is shown in figure 5, and the guide-surfatron [1,17]. Similar to resonant cavity plasmas, surface-wave sustained discharges are confined in a quartz tube. The microwave energy that sustains the plasma propagates along the quartz and plasma boundary, so that the plasma has no localized active zone and can be extended far outside the field applicator. Along the plasma column the EM field propagates in the TM mode, because only this mode can satisfy the field continuity relations across the boundary for axially symmetric surface waves [1]. Under normal operational conditions only the  $TM_{01}$  mode is excited (i.e. the only field components that are not equal to zero are the radial electric field  $E_r$ , the  $E_z$  and  $B_\phi$ , see figure 5). Other TM modes can only be excited if the product of the plasma tube radius and the microwave frequency exceeds 2 GHz·cm. Similar to the resonant cavities, plasmas can be created at reduced and atmospheric pressure. Whereas for the resonant cavities especially the radius of the cavity is important, for the surfatron it is the depth (in the axial z-direction, cf. figure 5) of the launcher that is critical, especially at atmospheric pressure. The guide-surfatron operates basically the same as the surfatron, but energy is coupled via waveguide system. Other examples of surface wave plasma devices<sup>e</sup> are the ro-box, the surfacan and the surfaguide. Since the introduction of surface-wave plasma launchers in the 1970's much effort has been put in the modeling of this type of discharges and consequently a highly developed theory is available, especially for the low-pressure regime [1].

<sup>e</sup> Not used as plasma sources for the experiments presented in this thesis.

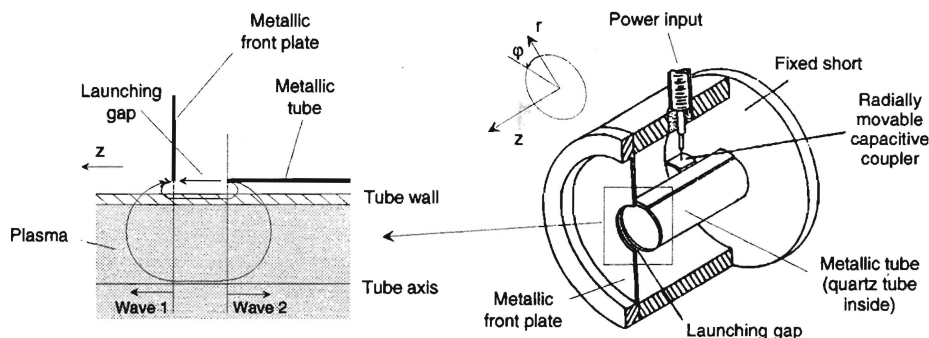


Figure 5. The surfatron, a field applicator that is used for launching surface waves. Plasmas are confined in a quartz tube and can be extended far outside the surfatron.

### 3. Spectrochemical analysis

Plasmas have acquired a dominant position in analytical chemistry, in which they are used as atomization and/or excitation source of analytes<sup>f</sup> [12,13]. Especially Atomic Emission Spectroscopy (AES) is nowadays a widely used technique in analytical laboratories for elemental analysis. For this purpose usually aqueous samples are nebulized and introduced into a plasma. In the plasma the aerosol is evaporated and the atoms present in the flow are excited. The emission, being a result of the spontaneous radiative de-excitation of excited species, then provides information on the composition of the sample, both qualitative and quantitative. The Inductively Coupled Plasma (ICP) is by far the most applied excitation source and detection limits achieved by ICP-AES are in the sub-ppb range for most elements (in aqueous samples 1 ppb  $\equiv$  1 ng/ml). Since the first ICP-AES systems were introduced on the market around 1975, this powerful analysis technique has expanded enormously. Fully automated ICP-AES systems are now readily commercially available and often equipped with the possibility of stand-alone operation (for instance for the continuous quality monitoring of river water). A current trend is to change from Atomic Emission Spectrometry to Mass Spectrometry (ICP-MS), which features even better detection limits, for most elements typically in the ppt range (1 ppt  $\equiv$  1 pg/ml)! Recently, further progress has been made with HR-MS (High Resolution MS), using a double focussing magnetic sector and TOF-MS (Time-Of-Flight MS) having a superior speed of analysis and resolution. An important additional advantage of ICP-MS is that it enables isotopic studies. Enriched isotopes can for instance be used as tracers to study migration and transport properties in living organisms. With TOF-MS even simultaneous isotopic analysis can be performed.

Apart from "simple" elemental analysis, usually applied in environmental, health or biological studies, the last ten years more and more focus is put on the rapidly evolving technique of speciation. This technique studies how elements are imbedded in molecular

<sup>f</sup> "Analytes" is the generic term for the elements (or molecules) of interest that are present in low concentrations in the sample.

structures of organic or inorganic substances. As an example, the toxicity and bioavailability of elements, in addition to their mobility and their impact on the environment, not only depend on their concentrations, but also strongly depend on the chemical form in which they occur. For instance, Cr(III) compounds are essential for living organisms, whereas Cr(VI) is toxic [18]. In speciation studies, molecular complexes are separated in time or space and then analyzed with an element-selective detector (ICP-AES or ICP-MS). Some of these separation techniques that are coupled to ICP-AES or ICP-MS are GC (Gas Chromatography), HPLC (High Performance Liquid Chromatography) and CZE (Capillary Zone Electrophoresis). Speciation can be an important support for several biological and medical studies or applications, and with the current stormy developments and progresses in these fields, it can be expected that the use of ICP-AES or ICP-MS will only increase in the near future.

Although the ICP is the most widely used excitation source for spectrochemical analysis, many other plasma sources are rather frequently applied as well. Some of these plasmas are Direct-Current Plasmas (DCPs), Glow discharges (GDs) and Microwave Induced Plasmas (MIPs). Since gas chromatographs can be easily coupled to capillary microwave-induced discharges, GC-MIP-AES is probably the most popular application of MIPs [19-21]. Especially capillary helium plasmas are often used, since, in contrast to argon plasmas, helium discharges can be utilized for the detection of halogens (F, Cl, Br, I and At). A major advantage of microwave-induced resonant cavities [22] as the Beenakker cavity [16], is that the same device can be used to create both argon and helium discharges. On the other hand, ICPs that are developed for operation on argon usually cannot be operated on helium (which requires smaller induction coils and torches [12]). Existing helium ICPs suffer from a high helium consumption (which is much more expensive than argon) and are therefore hardly used.

An important step in AES is the sample preparation and introduction [23]. The most applied introduction methods are based on the use of Pneumatic Nebulizers (PN), which exist in a variety of types, e.g. concentric, micro-concentric, cross-flow, Babington type and V-groove nebulizers. Better results are obtained with (the more expensive) Ultra-Sonic Nebulizers (USN) and in-line matrix removal systems. Laser Ablation (LA) is often used for solid samples, whereas ElectroThermal Vaporization (ETV) and Furnace Atomization (FA), as for instance in Furnace Atomization Plasma Emission Spectrometry (FAPES) [24], are very powerful if only micro samples are available.

Apart from AES or MS, several other analytical plasma-based techniques are used for elemental analysis, such as HCL-ICP-AFS (Hollow Cathode Lamp ICP Atomic Fluorescence Spectrometry) [12], in which the plasma can be used both as atomization cell and as excitation source. Obviously, there are many analysis techniques in which no discharges are involved. Examples are Atomic Absorption Spectrometry (AAS) and Laser Induced Breakdown Spectroscopy (LIBS), being used for direct solid sample analysis.

It is far beyond the scope of this work to give an extensive description of all these techniques. More information on spectrochemical analysis can be found in literature, e.g. in MONTASER and GOLIGHTLY [12] or BOUMANS [13].

ICPs that are developed for AES are usually operated on argon and are very sensitive for molecular gas injection (unless they are equipped with an automated impedance matching

system). This is related to the inductive character of the plasma, which acts as the second coil of a transformer. A consequence is that these plasmas are sensitive for impedance changes. The energy coupling into MIPs is totally different and especially the free expanding torches (i.e. the TIA and the MPT), in which the plasma dissipates energy at the end of a coaxial-like transmission line, are relatively insensitive for impedance changes. Together with the other plasma sources that are used in the presented study (i.e. the Beenakker cavity, the surfatron and the guide-surfatron) they enable the creation of plasmas under a widely varying range of conditions. This makes these plasma sources especially interesting for the study of molecular processes in plasmas.

#### 4. This thesis

This thesis represents an experimental study of spectroscopic features of various microwave-induced plasmas. It is focused on a better fundamental understanding of MIPs when they are used in analytical spectrochemistry, rather than on an improvement of the detection limits that are achieved by commercially available systems as discussed in section 3. For this reason various plasma properties and processes that are related to this application, such as excitation mechanisms, molecular dissociation and association reactions, transport phenomena and the influence of analyte or molecular gas injection on argon plasmas have been investigated by emission and absorption spectroscopy.

All next chapters in this thesis focus on specific aspects of the study. Some chapters have been published as papers [25,26] whereas the other chapters are submitted for publication [27,28] or will be submitted in near future [29,30]. As a result, all chapters can be read separately and unavoidably have some overlap. Here, an introductory overview is given:

- *Chapter 2* gives a general introduction into the use of microwave plasma torches as excitation sources in analytical chemistry. Spectroscopic measurements have been performed on argon plasmas produced by the TIA and the MPT.
- In *chapter 3* the TIA is used as an excitation source for the on-line analysis of combustion gases<sup>§</sup>. A system has been built for the monitoring of elements that are highly abundant in such gases, e.g. zinc, aluminum, lead and magnesium. Measurements have been performed at AVR-Chemie, the largest hazardous waste incinerator in The Netherlands. Combustion gases are extracted from the rotary kiln and subsequently evaporated and dissociated by the plasma.
- *Chapter 4* is devoted to dissociation processes of introduced molecules and association mechanisms of diatomic molecules in atmospheric discharges created by the TIA and the

---

<sup>§</sup> This chapter is basically a shortened report of a Master dissertation written within the framework of a 2-year post-graduate program on "Physical Instrumentation" by the Stan Ackermans Institute Centre of Technological Design. This dissertation was entitled "Design of a continuous gas analyzer based on MIP-AES for the on-line monitoring of metallic compounds in flue gases", ISBN 90-5282-770-2 (1997).



guide-surfatron. The emission of diatomic molecules is studied when molecular gases are introduced into argon discharges, either deliberately or by air entrainment.

- In *chapter 5* molecular processes in plasmas at reduced pressure (approximately 1-10 mbar) created by the surfatron and Beenakker cavity are studied. Since at these pressures volume processes are much less significant, it can be expected that results are different than obtained for the atmospheric discharges studied in chapter 4.
- In *chapter 6* so-called power interruption experiments performed on the TIA and MPT will be presented. From the time dependent behavior of line intensities during short plasma power interruptions, information is obtained on plasma transport properties and excitation mechanisms. The influence of analyte injection and molecular gases on argon plasmas is studied as well.
- Finally, in *Chapter 7* measurements on metastable argon 4s atoms in argon discharges created by the TIA are discussed. Density distributions of metastables have been deduced from diode laser absorption measurements. Moreover, it is studied how these metastables are quenched by molecular gas injection.

## References

1. M. Moisan and J. Pelletier, "*Microwave induced plasmas, Plasma Technonlogy*", Vol. 4, Elsevier science publishing, The Netherlands (1992).
2. M.I. Boulos, P. Fauchais and E. Pfender, "*Thermal plasmas: fundamentals and applications*", Plenum press, New York (1994).
3. L. Paquin D. Masson, M.R. Wertheimer and M. Moisan, *Can. J. Phys.* **63**, 831 (1985).
4. C.L. Hartz, J.W. Bevan, M.W. Jackson and B.A. Wofford, *Environ. Sci. Technol.* **32**, 682 (1998).
5. J. Asmussen, *J. Vac. Sci. Techn.* **A7**, 883 (1989).
6. F. Werner, D. Korzec and J. Engemann *Surf. Coat. Techn.* **91**, 101(1997).
7. F. Werner, D. Korzec and J. Engemann *Plasma sources sci. and techn.* **3**, 473(1994).
8. V.T. Airoldi, C.F.M. Borges, M. Moisan and D. Guay, *Appl. Optics* **36**, 4400 (1997).
9. L. Pomathiod, J.L. Michau and M. Hamelin, *Rev. Sci. Instrum.* **59**, 2409 (1988).
10. H. Malvos, H. Michel and A. Ricard. *Phys. D: Appl. Phys.* **27**, 1328 (1994).
11. D.O. Wharmby, *IEEE Proceedings-A* **140**, 465 (1993).
12. A. Montaser and D.W. Golightly, "*Inductively coupled plasmas in analytical atomic spectrometry*", second edition VCH Publishers, Inc., New York (1992).
13. P.W.J.M. Boumans, "*Inductively coupled plasma emission spectroscopy*", part 1: *Methodology, Instrumentation and Performance* & part 2: "*Applications and fundamentals*", John Wiley & Sons, New York (1987).
14. M. Moisan, G. Sauvé, Z. Zakrzewski and J. Hubert, *Plasma sources, Sci. and Techn.* **3**, 584 (1994).
15. Q. Jin, C. Zhu, M.W. Borer and G.M. Hieftje, *Spectrochim. Acta* **46B**, 417 (1991).
16. C.I.M. Beenakker, B. Bosman and P.W.J.M. Boumans, *Spectrochim. Acta* **33B**, 373 (1978).
17. M. Moisan and Z. Zakrzewski, *J. Phys. D: Appl. Phys.* **24**, 1025 (1991).

18. C.M. Andrie and J.A.C. Broekaert, *Fres. J. Anal. Chem.*, **346**, 653 (1993).
19. Q. Jin, Y. Duan and J.A. Olivares, *Spectrochim. Acta* **52B**, 131 (1997).
20. A.E. Croslyn, B.W. Smith, and J.D. Winefordner, *Critical Rev. Anal. Chem.* **27**, 199 (1997).
21. A. Montaser, *CRC Critical Rev. Anal. Chem.* **18(1)**, 45 (1987).
22. H. Matusiewicz, *Spectrochim. Acta* **47B**, 1221 (1992).
23. J.A.C. Broekaert, R.F. Browner and R.K. Marcus (eds.), "Sample introduction in atomic spectrometry", *Spectrochim. Acta* **50B**, special issue N° 4-7 (1995).
24. R.E. Sturgeon, S.N. Willie and V.T. Luong, *Spectrochim. Acta* **46B**, 1021 (1991).
25. *Chapter 4 of this thesis*, E.A.H. Timmermans, J. Jonkers, I.A.J. Thomas, A. Rodero, M.C. Quintero, A. Sola, A. Gamero and J.A.M. van der Mullen, *Spectrochim. Acta* **53B**, 1553 (1998).
26. *Chapter 5 of this thesis*, E.A.H. Timmermans, J. Jonkers, A. Rodero, M.C. Quintero, A. Sola, A. Gamero, D.C. Schram and J.A.M. van der Mullen, *Spectrochim. Acta* **54B**, 1083 (1999).
27. *Chapter 3 of this thesis*, E.A.H. Timmermans, F.P.J. de Groot, J. Jonkers, D.C. Schram and J.A.M. van der Mullen, "AES for the on-line monitoring of incinerator processes", *submitted for publication in J. Anal. At. Spectrom.* (1999).
28. *Chapter 6 of this thesis*, E.A.H. Timmermans, I.A.J. Thomas, J. Jonkers and J.A.M. van der Mullen, "Excitation balances and transport properties in atmospheric microwave induced plasmas studied by power interruption experiments", *submitted for publication in Plasma Sources, Sci. and Techn.* (1999).
29. *Chapter 2 of this thesis*, E.A.H. Timmermans, I.A.J. Thomas, J.A.M. van der Mullen and D.C. Schram, "Spectrochemical characteristics of microwave induced plasma torches", *to be submitted for publication* (1999).
30. *Chapter 7 of this thesis*, E.A.H. Timmermans, I.A.J. Thomas, J.A.M. van der Mullen and D.C. Schram, "The behavior of argon  $4s^3P_2$  metastables in the TIA studied via diode laser absorption".



# 2

## Spectrochemical characteristics of microwave induced plasma torches

*E.A.H. Timmermans, I.A.J. Thomas, D.C. Schram and J.A.M. van der Mullen*  
to be submitted for publication (1999).

**SUMMARY** – Argon plasmas produced by two different atmospheric microwave induced plasmas (the *Torche à Injection Axiale* and the *Microwave Plasma Torch*) have been studied by means of optical emission spectroscopy. This in order to obtain more insight in the applicability of these plasma torches as excitation sources for spectrochemical analysis. Compared to the widely used Inductively Coupled Plasma these plasmas benefit from a compact setup and low gas consumption whereas they are less sensitive to water load than most other microwave induced plasmas. In the plasmas produced by either of these plasma sources three distinctive zones can be observed: an ionizing cone-like zone close to the nozzle, followed by a cone tip zone, being the optimum zone for analyte excitation in the MPT, and a tail flame, in which processes like chemi-luminescence generate visible radiation. Emission spectra from argon discharges are largely dominated by intense emission bands of diatomic association products in all zones due to air entrainment. Experiments with aqueous aerosol injection have shown that the best detection limits for elements are achieved with the MPT (typically 0.1 ppm versus 1 ppm with the TIA, using a standard pneumatic nebulizer without desolvation). For the analysis of aqueous samples, therefore the MPT seems to have the most potential. However, from experiments with nitrogen, carbon dioxide and air it is found that the TIA is less sensitive to molecular gases and, depending on the geometry of the nozzle, even can be operated on pure molecular gases. This makes the TIA a promising excitation source for the analysis of gaseous samples with high analyte concentrations (such as flue gases).

## 1. Introduction

For years various different plasmas have been used as excitation sources for the determination of elements using atomic emission spectroscopy (AES) [1,2]. Especially for the analysis of aqueous samples AES is nowadays widely used in analytical laboratories. The Inductively Coupled argon Plasma (ICP) is by far the most used plasma source for this application and complete analysis systems including the ICP, sample preparation and injection, optics and data acquisition are readily commercially available. These systems are usually fully automated and sometimes even equipped with the possibility of stand-alone operation. Detection limits achieved by ICP-AES usually are in the sub-ppb range. A current trend is to replace the emission spectroscopy by mass spectrometry, which for most elements leads to a further improvement of detection limits [3].

Microwave induced plasmas (MIPs) are used several times in analytical chemistry as well. Besides the well-known surfatron [4,5] and the Beenakker cavity [6] a variety of other field shaping applicators are used [7-9]. However, major restrictions of most types of MIPs are their sensitivity to water introduction and their limited evaporation and excitation power of analytes. Therefore detection limits of elements are usually worse than in case an ICP is used as excitation source [9]. Another limitation of MIPs is the generally intense and broad emission bands of molecular spectra. Detection limits are reduced even further if lines of the analyte interfere with those bands. These are some of the reasons why ICPs are used much more frequently in spectrochemical analysis than MIPs.

However, many applications can be imagined in which very low detection limits are not required and relatively cheap, compact and modular equipment is more desirable. Examples of

such applications are studies of environmental pollution in Third World countries or measurements at industrial sites at locations with accessibility problems [10]. The ICP is a large and heavy apparatus and is expensive in purchase and in maintenance due to its large gas consumption (10-20 l·min<sup>-1</sup>) and therefore has its limitations for these applications.

For this reason microwave induced plasmas produced by the TIA (from "Torche à Injection Axiale") and the MPT (from "Microwave Plasma Torch") have been investigated in this paper with respect to their analytical performances, although it thus can be expected that detection limits of elements are worse than as determined in most ICPs. The TIA which has been developed in 1993 by MOISAN *et al.* [11], creates atmospheric plasmas that expand into open air, similar to plasmas created by an ICP. The TIA benefits from a compact set-up and low gas consumption (typically 5 l·min<sup>-1</sup>), whereas the plasma has a relatively high electron density and temperature and seems to have overcome the large sensitivity to water vapor, being characteristic for many other MIPs. The MPT, which like the TIA produces atmospheric free expanding plasmas but is operated at much lower power levels, is developed by JIN *et al.* [12,13] and improved afterwards by BILGIC *et al.* [14]. Due to the low power requirements, the equipment is even more compact than for the TIA and moreover, the argon consumption is reduced to less than 1 l·min<sup>-1</sup>. The MPT already has been used as spectrochemical excitation source by different analytical research groups [12,14].

In the next section the TIA and the MPT will shortly be discussed and typical plasma parameters will be compared to those of an ICP. Experimental results will be given in section 3, whereas in section 4 an evaluation of the applicability of both microwave induced plasma torches as excitation sources will be given.

## 2. The TIA and the MPT compared to the ICP

The TIA, depicted in figure 1 on the left, is a high power plasma torch that can produce atmospheric discharges in various gases. In their first paper about the TIA, Moisan *et al.* already showed that this torch is relatively insensitive to plasma impedance changes [11]. Together with the relatively high electron density, electron temperature and heavy particle temperature (cf. table 1) this makes it a promising excitation source for spectrochemical analysis. The torch consists of a coaxial structure perpendicular to a rectangular waveguide (WR-340), cf. figure 1. Basically, the TIA converts the propagation mode of the incident microwave radiation from the TE<sub>01</sub> mode inside the rectangular waveguide into the coaxial TEM mode. The plasma carrier gases and aerosols are introduced through the central gas inlet at the bottom side of the coaxial inner conductor and expand through the nozzle, being the top end of the inner conductor. Due to the field shaping characteristics of the TIA, the microwave energy is dissipated on top of the nozzle, where the plasma is created. A cross-flow nebulizer has been used for the creation of aerosols [1,2]. A more extensive description of the TIA, the power generator, the waveguide structure and tuning devices can be found in TIMMERMANS *et al.* [10].

The MPT, depicted in the middle of figure 1, produces flame-like plasmas [13]. The main differences of this plasma torch compared to the TIA are its low power and gas consumption and its separate central gas channel through which analytes can be introduced (similar to the ICP, cf.

figure 1). Due to the low power requirements (50-300 W), a coaxial feed line is used to power the torch.

The ICP, depicted on the right of figure 1, is much more voluminous than the discussed microwave induced plasmas. This is largely due to the larger skin depth and the swirl induced by the tangential injection of the outer and intermediate gas flow. Because analytes are being introduced via the inner gas flow, there is a clear difference between the active plasma generating zone and the analyte excitation zone (being located further downstream along the plasma axis).

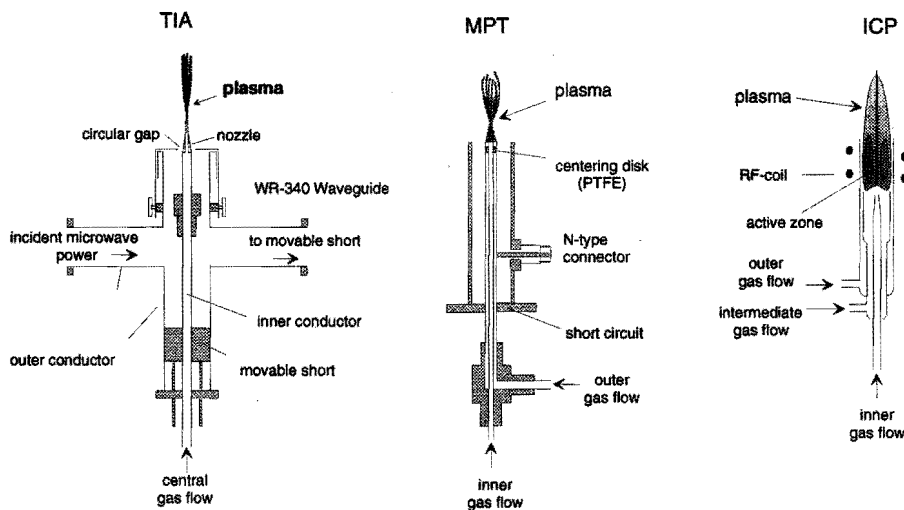


Figure 1. The TIA, depicted on the left, creates a free expanding plasma consisting of a thin (almost needle-like) converging filamentary cone with a tail flame on top of it. The MPT, depicted in the center, creates plasmas with similar structures although usually the (hollow) plasma cone has a larger diameter but a shorter length. The ICP, depicted on the right, creates a more voluminous plasma with a clear difference between the plasma generating active zone and the analyte excitation zone. Typical plasma parameters and operational settings are given in table 1.

Typical plasma parameters and operational settings for the three plasma sources are given in table 1. For the purpose of aerosol evaporation and analyte excitation especially the gas flow configuration, the plasma dimensions, the analyte residence time and the parameters  $n_e$ ,  $T_e$  and  $T_h$  are of importance. A plasma zone with a high heavy particle temperature is desired for an effective evaporation of the aerosol and the dissociation of molecules, whereas a high electron temperature (and density) is desired for the excitation of analytes with high excitation energies. Since for this latter reason usually noble gas discharges are used in the field of spectrochemical analysis, we mainly studied argon discharges in this paper (with and without analyte injection).

Parameter <sup>a</sup>	TIA	MPT	ICP
Electron density $n_e$ [ $m^{-3}$ ]	$3 \cdot 10^{21}$	$3 \cdot 10^{20}$	$2 \cdot 10^{21}$
Electron temperature $T_e$ [K]	$20 \cdot 10^3$	$18 \cdot 10^3$	$12 \cdot 10^3$
Heavy particle temperature $T_h$ [K]	$1 \cdot 10^3$ - $4 \cdot 10^3$	$1 \cdot 10^3$ - $3 \cdot 10^3$	$5 \cdot 10^3$ - $7 \cdot 10^3$
Ionization degree (%)	1	0.1	2
Applied power P [W]	300-2000	50-300	600-1800
Plasma dimensions [ $cm^2$ ]	$\varnothing 0.1 \times 5$	$\varnothing 0.2 \times 4$	$\varnothing 2 \times 5$
Typical $n_e$ gradient length [mm]	$\sim 0.07$	$\sim 0.07$	$\sim 1$
Typical $T_e$ gradient length [mm]	$\sim 0.1$	$\sim 0.1$	$\sim 2$
Used frequency f	2.46 GHz	2.46 GHz	10-100 MHz
Suitable gases	Ar, He, CO <sub>2</sub> , air	Ar, He	Ar
Gas flows (inner/interm./outer) $l \cdot min^{-1}$	(3-6)/-/-	(0.2-0.4)/(0.3-0.5)/-	1/(0-1)/(10-20)
Skin depth $\delta$ (mm)	$\sim 0.1$	$\sim 0.1$	$\sim 2$

Table 1: Typical plasma parameters and operational settings of the TIA, MPT and ICP compared. It should be noted that the TIA can be equipped with various types of nozzles. The tolerance for molecular gases is dependent on the geometry of the nozzle.

Emission measurements on the TIA and MPT have been performed with two different optical systems. In case a high spectral resolution was required, the plasma was imaged onto the entrance slit of a Jobin Yvon HR1000 monochromator (1 m focal length, 10  $\mu m$  slits, 1200 grooves/mm grating) and spectra were recorded with a photo-multiplier tube (Hamamatsu 928, side-on). In case high resolution was not required and large spectral ranges had to be measured, the plasma was focused onto a Monospec 18 monochromator (15.6 cm focal length, 10  $\mu m$  entrance slit, 1200 gr/mm grating) and spectra were recorded with a UV-enhanced CCD camera (SBIG ST6-UV, used as a 1D array of 750 pixels, each 11.5  $\mu m \times 6.53$  mm).

### 3. Experimental results

#### 3.1 General plasma observations

From the shape of the plasma and the distributions of  $n_e$ ,  $T_e$  and  $T_h$  as measured by JONKERS<sup>b</sup> *et al.* [15,16], it can be seen that plasmas created by the TIA can roughly be divided into three different zones<sup>c</sup>, cf. figure 2:

<sup>a</sup> These plasma parameters are typical for argon discharges and might be considerably different if aerosols are introduced.

<sup>b</sup> It should be noted that the insight in the spatial structure as obtained by JONKERS *et al.* is not fully applicable in this study since they studied argon discharges without water load.



1. A *cone-like zone*, being located directly above the nozzle. This is the ionizing part of the plasma and has the shape of a hollow filamentary converging cone. In this zone the gas temperature is low ( $T_h < 10^3$  K), whereas the electron density and temperature are high ( $n_e \approx 3 \cdot 10^{21} \text{ m}^{-3}$  and  $T_e \approx 22 \cdot 10^3$  respectively). This zone is 7-13 mm long whereas the cone has a diameter of 2 mm at the base (however, due to the hollow structure, gradient lengths for  $n_e$  and  $T_e$  are much smaller, cf. table 1).
2. A *cone tip zone*, starting at the converging point of the cone and continuing a few mm further downstream. Depending on the used gas flow this zone starts at 8-14 mm above the nozzle (AN). Compared to the ionizing zone, the gas temperature is higher ( $T_h \approx 2 \cdot 10^3 - 3 \cdot 10^3$  K), whereas the electron density and temperature have decreased ( $n_e \approx 1 \cdot 10^{20} \text{ m}^{-3}$  and  $T_e \approx 17 \cdot 10^3$  eV respectively). The shape of this plasma part is much like that of a filled cylinder with a height of 2-5 mm and a diameter of 2 mm.
3. A *tail flame*, in which the plasma widely fans out. For very low gas flows ( $< 0.5 \text{ l} \cdot \text{min}^{-1}$ ) and high power levels the tail flame can reach lengths up to 40 cm and a width of 6 cm, but under normal operational conditions ( $3-6 \text{ l} \cdot \text{min}^{-1}$ ) it is typically 4-6 cm long and 2 cm wide. In this part the gas temperature locally exceeds  $4 \cdot 10^3$  K whereas the electron density has dropped below the detection limit of the  $H\beta$  line emission broadening method ( $\sim 3 \cdot 10^{18} \text{ m}^{-3}$ ) and consequently could not be determined. The electron temperature could not be determined in this part either.

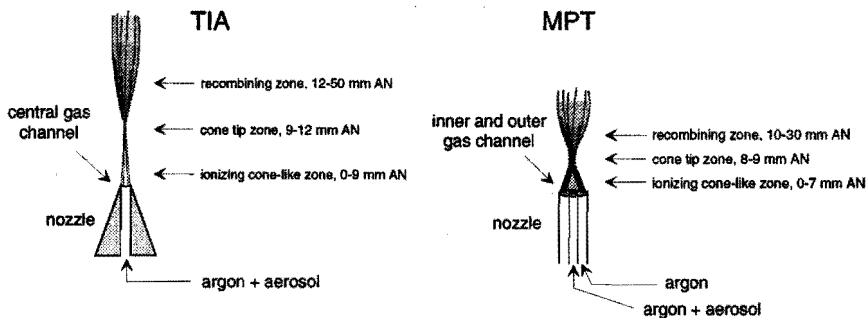


Figure 2. The three different zones that can be distinguished in typical plasmas as produced by the TIA and the MPT. The exact sizes of the zones mainly depend on the power and the gas flows.

In figure 2, a typical plasma shape of the MPT is given as well. Just as for the TIA, three different zones can be distinguished. The (hollow) cone has a diameter of typically 5 mm at the base and although it can be partly filamentary, its surface usually has a dense structure when the correct gas flows are used. In general, the MPT plasmas is shorter than that of the TIA.

<sup>c</sup> The given plasma description only applies when the "original" cone-like nozzle design with central gas injection is used. When different nozzle designs are used [10,17], the plasma shape is considerably different.

### 3.2 Spectroscopic characteristics

Spectroscopic measurements performed on the TIA and MPT showed that apart from numerous atomic lines, many different molecular bands are present as well, due to impurities in the argon gas and air entrainment. These emission bands are significantly less in ICPs, which are rather effectively shielded from the ambient air by the outer argon flow. The following molecular transitions are readily observed from argon TIA and MPT discharges:  $N_2$  ( $B^3\Pi \rightarrow A^3\Sigma$ ,  $C^3\Pi \rightarrow B^3\Pi$ ),  $N_2^+$  ( $B^2\Sigma_u^+ \rightarrow X^2\Sigma_g^+$ ),  $CN$  ( $B^2\Sigma \rightarrow A^2\Pi$ ),  $NH$  ( $A^3\Pi \rightarrow X^3\Sigma$ ),  $NO$  ( $A^2\Sigma^+ \rightarrow X^2\Pi$ ) and  $OH$  ( $A^2\Sigma \rightarrow X^2\Pi$ ). Emission of  $OH$  is strongly increased if aerosols are injected.

In figure 3 the relative intensities of a  $5p \rightarrow 4s$  argon line (at 420.1 nm) and the  $A^3\Pi \rightarrow X^3\Pi$  (1,1) band head of  $NH$  (at 337.0 nm) are given in a TIA plasma at different axial heights for different argon flows. As can be seen from the figure, the line intensities increase with increasing gas flow.

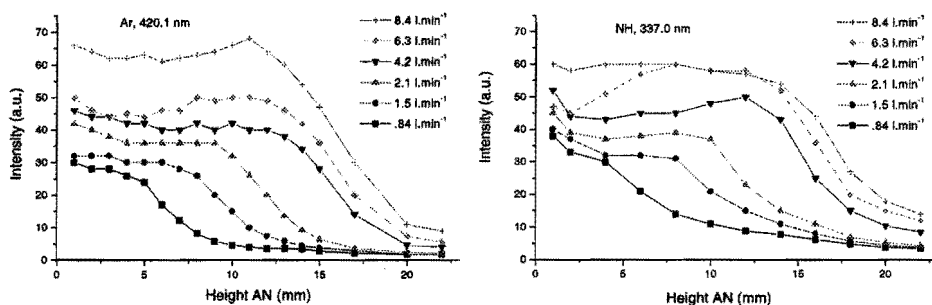


**Figure 3.** Relative intensities of a  $5p\text{-}4s$  argon line (at 420.1 nm) and the  $A^3\Pi \rightarrow X^3\Pi$  (1,1) band head of  $NH$  (at 337.0 nm) are given at different axial heights in a TIA plasma for different argon flows ( $P=1$  kW). It can be seen that intensities of both the argon line and the  $NH$  band head increase with an increasing flow rate.

It can be expected that the rate of the reaction chain of charge transfer between argon ions and molecular nitrogen:



followed by dissociative recombination:



will increase with an increasing gas flow due to turbulent mixing with surrounding air. Since this mechanism decreases the electron density  $n_e$ , whereas at the same time the emission increases, this indicates that the electron temperature  $T_e$  increases.

Moreover, it can be seen that with increasing gas flow the axial positions at which the emission intensities start to decay shift further downstream. The zone with more or less constant

(high) emission roughly defines the ionizing and cone tip zone, whereas intensities decay in the tail flame. The start of the tail flame is thus lifted further downstream when the gas flow is increased. This is illustrated by the photographs of TIA plasmas given in figure 4. On the left a photo of a plasma with low gas flow and on the right a plasma with high gas flow is given (1.0 and 5.0 l·min<sup>-1</sup> respectively). It should be noted that the tail flame shrinks with increasing gas flow and that the visible radiation emitted by this tail decreases drastically.

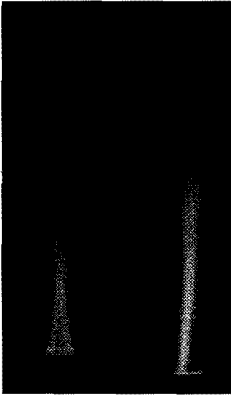


*Figure 4.*

*Photographs of argon TIA discharges with varying gas flows (on the left 1.0 and on the right and 5.0 l·min<sup>-1</sup> respectively). It should be noted that the plasma cone is extended further downstream with increasing gas flow. Radiation of the tail flame is so weak that it can hardly be distinguished on these photos.*

### 3.3 Emission from the tail flame

In figure 5, a typical spectrum measured from the weak white afterglow in the downstream end of the tail flame of a TIA plasma is given. The only emission lines that are still present are 4p→4s argon lines and the 3p5P→3s5S atomic oxygen lines around 777 nm. The continuum-like emission between 450-800 nm is probably largely due to NO<sub>2</sub> radiation created through the chemi-luminescent reactions [18,19]:



followed by:



The origin of the argon and oxygen lines is less obvious in this plasma part. Since excitation energies of the radiative levels are around 13.1 and 10.7 eV respectively, T<sub>e</sub> and T<sub>h</sub> are far inadequate to excite these levels. Most likely, the atomic species are created in the excited radiative state by the dissociative recombination of Ar<sub>2</sub><sup>+</sup> and O<sub>2</sub><sup>+</sup>, e.g.:



Emission of diatomic association products (such as CN, NH, C<sub>2</sub>) is not present in the extremity of the afterglow. Since at atmospheric pressure these molecules usually are produced in an excited (radiative) state by the three-particle association process given by [20]:



with A and B atomic radicals and C a heavy particle, it can be concluded that concentrations of atomic radicals (such as O, N, H, C) are low in this plasma zone. This in contrast to the cone-like ionizing plasma zone, the cone tip zone and the upstream part of the tail flame, where emission of diatomic association products is readily observed (cf. figure 3b for the emission intensity of NH).

For spectrochemical analysis however, the extremity of the tail flame hardly seems to have applications, so in the remainder of this paper we will focus on the plasma zone between the nozzle and the bottom part of the tail flame.

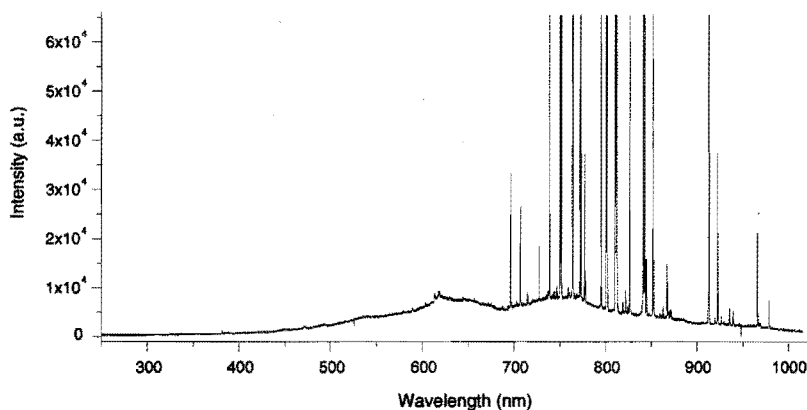


Figure 5. Typical spectrum obtained from argon TIA discharges in the white/yellow glow in the downstream end of the tail flame. Emission in this part is very weak and intensities should not be compared to the line intensities given in figure 3.

### 3.4 Detection limits

Similar to the profiles given in figure 4, analyte emission intensities are at a maximum in the ionizing cone and the cone tip zone of the TIA. Experiments with different analytes (Zn, Mg, Na, Cd) have shown that detection limits in the TIA are around 1 ppm for these elements. It should be noted that the aerosol was injected directly into the plasma without any preliminary desolvation process.

The distribution of analyte emission is rather different in the MPT, where just above nozzle (almost) no analyte signal is present and a distinctive maximal excitation is found at a height of 8 mm, cf. figure 6, where the intensities of an analyte (magnesium) are given as functions of the axial heights in the TIA and the MPT. The intensities of the Mg 3p-3s ion line at 279.6 nm show a similar dependence on the height (not shown in the figure). The profile for the magnesium atom line in the MPT (cf. figure 6), is largely similar to the heavy particle temperature profile as determined by PROKISCH *et al.* [21].

The differences between TIA and MPT can be largely ascribed to the different analyte injection methods: in the TIA aerosols and argon are mixed before being injected into the

plasma, whereas in the MPT the analyte is introduced through the central channel along the axis of the (hollow) plasma cone so that the actual plasma penetration of the aerosol takes place in the central zone. Detection limits have not been determined for the MPT in this paper but are reported by JIN *et al.* [13]. In case of analyte introduction with a pneumatic nebulizer without desolvation these detection limits are around 0.1 ppm, and significantly improve if a ultrasonic nebulizer with desolvation is used (to typically 1-10 ppb).

The better detection limits that are reported for the MPT can be largely attributed to a number of reasons:

- Due to the lower axial gas velocity in the MPT (typically 5 versus 15  $\text{ms}^{-1}$ ) the residence times of analytes in the plasma are longer.
- For the MPT the aerosol is introduced in a zone with high gas temperature, so that the droplets are evaporated more effectively.
- For the MPT the aerosol is injected along the axis of the hollow cone, ensuring a good sample penetration into the hot part of the plasma.

Moreover, problems with analyte injection into the TIA on a larger time scale were encountered. The long central gas channel of the TIA constitutes a significant resistance between nebulizer and plasma and condensation inside the tube deteriorates the analyte injection efficiency in the long run.

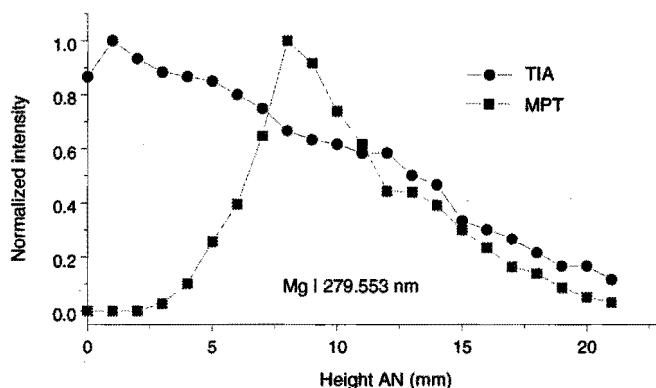


Figure 6. Normalized intensities of a Mg  $3p \rightarrow 3s$  atomic line (at 285.2 nm) measured from argon plasmas with magnesium analyte injection produced by the TIA and the MPT. It should be noted that for the MPT no analyte emission is observed close to the nozzle and that the plasma has a distinctive optimum analyte excitation zone (between 7 and 11 mm AN).

It should be noted that for both plasma torches, detection limits are worse than for the ICP (at least without aerosol desolvation). Main reasons probably are the higher heavy particle temperature in the ICP, which ensures a better droplet evaporation, and the lower molecular background due to an effective shielding of the plasma from the ambient air. The worse detection limits imply that the torches cannot be used in all applications in which ICP-AES is currently used.

If analyte concentrations in aqueous samples are high enough, the use of the MPT is

preferred (because of larger stability in time, its compact setup and its lower costs of acquisition and maintenance). An exception has to be made for the analysis of halogens: Since the TIA can be more easily operated on helium [11,22,23], it seems to be of special potential for this purpose.

### 3.5 Influence of molecular gases

Up to now we only studied aqueous analyte injection. However, many applications can be thought of in which gaseous samples have to be analyzed. It is found that, like the conventional argon ICP, the argon MPT is very sensitive to molecular gas injection. The TIA however, can handle much larger amounts of molecular gases, both in absolute and relative sense [24]. In figure 7, the intensity of a Zn emission line is given as a function of the amount of air added to a TIA plasma. As can be seen from the figure, the analyte intensity decreases rather smoothly.

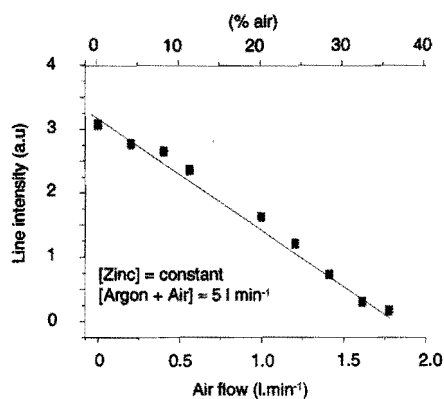


Figure 7.

Intensities of a Zn  $4p \rightarrow 4s$  atomic line (at 213.9 nm) as a function of the amount of air added to the argon TIA discharge. It should be noted that the total amount of gas and the amount of injected aqueous aerosol are kept at constant rate. Measurements are performed at 10 mm AN,  $P=1$  kW.

Depending on the nozzle geometry, even pure molecular gases can be used (cf. table 1). In figure 8 spectra from an argon plasma and an air plasma are given. The plasmas were created on top of a nozzle with a central tungsten tip [17,20]. Apart from the  $\text{NO}_x$  emission between 200 and 300 nm and numerous tungsten lines, the spectral background is rather flat, which is in favor for analytical applications.

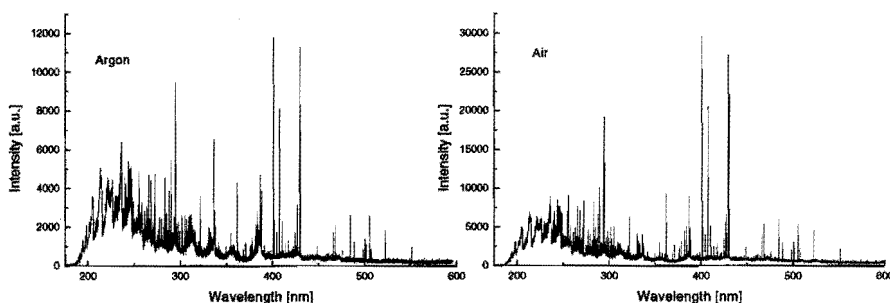


Figure 8. Typical spectra from an argon discharge (on the left) and an air discharge created by the TIA (on the right), measurement at 14 mm AN ( $P=400$  W).

The TIA thus seems to be especially promising for applications involving molecular gases. We already successfully used the TIA as dissociation and excitation source for the on-line analysis of combustion gases containing high levels of pollutants [10].

#### 4. Conclusions

Plasmas produced by the TIA (Torche à Injection Axiale) and the MPT (Microwave Plasma Torch) have been studied with respect to their applicability as excitation sources in spectrochemical analysis. Compared to the widely used Inductively Coupled Plasma these plasmas benefit from a compact setup and low gas consumption whereas they are less sensitive to water load than most other microwave induced plasmas. This makes these plasma torches interesting alternatives when size and cost reduction are desired and no extreme low detection limits are required.

In plasmas produced by both plasma sources three distinctive zones can be observed: an ionizing cone-like zone close to the nozzle, followed by a cylindrical-like cone tip zone and a tail flame, in which processes like chemi-luminescence generate weakly visible radiation. With increasing gas flow, the lengths of the cone and cone tip zones are increased whereas the size of the tail flame is reduced. Strong emission of diatomic association products (CN, N<sub>2</sub>, N<sub>2</sub><sup>+</sup>, NH, NO and OH) shows that air entrainment already takes place just above the nozzle.

For the analysis of aqueous samples the MPT seems to have the most potential since it features the best detection limits for elements (typically 0.1 ppm versus 1 ppm for the TIA). The better analytical performance of the MPT is probably due to the shorter analyte gas channel, the larger residence time of the aerosol in the plasma and the separation of the main gas flow and the analyte carrier gas flow carrying. In plasmas produced by the MPT, by far the strongest analyte radiation is emitted from the cone tip zone.

However, it is found that the TIA is less sensitive to molecular gases and, dependent on the geometry of the nozzle, even can be operated on pure molecular gases. This makes the TIA a promising excitation source for the analysis of gaseous samples, such as flue gases, with high analyte concentrations.

#### Acknowledgements

The authors would like to thank Prof. J.A.C. Broekaert, C. Prokisch and A.M. Bilgic from the University of Dortmund for lending the MPT and Prof. M. Moisan from the University of Montréal for giving permission to use the TIA design. Financial support was given by the Dutch Technology Foundation (STW) and by the Eindhoven Centre Technology for Sustainable Development (TDO).

## References

1. P.W.J.M. Boumans, "Inductively coupled plasma emission spectroscopy", part 2: "Applications and fundamentals", John Wiley & Sons, New York (1987).
2. A. Montaser and D.W. Golightly, "Inductively coupled plasmas in analytical atomic spectrometry", second edition VCH Publishers, Inc., New York (1992).
3. A. Montaser, *CRC Critical Rev.* **18(1)**, 45 (1987)
4. M. Moisan and Z. Zakrewski, *Rev. Sci. Instrum.* **58**, 1895 (1987).
5. M. Moisan and Z. Zakrewski, *J. Phys. D: Appl. Phys.* **24**, 1025 (1991).
6. C.I.M. Beenakker, B. Bosman and P.W.J.M. Boumans, *Spectrochim. Acta* **33B**, 373 (1978).
7. R.E. Sturgeon, S.N. Willie and V.T. Luong, *Spectrochim. Acta* **46B**, 1021 (1991).
8. H. Matusiewicz, *Spectrochim. Acta* **47B**, 1221 (1992).
9. Q. Jin, Y. Duan and J.A. Olivares, *Spectrochim. Acta* **52B**, 131 (1997).
10. Chapter 3 of this thesis, E.A.H. Timmermans, F.P.J. de Groote, J. Jonkers, D.C. Schram and J.A.M. van der Mullen, "AES for the on-line monitoring of incinerator processes", submitted for publication in *J. Anal. At. Spectrom.* (1999).
11. M. Moisan, G. Sauvé, Z. Zakrzewski and J. Hubert, *Plasma sources, Sci. and Techn.* **3**, 584 (1994).
12. Q. Jin, F. Wang, C. Zu, D.M. Chambers and G.M. Hieftje, *J. Anal. At. Spectrom.*
13. Q. Jin, C. Zhu, M.W. Borer and G.M. Hieftje, *Spectrochim. Acta* **46B**, 417 (1991).
14. A.M. Bilgic, C. Prokisch, J.A.C. Broekaert and E. Voges, *Spectrochim. Acta* **53B**, 773 (1998).
15. J. Jonkers, L.J.M. Selen, J.A.M. van der Mullen, E.A.H. Timmermans and D.C. Schram, *Plasma Sources, Sci. and Techn.* **6**, 533 (1997).
16. J. Jonkers, "Excitation and transport in small scale plasmas", Ph.D. Thesis, Eindhoven University of Technology, The Netherlands (1998).
17. A. Ricard, L. St-Onge, H. Malvos, A. Gicquel, J. Hubert and M. Moisan, *J. Phys. III France* **5**, 1269 (1995).
18. J.C. Greaves and D. Garvin, *J. Chem. Phys.* **30**, 348 (1959).
19. J.V. Michael, J.E. Allen Jr. and W.D. Brobst, *J. Phys. Chem.* **85**, 4109 (1981).
20. Chapter 4 of this thesis, E.A.H. Timmermans, J. Jonkers, I.A.J. Thomas, A. Rodero, M.C. Quintero, A. Sola, A. Gamero and J.A.M. van der Mullen, *Spectrochim. Acta* **53B**, 1553 (1998).
21. C. Prokisch and J.A.C. Broekaert, *Spectrochim. Acta* **53B**, 1109 (1998).
22. A. Rodero, M.C. García, M.C. Quintero, A. Sola and A. Gamero, *J. Phys. D: Appl. Phys* **29**, 681 (1996).
23. A. Rodero, M.C. Quintero, A. Sola and A. Gamero, *Spectrochim. Acta* **51B**, 467 (1996).
24. E.A.H. Timmermans, I.A.J. Thomas, J. Jonkers, J.A.M. van der Mullen and D.C. Schram, *Fresenius J. Anal. Chem.* **362(5)**, 440 (1998).





# 3

## AES for the on-line monitoring of incineration processes

*E.A.H. Timmermans, F.P.J. de Groot, J. Jonkers, D.C. Schram and J.A.M. van der Mullen*  
Submitted for publication in *J. Anal. At. Spec.* (1999).

**SUMMARY** - *A diagnostic measurement system based on atomic emission spectroscopy (AES) has been developed for the purpose of on-line monitoring of hazardous elements in industrial combustion gases. The aim was to construct a setup with a high durability for rough and variable experimental conditions, e.g. a strongly fluctuating gas composition, a high gas temperature and the presence of fly ash and aggressive effluents. Since the setup is primarily intended for the analysis of combustion gases with extremely high concentrations of pollutants, not much effort has been made to achieve very low detection limits. It was found that an inductively coupled argon plasma was too sensitive for molecular gas introduction. Therefore a microwave induced plasma torch, compromising both the demands of a high durability and an effective evaporation and excitation of the analyte was used as excitation source. The analysis system has been installed at AVR-Chemie, a Dutch industrial hazardous waste incinerator, and successfully tested on combustion gases present above the incineration process. Highly abundant elements as zinc, lead and sodium could easily be monitored. On-line information of relative fluctuations of these elements in the combustion gases may be used for process control and contribute to a more efficient incineration process.*

## 1. Introduction, the aims of combustion gas analysis

During the last decade worldwide several groups have been studying the feasibility of AES (Atomic Emission Spectroscopy) for the on-line analysis of flue gases. As far as we know these investigations are without exceptions focused on off-stream exhaust gases, i.e. relatively "clean and cold" end-of-pipe gases just before their ejection into the atmosphere takes place. Main reason for the exploration of this research field is the expectation that within a few years European and American legislation will enforce continuous emission monitoring of flue gases for several industries, e.g. power plants, cement industries and waste incinerators [1]. Therefore a strong need exists for the development of analysis methods for which the measuring time is significantly reduced compared to the methods that are currently in use.

Clear progress has been made with ICP-AES, in which an inductively coupled plasma ("ICP") has been used as the excitation source of the flue gases [1-6] and in 1997 the first systems for quantitative continuous emission monitoring based on ICP-AES became commercially available [1]. Other research groups focused their attention onto LIBS (Laser-Induced Breakdown Spectroscopy), in which a laser is directly focused into the off-stream gas flow creating discharges inside the stack [7,8]. Although gas sampling, a critical stage when ICP-AES is used, can be avoided with the LIBS technique, serious problems have been encountered with the calibration due to the very large gradients in the laser-induced plasma and the presence of fly ashes.

Apart from legislation purposes, on-line monitoring can also be used to control the combustion process. Opposite to the groups mentioned, our aim is to investigate whether it is possible to develop analytical equipment that can be used for process control. Therefore, a project was started in co-operation with AVR-Chemie, a large industrial hazardous waste incinerator in Rozenburg (close to Rotterdam), with the aim of on-line monitoring of heavy metals present in the combustion gases just above the flames of the incineration process itself, i.e. in gases which have not been cleaned yet.

The process of waste incineration at AVR-Chemie is sketched in figure 1. Measurements should be performed on the combustion gases in the so-called secondary combustion chamber, which has the function of incinerating hazardous waste that has not been completely burnt inside a slowly rotary kiln. The solid slag remaining after the combustion process inside the after burning-chamber is removed through various outlets, whereas the combustion gases undergo several cleaning stages, before they are ejected into the atmosphere. The energy that is liberated from the combustion is used to create steam inside the boilers for the production of electricity, cf. figure 1.

A possible application of on-line information on temporal fluctuations of metals in the combustion gases present in the secondary combustion chamber could be the adjustment of the incineration composition, in order to optimize the combustion process or to minimize peak loads of metal flows. This may increase the electricity production and the lifetime of the equipment used in the cleaning stages that follow after the two-stage incineration [9].

A	Introduction hazardous waste	5,7	Wet and dry ash outlet	12	Alkaline scrubber
1	Rotary kiln	8	Quench	13	Heat exchanger
2	Secondary combustion chamber	9	Electrostatic filter	14	Ventilator
3	Bottom ash outlet	10	Acid scrubber	15	Active carbon filter
4,6	Boiler	11	16	Stack	

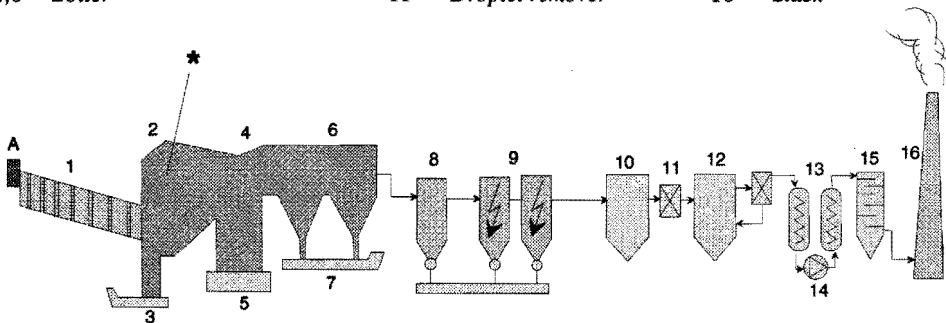


Figure 1.1 Schematic drawing of DTO9 at AVR-Chemie. Measurements have been performed above the combustion in the secondary combustion chamber, marked with an asterisk.

The analysis of non-cleaned gases implies that the merits of the previous groups - achieving good detection limits and an accurate quantification of concentrations - are less important in our case, whereas flexibility, cost reduction, the withstand against changing experimental conditions and the presence of acids and dust particles are of much more importance [9]. As a consequence, it is not straightforward to use commercially available ICP-AES equipment, since this is developed and optimized for relatively clean off-stream gases and should be used under laboratory-like conditions. The combustion gases above the incineration process inside the secondary combustion chamber contain high levels of pollutants and measurement conditions are far from laboratory-like. Especially due to the high temperature of the combustion gases and the presence of acid compounds great care has to be given to the materials used in the analysis system.

Since no methods are in use for monitoring metals inside the incineration oven itself, it is obvious that new developments in this area are of great importance. It is the aim of this study to find strategies to speed up these developments.

In the next section the advantages and disadvantages of the use of AES for analytical gas analysis will be discussed. In section 3 the used experimental setup will be given while in section 4 preliminary results obtained at AVR-Chemie will be presented. An evaluation and concluding remarks will be given in section 5.

## 2. Atomic emission spectroscopy (AES) for combustion gas analysis

Spectroscopy is a logical choice when the on-line analysis of multiple species is demanded. For the analysis of molecules in off-stream flue gases, (infrared) absorption spectroscopy is often used. However, since atoms cannot be excited rotationally or vibrationally, infrared absorption spectroscopy cannot be used for the analysis of elements, such as heavy metals. Atomic spectroscopy can either be based on absorption (AAS) or emission (AES). Since in combustion gases varying concentration of solid particles are present which easily absorb radiation wavelength-independently, AAS would have several complications and has been ruled out. This study has been focused on diagnostics based on atomic emission spectroscopy, which does not have these problems, and moreover, is a very fast and sensitive analysis method that can provide information on several elements simultaneously. Furthermore, AES is very useful for the analysis of atoms present in concentrations as are expected for several heavy metals in the combustion gases of waste incinerators.

AES is widely used for the analysis of liquids. The analysis of combustion gases at AVR-Chemie however, involves various new problems:

1. The combustion gases in the secondary combustion chamber form a complex and aggressive acid medium which reaches temperatures up to 1200 °C.
2. During the extraction, condensation of incinerator gases easily results in the loss of particles, e.g. to the walls of the extraction system. Since heavy metals are largely concentrated in or on these particulates, their loss should be avoided.
3. Due to an under-pressure in the range of 1 mbar that is present inside the secondary combustion chamber, a gas sampling technique based on pumping is required for the gas extraction.
4. Significant fluctuations in this pressure complicate the extraction of the gases.
5. The measurement site is subject to strong vibrations and strong temperature fluctuations [9].
6. There is a lack of calibration samples for quantitative measurements.

### 3. The experimental setup

#### 3.1. Introduction

Three largely separated steps can be distinguished in AES in the case of combustion gas analysis (cf. figure 2):

1. Gas sampling, i.e. the extraction of the combustion gases out of the waste incinerator and transport towards the excitation source.
2. Dissociation and the excitation of the combustion gases by an excitation source, e.g. a laser or plasma.
3. Acquisition and analysis of the emission spectra.

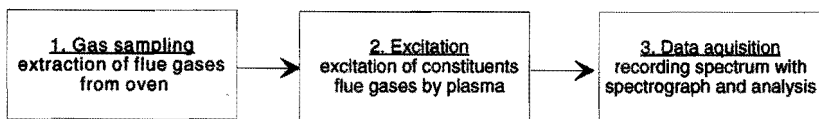


Figure 2. A diagram showing the three main steps in combustion gas analysis.

These three steps will be discussed separately. Since the excitation source plays a central role in atomic emission spectroscopy, the applied plasma source will be discussed at first. The data-acquisition and gas sampling will be treated afterwards.

#### 3.2. The "conventional" ICP as excitation source for molecular gases

Plasmas and lasers are the most common sources used for the excitation of atomic or molecular species. In analytical chemistry the so-called inductively coupled plasma (ICP) is by far the most popular excitation source, especially when heavy metals in aqueous aerosols have to be analyzed [10,11]. As a result, several ICP-AES systems have become commercially available. These systems usually are completely computer-controlled and optimized for the analysis of aqueous samples. Experimental settings (as gas flows) can only be varied to a limited extent. Since it is likely that for gas analysis other experimental conditions are required, the use of these commercially available systems is not straightforward. For this reason our initial efforts to analyze gases were done with a non-commercially available 50 MHz ICP (Philips [11]), cf. figure 3, requiring fully manual control. Within a certain range, increasing the flow of combustion gases into the argon-ICP will result in an increase of the emission signals of the present species and thus improve the signal to noise ratios, since the total number of elements introduced into the plasma will increase consequently. It therefore is important that a considerable amount of combustion gases can be introduced into the plasma.

However, it is well known that molecular gases can have a large influence on noble gas discharges and that the excitation power of the plasma might be severely altered [10,11]. When too much molecular gases are introduced, the plasma even might extinguish. Therefore, an extensive study on the effects of molecular gases on the ICP is needed.

The effects of incinerator gases on the excitation power of the argon ICP are simulated by simultaneously introducing air and an aqueous analyte. The analyte (30 ppm zinc in 10% HNO<sub>3</sub>) is introduced through the central channel of an ICP Fassel torch [12] with the use of an argon-fed cross-flow nebulizer (typical aerosol injection rate: 2 ml·hr<sup>-1</sup>). Additional air, being a substitute for the combustion gases, has been added to the central argon/aerosol flow just before the central channel in the ICP torch. It should be noted that only the air flow  $Q_{\text{air}}$  is varied during the experiments and that the amount of Zn introduced into the plasma is kept at a constant rate.

Results are shown in figure 4, in which the dimensionless quantity PDR (Peak intensity to Detection limit Ratio) is used. It is defined as

$$\text{PDR} = \frac{c}{c_L} = \frac{I(c)}{z_A \sigma_B}, \quad (1)$$

with  $c$  being the concentration of Zn in the simulated incinerator gas (in mg·m<sup>-3</sup>),  $c_L$  the detection limit of Zn (in mg·m<sup>-3</sup>),  $I(c)$  the measured Zn line intensity (cf. figure 4a),  $z_A$  an arbitrary constant (taken 2 in our case) and  $\sigma_B$  the noise in the measured background (cf. figure 4a). In figure 4b the PDR of the most intense emission line of zinc (at 213.86 nm) is given as a function of the amount of air added to an argon plasma with a RF power supply of 2.0 kW. It is found that the introduction of more than 0.21 l·min<sup>-1</sup> of air leads to a strong decrease of the PDR. This corresponds to the experimental findings that for  $Q_{\text{air}} > 0.21 \text{ l}\cdot\text{min}^{-1}$  the intensity of the Zn line sharply drops, whereas the background noise  $\sigma_B$  remains more or less constant. Apparently, the excitation power of the plasma is severely disturbed if  $Q_{\text{air}} > 0.21 \text{ l}\cdot\text{min}^{-1}$ .

From equation 1 it can be seen that if the PDR and the concentration  $c$  are known, the theoretical detection limit of Zn in air (or combustion gases) can be calculated. The concentration  $c$  can simply be deduced from the known mass flow of zinc and the known volume flow of air into the plasma. Results are given in figure 4c and obtained using the PDR values of figure 4b). Figure 4c once more shows that the best detection limits would be achieved combustion gases are introduced with a rate of 0.21 l·min<sup>-1</sup>.

In figure 4d the relationship between the applied RF power and the minimum value of the detection limit of zinc is shown for an argon ICP with analyte and 0.21 l·min<sup>-1</sup> air injection. From the plot it can be seen that the detection limit depends rather strongly on the RF power and clearly deteriorates if less than 1.5 kW is applied. In that case the drop in the PDR will appear at air flow rates below 0.21 l·min<sup>-1</sup>.

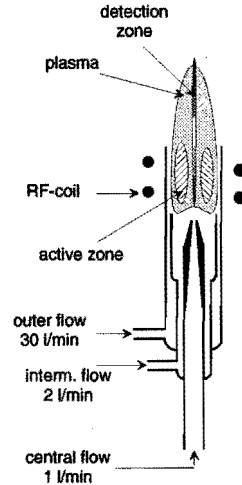
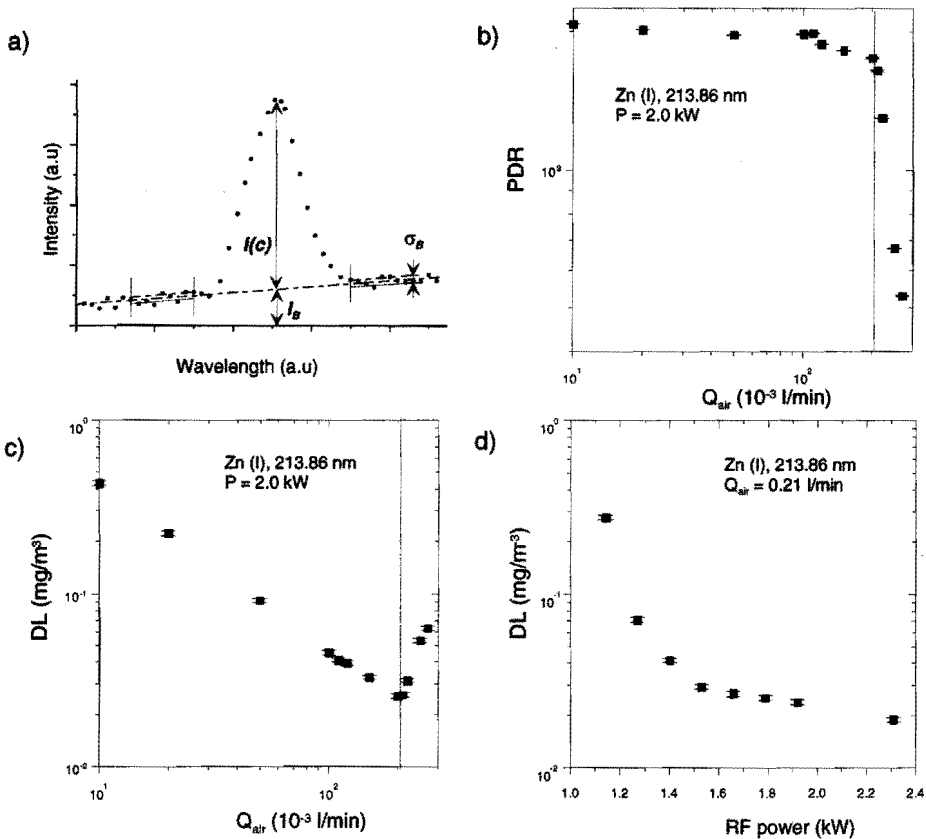


Figure 3. A schematic illustration of the 50 MHz inductively coupled plasma and the quartz plasma torch.



**Figure 4.** In a) it can be seen how the measured parameters in the peak intensity to detection limit ratio (PDR) are defined. In b) the PDR and in c) the deduced detection limit DL for an atomic Zinc line are given as functions of the air flow  $Q_{air}$  introduced into the argon ICP. In d) the minimum detection limit is shown as a function of the HF-power when  $Q_{air}$  is kept constant.

The measurements show that air introduction has a dramatic impact on the excitation power of the argon ICP. Assuming that combustion gases have the same effect on the excitation power of the plasma as air, it is obvious that the combustion gases can only constitute a little fraction of the total plasma gas (maximally  $0.21 \text{ l}\cdot\text{min}^{-1}$  of combustion gases versus  $> 25 \text{ l}\cdot\text{min}^{-1}$  of argon). As a result, concentrations of several trace elements can easily become too low for detection.

It is interesting to compare our experimental findings with the normal molecular load of the ICP by means of water inlet when it is used for liquid analysis. It is found that the plasma can endure a number of air molecules which is approximately equal to the number of water molecules that normally is introduced for liquid analysis, before getting noticeably disturbed. For the detection of some elements in combustion gases however, a higher gas flow might be needed in order to ensure that sufficient atoms are present in the plasma. Moreover, due to the risk of condensation of the hot combustion gases and the presence of particulates, which would



easily obstruct capillary gas handling systems, it is very difficult to control small gas flows. Apart from the flow capacity control problems, it can be expected that the composition of combustion gases strongly fluctuates with respect to the molecular species, particulates and acid compounds. Especially for plasmas that are sensitive for molecular injection, this might affect the excitation power as a function of time. All these factors suggest that a plasma is required which is less sensitive to molecular injection and in which significantly more than  $0.21 \text{ l}\cdot\text{min}^{-1}$  of molecular gases can be introduced.

### 3.3. The "Torche à Injection Axiale" (TIA)

As discussed in section 3.2, the investigated argon ICP shows several shortcomings as excitation source for combustion gases. In literature, several ICPs have been reported which, unlike the ICP we studied, have a very high resistance against molecular gases or even can be operated on pure molecular gases [10,11]. However, these plasmas usually require a high power input (>3 kW) and consequently a large and heavy setup. Because a compact and modular setup is desired for the measurements at the secondary combustion chamber of AVR-Chemie, we have looked for a plasma source in the category of microwave induced plasmas (MIPs).

Microwave induced plasmas have already been used several times in analytical chemistry [13]. Besides the well-known surfatron [14-16] and Beenakker cavity [17], several other field shaping applicators have been used as well [18,19]. However, due to their limited operating powers (< 400 W), these plasmas show a strong sensitivity to water introduction. For this reason their practical use is mainly restricted to applications in combination with gas chromatography and the ICP, combining a better  $\text{H}_2\text{O}$  resistance and much better detection limits, is still far more popular for the analysis of aqueous samples.

Recent developments in the field of microwave induced plasma technology however, have resulted in new compact plasma sources which have overcome these power restrictions and can be operated at power levels up to several kilowatts. This is mainly due to the avoidance of quartz materials and an increasing availability of waveguide sustained power supplies. Through waveguides much higher power levels can be transmitted than through coaxial lines.

One of these new microwave induced plasma sources is the so-called "TIA" (from "Torche à Injection Axiale") [20,21], producing needle-like plasmas which seem very suitable for atomic emission spectroscopy. Due to its design, the TIA is rather insensitive for impedance changes [22] (unlike the argon ICP discussed in section 3.1) and therefore fulfills the demand of a high resistance to molecular gases. Depending on the geometry of the TIA-nozzle even pure molecular gases can be used as plasma gas [21,23]. This is one of the main reasons why this plasma source has been used for the measurements at AVR-Chemie.

The TIA is based on the original design from MOISAN *et al.*, who also studied the tuning and matching properties and characteristics of the torch when creating atmospheric helium or argon plasmas [20]. Remarkable is the large power range over which the TIA can be operated: from 150 W up to at least 5 kW. The plasma has a diameter of typically 1-2 mm and a height of 6 cm (at a microwave power of 1 kW and  $5 \text{ l}\cdot\text{min}^{-1}$  of argon gas supply). Typical maximum electron densities and temperatures in an argon plasma at these conditions are  $2\cdot 10^{21} \text{ m}^{-3}$  and

$2 \cdot 10^4$  K respectively while the maximum heavy particle temperature is approximately  $5 \cdot 10^3$  K [24,25].

The TIA and the accompanying waveguide structures are shown in figure 5. Microwave radiation with a frequency of 2.46 GHz is introduced into a rectangular waveguide structure (WR-340, inner dimensions  $86.4 \times 43.2$  mm<sup>2</sup>) by means of an antenna and propagates inside the waveguide in the dominant TE<sub>01</sub> mode. Inside the TIA-structure, this wave propagation mode is converted into the coaxial TEM mode. After impedance matching and tuning, which can be achieved with a movable short and three tuning screws inside the waveguide and several elements inside the TIA, the microwave energy can be transmitted and focused in the vicinity of the gap between the nozzle and the outer cover. A plasma breakdown can be created above the nozzle at sufficiently high power densities after supplying a (noble) gas flow. Depending on the matching, the plasma will dissipate almost all energy and hardly any EM energy will be reflected. Electromagnetic shielding is necessary to maintain the microwave energy leakage within allowed limits. When the system is mismatched, part of the power will be reflected towards the magnetron. Since reflected power easily causes damage to the magnetron tube, a circulator is inserted between the antenna and the tuning screws. This three-gate device directs incident power in the direction of the TIA and the reflected waves towards the auxiliary load. The amount of reflected power, and thus the efficiency of the power transfer towards the plasma, is measured with a diode connected to the load of the absorber. The power supply (Muegge, MW-GIR2M130-2K) is limited to 2 kW.

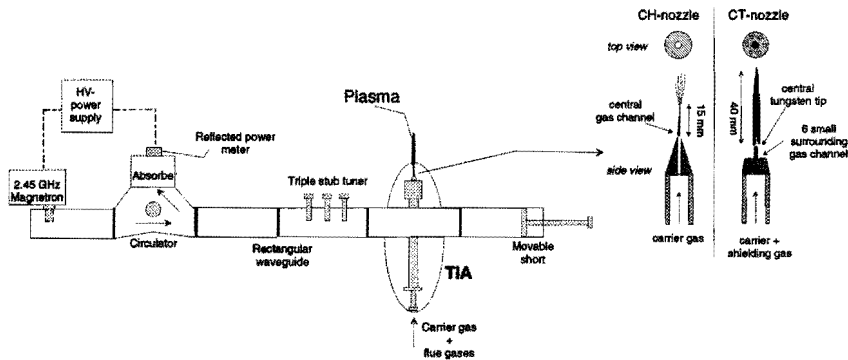


Figure 5. The microwave set-up with the TIA in central position. On the right the two different applied nozzles are depicted.

Two different nozzle designs have been used to control the gas flow and field shaping properties [21,22], cf. figure 5. When using a copper nozzle with a central hole for gas injection (CH-nozzle), only plasmas can be created if noble carrier gases are used, e.g. argon or helium. However, when the plasma is created on top of a nozzle with a central tungsten tip (CT-nozzle), purely molecular gases, like air or flue gases, can be used as well. A limitation of the CT-nozzle is that the maximum applied power is approximately 1 kW (when a total gas flow of about 4 l·min<sup>-1</sup> is used). At higher power levels the tungsten tip will erode and emission lines of tungsten

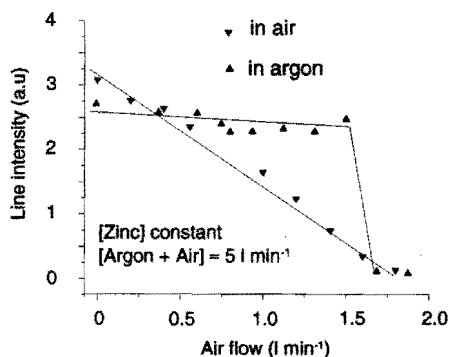
can be observed in the spectrum. Because this element has many very strong emission lines, analyzing the spectra becomes rather difficult. Other possible tip materials suffer from the disadvantage of a lower melting point. Typical diameters of the gas channels are 1.5-2 mm for the CH-nozzle and 0.5-1 mm for the CT-nozzle.

In order to investigate the influence of molecules on the detection limit we applied the same method as described in section 3.2 for the ICP. In figure 6 the intensity of a zinc line from an argon plasma with Zn analyte and air additives (created with the CH-nozzle) is shown as a function of the amount of introduced air. If we assume that the air addition has no influence on the noise in the spectral background ( $\sigma_B$ ), we can compare the results with figure 4c, giving the PDR for the investigated argon ICP. It is obvious that in case of the TIA plasma much more air can be introduced as in the ICP, both in absolute as in relative sense (1.5 versus 0.2 l·min<sup>-1</sup> and 30 versus 0.8% respectively).

A remarkable difference can be seen between TIA plasmas expanding into air and plasmas expanding into an argon environment (controlled by a large vessel). For plasmas expanding into an air environment we observed a steady decrease of the Zn emission as a function of the amount of air introduced with the argon carrier gas. However, for plasmas expanding into an argon environment, the emission signal remained more or less constant for low airflow rates and dropped sharply if the amount of added air exceeded 1.5 l·min<sup>-1</sup>. This shows some resemblance with the case of the ICP expanding into air (cf. figure 4b), in which the emission intensity also showed a sharp drop. The resemblance is probably due to an effective shielding of the ICP from the air environment by the outer argon gas flow. However, the similarity is only relative, since, as stated before, much more air can be introduced into the TIA plasma.

Figure 6.

*The intensity of a zinc line (introduced as aerosol) measured from an argon discharge created with the CA nozzle as a function of the additionally introduced amount of air (measured at 7 mm above the nozzle, P=1 kW). It should be noted that there is a large difference between plasmas expanding in the open air and plasmas expanding into an argon environment.*



### 3.4. The optical set-up

The optical setup that was used for spectroscopic measurements at the waste incinerator plant is given in figure 7. With a parabolic mirror the plasma is imaged onto the entrance slit of the compact crossed Czerny-Turner monochromator (Monospec 18, focal length 15.6 cm, 2400 gr/mm grating blazed at 260 nm, produced by Thermo Jarrell Ash). The use of the parabolic mirror ensures a large solid angle and avoids problems that the use of lenses would entail (like a wavelength-dependent diffraction index).

The dispersed emission signal is focused onto an UV-enhanced CCD-camera (ST6-UV, manufactured by Santa Barbara Instrument Group), used in the spectroscopic mode. In this mode the camera has an array of 750 pixels, each  $11.5 \mu\text{m} \times 6.53 \text{mm}$  in size. The resolution of the optics is approximately  $0.016 \text{nm/pixel}$  at  $210 \text{nm}$ , ample to identify atomic lines and molecular bands. At this resolution thus approximately  $12 \text{nm}$  is depicted simultaneously on the CCD, whereas at  $400 \text{nm}$  around  $16 \text{nm}$  is depicted simultaneously. As a result, only about 15 measurements are necessary to scan the most relevant wavelength interval ( $200\text{--}400 \text{nm}$ ). Apart from the compact size and the relatively low price, another major advantage of the used system is its robustness: re-calibration after transport is hardly ever required.

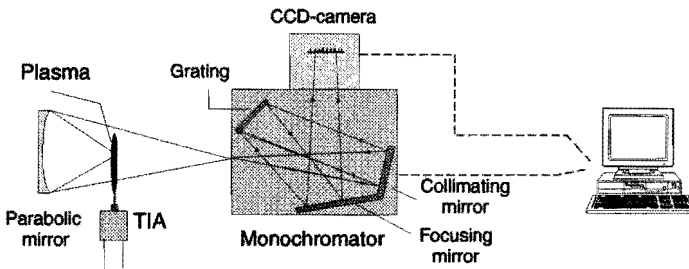


Figure 7. The optical system. The plasma is focused onto the entrance slit of the monochromator using a parabolic mirror. Both the grating inside the monochromator and the CCD-camera are computer-controlled.

### 3.5. Combustion gas sampling

In principal, there are two different methods for analyzing combustion gases with plasma-AES [9]. These methods are based on:

1. Plasma implementation; the plasma is created inside the incinerator oven so that no further gas handling is required.
2. Gas extraction; the gases are extracted from the oven and introduced into a plasma which is created outside the oven. Due to the slight under-pressure that is present in the oven (approximately  $-1 \text{mbar}$ ) a pump will be required.

The first option has to be ruled out: The geometry of the oven does not allow the creation of a plasma jet inside the oven since the oven wall is approximately  $1 \text{m}$  thick whereas the sampling orifice has an inner diameter of only  $2 \text{cm}$ . It is therefore impossible to introduce a plasma device into the oven. Moreover, due to the aggressive medium, the plasma device would be affected within a few hours. Apart from that, it is not to be expected that due to the viscosity of a plasma, incinerator gases easily diffuse into the hot plasma zone. Only with techniques in which plasmas are created within a very short time scale (within a few  $\mu\text{s}$  or  $\text{ns}$ ), such as LIBS, this problem can be avoided. However, as stated in section 1, LIBS suffers from calibration problems due to large plasma gradients and the presence of fly ash. Even if it would be possible to create a plasma inside the oven, a remaining problem is the plasma observation, since only

one small sampling orifice is available. Therefore we had to select the second option: the extraction of the combustion gases from the incinerator oven and introducing them into a plasma.

As far as we know, in literature only gas samplers are reported for end-of-pipe measurements on exhaust gas flows of plants, i.e. the much cleaner and colder gases inside the stack. The most important in these designs is the iso-kinetic sampling [1], a feature that is not relevant in the highly turbulent secondary combustion chamber. However, what is relevant for the sampling of combustion gases is that the medium is extremely aggressive. Because of the extreme high temperatures and acidity at AVR-Chemie, we had to find alternatives for the normal probes which are in use for end-of-pipe analysis. Two different gas sampling methods have been developed and tested:

1. The first method is based on a dilution probe that consists of two parallel placed  $\text{Al}_2\text{O}_3$  tubes that can be inserted through an aperture in the incinerator oven wall. The principle of the dilution probe is based on Bernoulli's theorem (the "Venturi effect", which is also used in nebulizers), cf. figure 8: The incinerator gases are diluted within an incoming argon carrier gas flow [9] and a mixture of both gases is obtained at the outlet of the probe. The dilution process will decrease the partial pressure of the combustion gases so that condensation after cooling may be avoided.

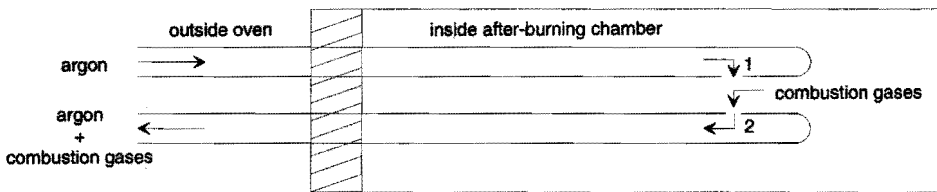


*Figure 8. At the small orifice "1" an expansion in the argon flow is created. Since this creates an under-pressure, incinerator gases are sucked in from the vicinity of the gap. Subsequently, a mixture of argon with incinerator gases is directed towards the plasma through orifice "2".*

2. The second method is based on the creation of a plasma at under-pressure. Due to the pressure gradient produced in this way, combustion gases will be extracted from the oven and introduced into the plasma without the need of a pump between oven and plasma [9].

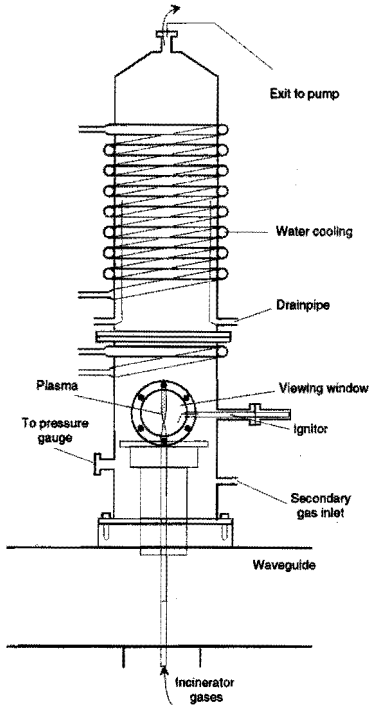


Figure 9. The plasma column used for the creation of plasmas at under-pressure.

For the creation of plasmas at under-pressure, a chimney-like vessel has been constructed (cf. figure 9), which can be mounted on top of the waveguide section of the TIA and evacuated by a vacuum pump. Since the pressure inside the vessel (typically between 950 and 990 mbar) is kept lower than the pressure inside the incinerator oven, combustion gases can be automatically extracted from the incinerator oven and sucked through the nozzle of the inner conductor of the TIA. The stainless steel or alumina sampling line between the incinerator oven and the central pipe of the TIA plasma is heated to approximately 150 °C in order to avoid condensation of the combustion gases. If desired, the combustion gases can be diluted with argon, just before entering the TIA.

With a variable pumping capacity the pressure, and consequently the gas flow, can be controlled.

## 4. Experimental results

### 4.1. General results

Both sampling methods discussed in section 3.5 have been extensively tested at the secondary combustion chamber of AVR-Chemie.

Before using the dilution probe at AVR-Chemie, it had been tested in the laboratory in a wood furnace in order to study the dilution ratio. After several days of testing no instabilities or visible damage to the probe could be observed. However, at AVR-Chemie, the probe suffered from several major disadvantages:

1. The tip of the probe, being exposed to the aggressive medium inside the combustion oven, was subject to a fast vitrification.
2. Obstruction of the down-stream orifice of the probe by fly ash during operation even increased the rate of vitrification and changed the dilution ratio continuously
3. As a result it was difficult to keep the total combustion gas flow constant since the dilution ratio of the argon carrier gas with the combustion gases was variable.

4. The expectation that condensation of the combustion gases would be avoided due to a decrease of the partial pressure was incorrect and a wet aerosol was obtained at the outlet of the second  $\text{Al}_2\text{O}_3$  tube. Possibly part of the heavy metals present in the combustion gases got lost (due to sticking at the wall) in the channel between the incinerator oven and the plasma.

The corrosion processes reduced the lifetime of the dilution probe significantly. Some probes were seriously damaged after a few hours of use only. This is thus in sharp contrast to the laboratory tests in a wood furnace. Apparently it is very difficult to simulate the aggressive conditions present at a waste incinerator plant (e.g. the presence of fly ashes, volatile acids and other pollutants).

Much better results were obtained with plasmas created at under-pressure using the chimney-like column (cf. figure 9) and a heated interface between the incinerator wall and plasma source. This method offered the major advantages that condensation of combustion gases in the sampling line could indeed be avoided and that the gas flow was stable in time and well adjustable. In the case of "hot" sampling, i.e. sampling with the use of heating ribbons, no condensation was observed and a representative sample could be obtained. Particulates present in the combustion gases were introduced into the plasma without noticeable losses and effectively evaporated in the hot medium. In the case of "cold" sampling however, i.e. sampling without a heated interface, condensation precipitated inside the extraction line, affecting the characteristics of the system in time. Therefore all presented measurements were done with a heated sampling line.

A limitation is that argon plasmas created at under-pressure with the use of the CH-nozzle (cf. section 3.3) showed instabilities if relatively large amounts of combustion gases were introduced ( $>0.5 \text{ l}\cdot\text{min}^{-1}$ , i.e. approximately 10%). The use of the CT-nozzle however, resulted in stable plasmas over a large range of experimental conditions ( $P = 300\text{-}1000 \text{ W}$ , gas flow =  $3\text{-}6 \text{ l}\cdot\text{min}^{-1}$ ) that could be created in pure combustion as well. As discussed before in section 3.3, higher power levels cannot be employed using this nozzle, in order to avoid erosion of the tungsten tip.

#### **4.2. Observed elements**

As discussed in section 4.1, best results were obtained from plasmas created at under-pressure using a CT-nozzle and the plasma column. Despite the extreme measurement conditions and the aggressive medium, which had to be analyzed, the analysis system operated stable for a long period (a few weeks), in which it had been used several hours per day. Presented results hence are obtained from this type of discharges.

A part of a typical spectrum measured from a discharge in pure combustion gases is given in figure 10. Many atomic lines and molecular bands can be distinguished in the shown spectral range between 340 and 425 nm. It should be noted that the CCD camera is over-exposed at several spectral ranges due to intense molecular or atomic radiation.

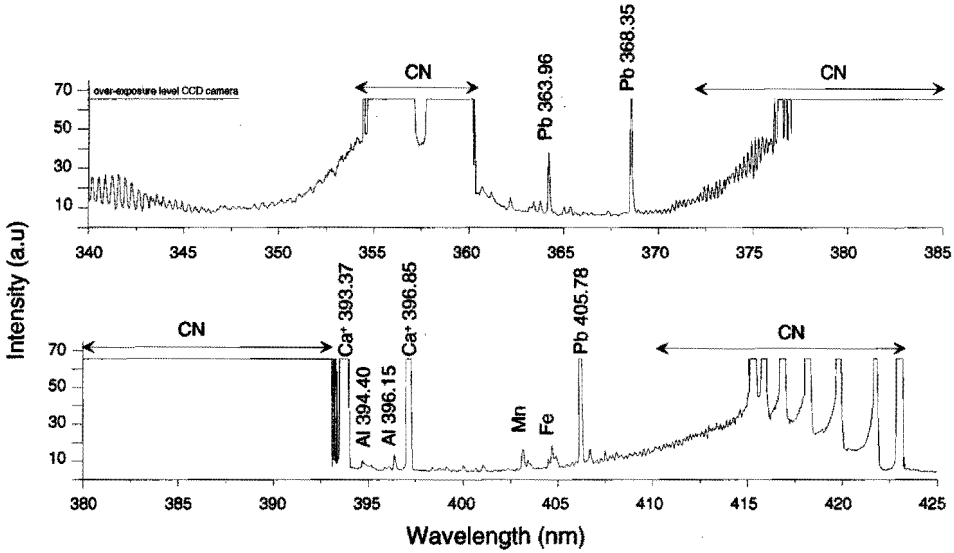


Figure 10. A part of a typical spectrum as measured from a discharge in pure combustion gases (at an under-pressure of -10 mbar). The absorbed microwave power was 600 W and the measurement was done at app. 10 mm above the CT-nozzle. It should be noted that molecular bands cover a considerable part of the shown spectral range.

The elements that have been identified unambiguously and their corresponding strongest emission lines are given in figure 11. The underlined wavelength represents the line that can best be used for monitoring, taking into account its strength and the absence of interference with other lines or bands. Several elements, such as oxygen, could not be detected due to the operating range of the monochromator ( $\lambda < 600$  nm).

Element	Wavelength (nm)	Ionization State	Monitoring Line
Al	394.40 (I)		<u>396.15 (I)</u>
Ba	<u>455.40 (II)</u>		493.41 (II)
C	<u>193.09 (I)</u>		247.86 (I)
Ca	393.37 (II)		<u>396.85 (II)</u>
Cr	<u>425.44 (I)</u>		427.48 (I)
Cu <sup>+</sup>	<u>324.75 (I)</u>		327.40 (I)
Fe	248.33 (I)		371.99 (I)
Mg	<u>285.21 (I)</u>		516.73 (I)
Mn	<u>403.08 (I)</u>		403.31 (I)
Na	<u>589.00 (I)</u>		589.59 (I)
Pb	363.96 (I)		368.35 (I)
Si	250.69 (I)		251.61 (I)
Ti	399.86 (I)		252.41 (I)
W <sup>+</sup>	272.44 (I)		<u>400.88 (I)</u>
Zn	202.55 (II)		<u>206.20 (II)</u>
			<u>213.86 (I)</u>

detected at AVR-Chemie	
1 H	2 He
3 Li	4 Be
5 B	6 C
7 N	8 O
9 F	10 Ne
11 Na	12 Mg
13 Al	14 Si
15 P	16 S
17 Cl	18 Ar
19 K	20 Ca
21 Sc	22 Ti
23 V	24 Cr
25 Mn	26 Fe
27 Co	28 Ni
29 Cu	30 Zn
31 Ga	32 Ge
33 As	34 Se
35 Br	36 Kr
37 Rb	38 Sr
39 Y	40 Zr
41 Nb	42 Mo
43 Tc	44 Ru
45 Rh	46 Pd
47 Ag	48 Cd
49 In	50 Sn
51 Sb	52 Te
53 I	54 Xe
55 Cs	56 Ba
57 La	58 Ce-Lu
59 Pr	60 Nd
61 Pm	62 Sm
63 Eu	64 Gd
65 Tb	66 Dy
67 Ho	68 Er
69 Tm	70 Yb
71 Lu	72 Hf
73 Ta	74 W
75 Re	76 Os
77 Ir	78 Pt
79 Au	80 Hg
81 Tl	82 Pb
83 Bi	84 Po
85 At	86 Rn
87 Fr	88 Ra
89 Ac	90-103 Th-Lr
104 Uuq	105 Uup
106 Uuh	

Figure 11. An overview of the elements observed at AVR-Chemie, together with their strongest emission lines (in nm). Atomic lines are labeled with "I" and ionic with "II". Emission lines that can best be used for monitoring are underlined. († probably originating from eroding nozzle)



The list of detected elements has been compared to the composition of fly ash that was collected at the waste incinerator plant as well [9]. Although the fly ash, being analyzed by a laboratory sieve analysis, was collected during another period and at a different location, it provided a global impression of the abundance of present elements. All elements detected by AES were found to be highly abundant in the fly ashes ( $> 2$  mg/g). Halogens, like Br, Cl and F, were not detected by emission spectroscopy although they were found to be highly abundant in the fly ash as well. It is well known from ICP-AES that a helium plasma is required for the detection of these elements [10], since their radiative levels are hardly populated in an argon or air plasma.

It should be noted that, although not yet determined, detection limits for elements present in combustion gases will be rather poor compared to the detection limits as achieved with ICP-AES for aerosol analysis. Argon ICP-AES normally features a high accuracy, very low detection and linearity over several orders of magnitude for aqueous aerosol analysis. This has its origins in the voluminous argon plasma and a restricted sample injection, outside of the active zone of the plasma. In the case of the TIA, the carrier gas and analyte are mixed before entering the plasma and consequently, the analyte has a strong impact on the plasma properties. Laboratory measurements have shown that in TIA plasmas detection limits of most heavy metals in aerosols are around 1 ppm level [26], substantially worse than most ICP-AES systems. Therefore, it can be expected that the detection limits of the combustion gas monitoring system, are rather poor and worse than those for ICPs reported by other authors who focused on the analysis of cleaned end-of-pipe gases. On the other hand, their systems do not benefit from a very compact and modular set-up and moreover, very likely are not suitable for the extreme conditions as can be expected when monitoring incinerator processes for process control, which is the purpose of our work (cf. section 1 and 2).

Since only very short measurement times are necessary for the detection of the elements listed in figure 11 (or even allowed in order avoiding over-exposure of the CCD-camera), the system can be used very well for continuous gas monitoring of those elements. The measurement time is almost entirely determined by the data transfer from the camera to the computer (approximately 5 s per frame). The analysis of the spectra requires more time but can be performed afterwards since they are stored on a computer. However, if desirable, software can be developed that provides a full automatic (on-line) data-acquisition and analysis.

### ***4.3. Molecular interference***

In the measured spectra several molecular bands are dominantly present, as for example can be seen from figure 10. The vast majority of these bands originate from molecular association products that are created in the plasma [23,27]. The observed molecular transitions are listed in table 1, including the wavelength ranges in which the most intense emission bands appear. Molecular transitions labeled as "intense" or "very intense" create such a strong spectral background that the corresponding wavelength ranges cannot be used for AES due to the over-exposure of the CCD camera.

Molecule	Name system	Transition	Spectra (nm)	Relative strength
CN	Violet system	$B^2\Sigma \rightarrow A^2\Pi$	335-360	very intense
			373-389	very intense
			410-422	very intense
			450-460	very weak
NH	3360 Å system	$A^3\Pi \rightarrow X^3\Sigma$	326-338	intense
N <sub>2</sub>	First positive system	$B^3\Pi \rightarrow A^3\Sigma$	503-600	very weak <sup>‡</sup>
	Second positive system	$C^3\Pi \rightarrow B^3\Pi$	290-298	intense <sup>‡</sup>
N <sub>2</sub> <sup>+</sup>	first negative system	$B^2\Sigma_u^+ \rightarrow X^2\Sigma_g^+$	330-500	weak <sup>‡</sup>
			380-392	weak <sup>‡</sup>
			420-428	very weak <sup>‡</sup>
NO	γ system	$A^2\Sigma^+ \rightarrow X^2\Pi$	190-280	weak
OH	3064 Ångström system	$A^2\Sigma \rightarrow X^2\Pi$	260-297	very weak
			306-324	intense

<sup>‡</sup> Only present in air plasmas. After introduction of incinerator gases these bands disappear, possibly due to the presence of water.

*Table 1. List of the observed molecules, including the wavelength ranges with their most intense emission bands. Some of these molecules can be observed in the spectrum shown in figure 10.*

In the spectrum of figure 10 it can be seen that the intensities of the shown Al lines are a few orders of magnitude weaker than the Ca<sup>+</sup> lines and the CN band. Atomic lines in different wavelength intervals with comparable weak intensities might easily be lost in the molecular bands given in table 1, even if they are indicated as being "weak" or "very weak". Therefore it is important to reduce the intensities of these bands to a minimum. It is observed that spectra from pure combustion gas plasmas have a very high molecular background. This background can be reduced by the addition of a considerable amount of argon. Probably the argon metastables or ions effectively quench the diatomic species. Experimentally it is found that the best results are obtained if approximately 2 l·min<sup>-1</sup> of combustion gases and 3 l·min<sup>-1</sup> of argon are used. However, it should be noted that this mixture still contains much more molecular sample gases, than the amount that could be introduced into the ICP without deteriorating the analyte signal (cf. section 3.2).

#### 4.4. Towards quantitative measurements

The presented measurements are not yet quantitative and hitherto the measurement system can only be used to follow relative fluctuations in the gas composition in time. To enhance process control, quantitative measurements would be desirable. A major possible error source for quantitative measurements is related to the loss of particulates during the gas extraction. Heating of the joint between incinerator oven and plasma torch can minimize this loss.

However, even if the gases can be extracted without losses and if we assume that the particulates are totally evaporated inside the plasma, several other problems remain.

In contrast to liquid analysis, where calibration is rather straightforward, calibration of combustion gas analysis is quite complex, mainly because gaseous standards containing all relevant elements are not yet available. Probably a gaseous standard, preferably air or argon, containing one element can be used. For some elements these standards are commercially available. Knowledge of relevant excitation energies, excitation mechanisms, transition probabilities and the electron temperature can provide a relationship between the measured emission of the calibration standard and the concentration of the elements in the combustion gases. One step further is a completely standard-less calibration. For such a standard-less calibration a thorough understanding of plasma properties will be required. Apart from practical problems such as the difficulties of the "on-line" determining of parameters as electron density and temperature and the gas temperature, it will be difficult to take into account the matrix effects of the so-called easy ionizable elements. Especially the highly abundant element sodium ( $\approx 20$  mg/g in fly ashes, cf. section 4.2) will largely influence the argon or air plasma. If combustion gases are introduced into an argon plasma, the plasma color becomes yellow due to the extremely intense sodium  $3s^2S \rightarrow 3p^2P_0$  doublet at 589.0 and 589.6 nm. Since the excitation energy from the ground state towards the radiating level is only 2.1 eV, the electron energy distribution function can be severely affected. It is obvious that this influences the population of excited states of other elements as well. As an example, it is observed that intensities of argon lines significantly decrease, or even vanish, if large amounts of sample gas with high sodium concentrations are introduced. Therefore, it can be expected that for accurate quantitative measurements, one should work with relatively low combustion gas flows compared to the argon carrier gas flow.

## 5. Discussion

It is shown that plasma-AES can be used for the on-line monitoring of several elements which are highly abundant in combustion gases. Main goal was to construct a compact measurement system capable to withstand extreme gas conditions as present above an oven of hazardous waste incinerator plant (high temperature, high acidity, the presence of fly ashes and volatile compounds), rather than to achieve low detection limits, which usually is the merit of other research groups. With the built analysis system several heavy metals, such as Zn, Fe and Pb, could easily be monitored continuously, so that the system is usable for process control. After the extraction from the incinerator oven, the gases were dissociated and its constituents excited in a microwave-induced plasma produced by the "Torche à Injection Axiale" (TIA). Atomic emission spectroscopy finally provided information about the present metals. The torch was used as excitation source because plasmas created by the TIA could resist high concentrations of molecular gases and changing gas compositions.

The best results were obtained with discharges created at under-pressure in a mixture of flue gases and argon. Plasmas created at under-pressure enabled the use of a very short heated

sampling line between incinerator and plasma, so particle losses during the sampling will be minimal. The addition of argon reduced the intensity of molecular bands, which otherwise easily overgrow weak atomic lines, and has the advantage that plasma parameters such as the electron density and temperature are less sensitive to changing concentrations of easy ionizable elements (e.g. Na).

Hitherto, measurements provided relative results only. For quantitative analysis, a calibration technique has to be found to overcome this gap. Due to the lack of good calibration standards, the presence of dust particles and a high concentration of easy ionizable elements in combustion gases, it will not be easy to achieve an accurate calibration method and more insight in fundamental plasma processes will be demanded.

## Acknowledgements

The authors would like to thank AVR-Chemie and the Dutch Technology Foundation STW for their financial support and in particular W.J. van de Guchte (AVR-Chemie) for his assistance during the measurements at the incinerator site and J. Verwoerd (AVR-Chemie) for reviewing this paper. The authors furthermore would like to thank A.B.M. Hüsken, H.M.M. de Jong, G. ter Plegt and M.J.F. van de Sande for their technical assistance and A. Boekkooi for his fruitful discussions.

## References

1. G.A. Meyer and M. Seltzer, *International Laboratory*, March **10E** (1997).
2. G.A. Meyer and R. Barnes, *Spectrochim. Acta* **40B**, 893 (1985).
3. C. Trassy and R. Diemiaszonek, *High Temp. Chem. Proc.* **3**, 449 (1994).
4. C. Trassy and R. Diemiaszonek, *J. Analyt. At. Spectrom.* **10**, 661 (1995).
5. C. Trassy, *Spectroscopy Europe* **8/1**, 20 (1996).
6. D. Nore, A.M. Gomes, J. Bacri and J. Cabe, *Spectrochim. Acta* **48B**, 1411 (1993).
7. L.W. Peng, W.L. Flower, K.R. Hencken, H.A. Johnsen, R.F. Renzi and N.B. French, *Process Control and Quality* **7**, 39 (1995).
8. H. Zhang, J.P. Singh, F.Y. Yueh and R.L. Cook, *Appl. Spectrosc.* **49**, 1617 (1995).
9. E.A.H. Timmermans, "Design of a continuous gas analyzer based on MIP-AES for the on-line monitoring of metallic compounds in flue gases", dissertation 2-year post-graduate program of "Physical Instrumentation" at the Center of Technological Design, ISBN 90-5282-770-2 (1997).
10. A. Montaser and D.W. Golightly, *Inductively coupled plasmas in analytical atomic spectrometry*, second edition VCH Publishers, Inc., New York (1992).
11. P.W.J.M. Bouwmans, "Inductively Coupled Plasma Emission Spectroscopy", part I & II, John Wiley & Sons, USA (1984).
12. R.H. Scott, V.A. Fassel, R.N. Kniseley and D.E. Nixon, *Anal. Chem.* **46**, 75 (1974).
13. Q. Jin, Y. Duan and J. Olivares, *Spectrochim. Acta* **52B**, 131 (1979).

14. M. Moisan, Z. Zakrewski and R. Pantel, *J. Phys. D: Appl. Phys.* **12**, 219 (1979).
15. M. Moisan and J. Pelletier, "Microwave Excitation Plasmas" (Chap.V), Elsevier Science Publish. B.V., Amsterdam, The Netherlands (1992).
16. J. Hubert, M. Moisan and A. Ricard, *Spectrochim. Acta* **34B**, 1 (1979).
17. C.I.M. Beenakker, *Spectrochim. Acta* **31B**, 173 (1977).
18. H. Matusiewicz, *Spectrochim. Acta* **47B**, 1221 (1992).
19. Q. Jin, C.Zhu, M.Borer and G.Hieftje, *Spectrochimica Acta* **46B**, 417 (1991).
20. M. Moisan, G. Sauvé, Z. Zakrewski and J. Hubert, *Plasma Sources, Sci. and Techn.* **3**, 584 (1994).
21. A. Ricard, L. St-Onge, H. Malvos, A. Gicquel, J. Hubert and M. Moisan, *J. Phys. III France* **5**, 1269 (1995).
22. E.A.H. Timmermans, I.A.J. Thomas, J. Jonkers, J.A.M. van der Mullen and D.C. Schram, *Fresenius J. Anal. Chem.* **362-5**, 440 (1998).
23. Chapter 4 of this thesis, E.A.H. Timmermans, J. Jonkers, I.A.J. Thomas, A. Rodero, M.C. Quintero, A. Sola, A. Gamero, and J.A.M. van der Mullen, *Spectrochim. Acta* **53B** 1553-1566 (1998).
24. J. Jonkers, H.P.C. Vos, J.A.M. van der Mullen and E.A.H. Timmermans, *Spectrochim. Acta* **51B**, 457 (1996).
25. J. Jonkers, L.J.M. Selen, J.A.M. van der Mullen, J. van Dijk, E.A.H. Timmermans and D.C. Schram, *Plasma Sources, Sci. and Technol.* **6**, 533 (1997).
26. Chapter 2 of this thesis, E.A.H. Timmermans, I.A.J. Thomas, J.A.M. van der Mullen and D.C. Schram, "Spectrochemical characteristics of microwave induced plasma torches", to be submitted for publication (1999).
27. C. Truitt and J.W. Robinson, *Anal. Chim. Acta* **51**, 61 (1970).

# 4

## The behavior of molecules in microwave induced plasmas studied by optical emission spectroscopy: 1. plasmas at atmospheric pressure

*E.A.H. Timmermans, J. Jonkers, I.A.J. Thomas, A. Roderó<sup>(†)</sup>,  
M.C. Quintero<sup>(†)</sup>, A. Sola<sup>(†)</sup>, A. Gamero<sup>(†)</sup> and J.A.M. van der Mullen*  
published in *Spectrochim. Acta.* **53B** 1553-1566 (1998).

*(†) Departamento de Física Aplicada, Universidad de Córdoba,  
14071 Córdoba (Spain).*

**SUMMARY** - *The behavior of molecules in different atmospheric microwave induced plasmas (MIPs) has been studied by means of optical emission spectroscopy. This in order to obtain more insight in molecular processes in plasmas and to investigate the feasibility of emission spectroscopy for the analysis of molecular compounds in gases, e.g. flue gases. Various molecular species (i.e. N<sub>2</sub>, CO<sub>2</sub>, H<sub>2</sub>O, SF<sub>6</sub> and SO<sub>2</sub>) have been introduced into discharges in argon or in molecular gases such as carbon dioxide or nitrogen. The plasmas were created and sustained by a guide-surfatron or a torch in the power range of 150 W to 2 kW. Only nitrogen sometimes yielded observable emission from the non-dissociated molecule (first and second positive system). Using other molecular gases, only dissociation and association products were observed (i.e. atomic species and diatomic molecules such as CN, C<sub>2</sub>, OH and NH). The intensities of these products have been studied as a function of the concentration of introduced molecules, the position in the plasma and the composition of the plasma environment. Since in most cases the same diatomic association products are seen, observed associated molecules can only to some extent be related to the molecules originally present in the plasma gas. Therefore it will be difficult to use atmospheric microwave discharges for the analysis of gas mixtures under the studied experimental conditions.*

## 1. Introduction

For years inductively coupled plasmas (ICPs) [1,2] and microwave induced plasmas (MIPs) [3,4] have been used as excitation sources for the determination of elements using atomic emission spectroscopy (AES).

One of the major restrictions of most types of MIPs is their limited evaporation and excitation power of analytes, being a result of a relatively low gas temperature and a short analyte residence time. Therefore, detection limits of elements are usually worse than in case an ICP is used as excitation source. Another limitation of MIPs is the generally intense and broad emission of molecules. Detection limits are reduced even further if lines of the analyte interfere with those bands. These are some of the reasons why ICPs are used more frequently in the spectrochemical analysis of elements than MIPs.

An interesting idea is to use this presence of molecular spectra, being a disadvantage in AES, as a benefit. This paper therefore deals with the analysis of molecular gases instead of atomic species. For molecular gas analysis other plasma conditions than for atomic emission spectroscopy will be required. In an ICP the heavy particle temperature is rather high (typically  $7 \cdot 10^3$  K) and molecules are dissociated almost instantaneously [5]. MIPs on the other hand, have a substantially lower heavy particle temperature and therefore it can be expected that molecular dissociation will be less effective in these plasmas. The rather strong molecular emission spectra also support this expectation. MIPs could therefore be useful for the analysis of molecular gases.

The aim of this paper is to provide a better insight in the molecular processes involved in MIPs. Especially an unambiguous relationship between observed emission and introduced molecules would be of great importance, considering industrial applications as e.g. the on-line monitoring of hazardous molecules in flue gases.

Two field applicators, a torch called "Torche à Injection Axiale" (TIA) [6] and a surface wave plasma launcher called "Guide-Surfatron" (GS) [7], have been used to obtain a widely varying range of plasma conditions (heavy particle temperature  $T_h \approx 1 \cdot 10^3 - 4 \cdot 10^3$  K, electron temperature  $T_e \approx 1 \cdot 10^4 - 2 \cdot 10^4$  K and electron density  $n_e \approx 10^{21} \text{ m}^{-3}$ ).

Line intensities have been used to estimate several plasma parameters for atmospheric argon discharges produced by both field applicators: the electron density (from  $H\beta$  broadening), the rotation temperature (using the 3064 Ångström system of the OH radical) and the excitation temperature (using atomic argon lines).

In order to study the feasibility of both plasma sources as excitation sources for molecular analysis, several experiments based on optical emission spectroscopy (OES) have been carried out. The emission of both atomic and molecular species has been studied after introducing different molecular species (i.e.  $N_2$ ,  $CO_2$ ,  $SF_6$ ,  $H_2O$  and  $SO_2$  or mixtures of these gases) into argon plasma discharges. Argon discharges produced by the TIA in which  $CO_2$  and  $N_2$  are introduced have been studied most intensively. In these plasmas the molecular analyte gases have been introduced with varying concentrations and the emission has been studied at different positions in the plasma. Depending on the used nozzle configuration, discharges in purely molecular gases (i.e. nitrogen and carbon dioxide) could be created with the TIA as well. To study the interaction of the plasma with molecules from the surroundings in which the plasma is created, measurements have been performed on plasmas produced by the TIA expanding into air and carbon dioxide environments. The guide-surfatron has been used to produce confined plasmas which have no interaction with the ambient air.

## 2. Experiments and instrumentation

In order to create a range of plasma conditions, two different plasma sources have been used. With the "torche à injection axiale" (TIA) microwave induced plasmas are created which freely expand into the open air, whereas the guide-surfatron (GS) is used to create capillary plasmas inside a quartz tube. Both plasma sources are shown in figure 1 and will be discussed separately.

The TIA (from "torche à injection axiale", using the nomenclature of the developers, MOISAN *et al.* [6]) produces an atmospheric flame-like argon or air plasma expanding into the open air. Basically, inside the TIA the propagation mode of the incident microwave radiation is converted from the rectangular  $TE_{01}$  into the coaxial TEM mode. Energy is dissipated just above the top of the inner conductor, where the plasma is created. The inner conductor is terminated by a nozzle through which the plasma gas is supplied. Due to its field and flow shaping characteristics, the nozzle design exerts a strong influence on the plasma shape. Three different nozzles have been used:



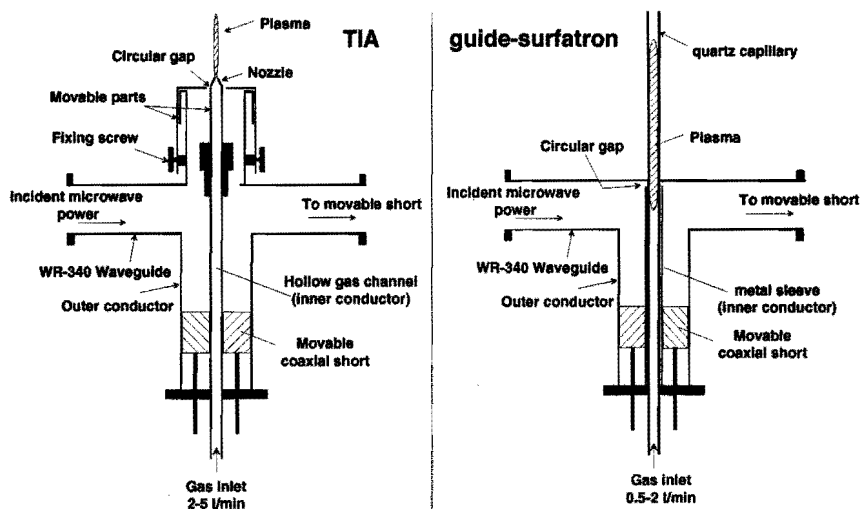


Figure 1. The torche à injection axiale (left) and the guide-surfatron (right). It should be noticed that the TIA can be equipped with different nozzles (cf. figure 2)

- CH: a copper nozzle with gas injection through a central hole (CH) with an inner diameter of 1.8 mm, as proposed by MOISAN *et al.* in their first publication about the TIA [6], cf. figure 2 (left),
- CT: a copper nozzle containing a central closed tip (CT) of tungsten with parallel gas injection, as reported by RICARD *et al.* [8], cf. figure 2 (center). Since the plasma is created on top of this tip, a heat resistant metal like tungsten is necessary.
- HT: a copper nozzle with a central hollow tip (HT) of tantalum ( $\varnothing$  1 mm inner dimensions) and additional parallel gas injection. Gas flows through the inner channel (i.e. through the tip) and the outer channels (i.e. through the surrounding apertures) can be regulated separately, cf. figure 2 (right). The carrier gas and analyte are introduced through the inner tip whereas a shielding gas can be injected through the outer channel. This configuration enables a good analyte penetration into the plasma and reduces entrainment of ambient air. A disadvantage of the currently used design is that it suffers from strong erosion due to a physical contact of the plasma with the tantalum tip. Scale-up of the torch would enable water cooling and could increase the lifetime of the nozzle.

The nozzles will be referred to as the CH, CT and HT nozzle. Due to the geometry and field shaping characteristics of the CT and HT nozzle, discharges in air or other molecular gases can be created. With the CH nozzle noble gases, e.g. argon or helium, have to be used as carrier gas.

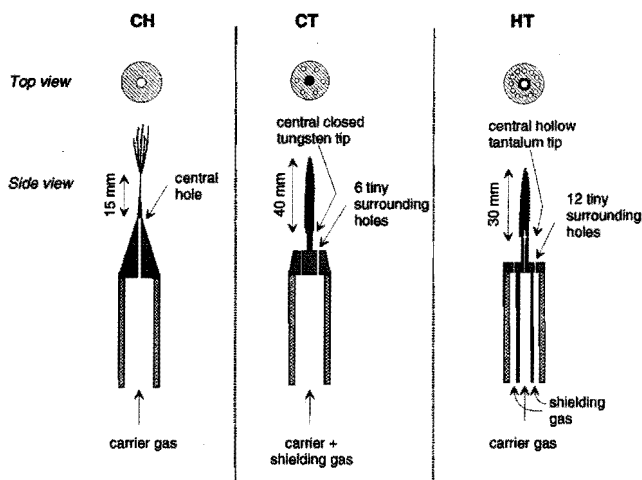


Figure 2. The central hole (CH), closed tip (CT) and hollow tip (HT) nozzle respectively. Due to the geometry and field shaping characteristics of the CT and HT nozzle, discharges in air or other molecular gases can be created. Plasma dimensions depend on the power input and applied gas flow through the nozzle.

The guide-surfatron (GS) [7,9,10], shown in figure 1, creates atmospheric capillary argon surface wave discharges enclosed by a quartz tube with an inner diameter of typically 1.5 mm. Inside the guide-surfatron the propagation mode of the incident microwave radiation is converted from the rectangular  $TE_{01}$  into the coaxial  $TM_{01}$  mode. Since the electromagnetic field of the microwaves propagates along the interface between the quartz tube and the plasma, plasmas can be extended over long distances. In contrast to plasmas created by the TIA, this plasma has no interaction with the ambient air. The use of the fused silica tube limits the applicable HF power to approximately 600 W.

In table 1 the major components of the system are listed. A waveguide structure (WR-340, inner dimensions 86.4×43.2 mm) is used for the energy transfer from the generator to the TIA or the guide-surfatron. All plasmas are created and sustained by 2.45 GHz microwaves.

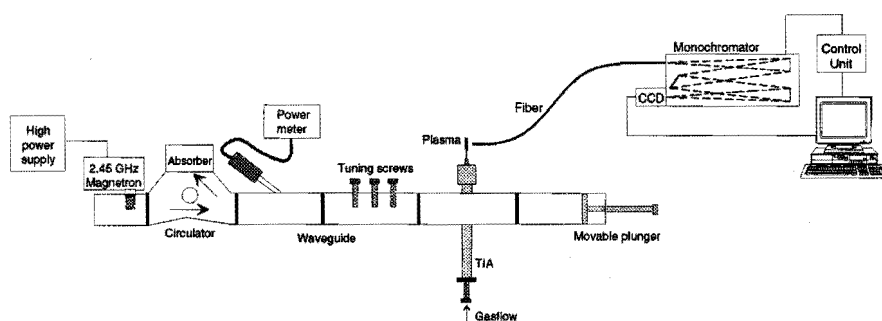
Component	Model	Manufacturer
Magnetron	Philips YJ 1442, 2.45 GHz	Philips
HV power supply	HTN 7000-6500	FUG
Field Applicators	Torche à Injection Axiale	Laboratory built
	Guide-Surfatron	
Monochromators	Monospek 1000, 1200 gr/mm, 420 nm blaze-angle	Jobin Yvon
	Monospek 18, 1200 gr/mm, 500 nm blaze-angle	SMS
CCD camera	ST6-UV	SBIG
Massflow controllers	FC-260 series	Tylan General

Table 1. Instrumental components.

The (simplified) setup in combination with the TIA is shown in figure 3. A triple stub-tuner, movable plungers and tuning elements inside the TIA or GS allow impedance matching and tuning. A circulator prevents the magnetron from being damaged by reflected microwave power.

Gas flows are regulated with mass-flow controllers. In case mixtures of gases are used, mixing is carried out inside a mixing chamber (not shown in figure 3), just before entering the central gas tube of the TIA or the quartz capillary inside the GS.

The emission signal of the plasma is guided through an optical fiber and focused onto the entrance slit (10-13  $\mu\text{m}$ ) of either a 1 meter or a 15.6 cm monochromator (the Monospek 1000 and Monospek 18 respectively). A computer-controlled CCD camera is used to measure the spectra. The camera has been used in the so-called spectroscopic mode, featuring an array of  $750 \times 1$  pixels, each  $11.5 \mu\text{m} \times 6.53 \text{ mm}$  in size.



**Figure 3.** Schematic diagram in which the TIA is used to create a freely expanding plasma. The emission signal of the plasma is guided through an optical fiber and focused onto the entrance slit of a monochromator. Spectra are acquired with a CCD camera. Basically the same setup is used for GS experiments.

Table 2 shows some typical operating conditions for both plasma sources. The given plasma lengths are for pure argon plasmas. It should be realized that (especially for the GS) these lengths are strongly dependent on the composition of the gas mixture and the applied power.

	TIA	Guide-surfatron
Power input P (W)	150-2000	150-600
Carrier gas	argon, air, N <sub>2</sub> , CO <sub>2</sub>	argon
Max. concentration molecular gases (%)	100	15
Gas flow (l·min <sup>-1</sup> )	2-6	0.5-2
Confinement	open air	quartz tube
Plasma length L <sub>pl</sub> (cm)	3-6	10-25

**Table 2.** Typical operating conditions of the two field applicators.

The electron density, the excitation temperature and the rotation temperature have been determined for argon plasmas (containing molecular impurities) under normal operating conditions. The electron density  $n_e$  is calculated from the broadening of  $H_\beta$  (at 486.132 nm), using data from CZERNIKOWSKI *et al.* [11]. The excitation temperature  $T_{exc}$  is deduced from a Boltzmann-plot of several argon lines, using statistical weights and transition probabilities from WIESE *et al.* [12]. Similar, the rotational temperature  $T_{rot}$  is found from the rotational distribution of emission lines from the 3064 Ångström system of OH, using data from DIEKE *et al.* [13]. The OH emission is due to impurities of  $H_2O$  in the argon gas.  $T_{exc}$  is often regarded as a lower limit of the electron temperature  $T_e$ , while  $T_{rot}$  is regarded as an indication for the heavy particle temperature  $T_h$ . It should be noticed that the data are not Abel-inverted and that MOUSSOUNDA *et al.* [14] have shown that OH emission in a surfatron discharge mainly appears from the outer region of the plasma. For confined plasmas created by the guide-surfatron  $T_{rot}$  therefore might be a good indication for the heavy particle temperature in the outer region of the plasma. Since plasmas produced by the TIA and the GS show very steep gradients in temperatures and electron densities,  $T_{rot}$  should be measured with a very high spatial resolution in order to obtain reliable radially resolved results. Emission of  $N_2^+$ , which might provide information about  $T_{rot}$  in the center of the plasma [14], was too weak for the determination of the rotational temperature.

Since the spectral resolving power restricts the accuracy of the rotational temperature as obtained by the slope of Boltzmann plots, spectra have been simulated as well. Also in this case the wavelengths and transition probabilities have been taken from DIEKE *et al.* [16]. Simulations are found to be in good agreement with the Boltzmann plot method and reduced the possible error margins to within a few hundred Kelvin. As an example a measured and calculated spectrum are shown in figure 4.

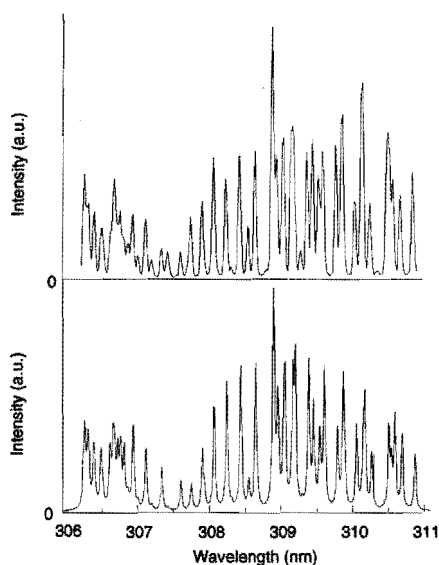


Figure 4.

Examples of a measured (above) and a calculated spectrum (below) of the OH radical (3064 Ångström system of OH,  $A^2\Sigma^+ \rightarrow X^2\Pi$ ). The measured spectrum is taken from an argon discharge produced by the GS ( $P=100$  W,  $[Ar]=0.25$  l·min<sup>-1</sup>). The reasonable good agreement between both spectra should be noted. The rotational temperature used for the simulated spectrum is  $T_{rot}=1100$  K.

### 3. Results and discussion

#### 3.1. Characteristics of argon plasmas created by the TIA and the GS

In order to compare plasmas produced by the TIA and the guide-surfatron,  $T_{rot}$ ,  $T_{exc}$  and  $n_e$  have been determined experimentally. Typical parameters found for argon plasmas created by the TIA are  $T_{rot} \approx 3 \cdot 10^3$  K,  $T_{exc} \approx 5.5 \cdot 10^3$  K and  $n_e \approx 10^{21}$  m<sup>-3</sup>. These values are obtained just above the CH nozzle using an argon flow [Ar]=3 l·min<sup>-1</sup> and a power input P=320 W leading to a plasma with a length of  $L_{pl} \approx 5$  cm. The obtained  $T_{exc} \approx 5.5 \cdot 10^3$  K is significantly lower than the electron temperatures reported by JONKERS *et al.* [15,16], showing that plasmas produced by the TIA are far from Boltzmann- or Saha-equilibrium. The Thomson scattering experiments reported in [15,16] give electron temperatures between  $1.7 \cdot 10^4$  and  $2.5 \cdot 10^4$  K for argon plasmas produced by the TIA under comparable experimental conditions. Therefore  $T_{exc}$  cannot be identified as the electron temperature [17].

Measurements performed on plasmas produced by the guide-surfatron reveal that for a "pure" argon plasma  $T_{exc} \approx 5.2 \cdot 10^3$  K,  $T_{rot} \approx 1.7 \cdot 10^3$  K and  $n_e \approx 4 \cdot 10^{20}$  m<sup>-3</sup>. It should be noted that both  $T_{rot}$  and  $n_e$  are lower than for the TIA plasma but that  $T_{exc}$  is comparable. These are typical values close to the guide-surfatron gap (the energy transfer zone) and decrease slowly towards the end of the plasma column. The given values are obtained for a HF power input P=150 W, an argon flux [Ar]=1 l·min<sup>-1</sup> and a quartz tube inner radius  $r_i=1$  mm, leading to a plasma length  $L_{pl} \approx 12$  cm.

#### 3.2. TIA spectra for different molecular analyte gases

To study the feasibility of the use of the TIA for detection of molecules, experiments with various molecular gases (i.e. N<sub>2</sub>, CO<sub>2</sub>, H<sub>2</sub>O and SF<sub>6</sub> and mixtures) have been performed. The emission spectra have been studied after the introduction of these molecular gases into argon plasmas produced by TIA using the CH nozzle. Figure 5 shows a typical spectrum of an argon plasma in which small amounts of CO<sub>2</sub> and N<sub>2</sub> have been introduced (0.30 and 0.030 l·min<sup>-1</sup> respectively, compared to 4.0 l·min<sup>-1</sup> of argon). It is remarkable that emission of the original analyte gases CO<sub>2</sub> and N<sub>2</sub> (which have dissociation energies of  $E_{dis}=5.45$  and 9.76 eV respectively) cannot be observed in the spectrum. Instead, ionic molecular nitrogen, atomic lines (Ar, C, N, O and H) and several association products (CN, C<sub>2</sub>, NH and OH) can be seen. In the far UV, beyond the shown wavelength range, the  $\gamma$  system of NO is found to be fairly present as well.

However, by far the most intense is emission of CN. It should be noted that the band head of the violet system of CN at 388.34 nm ( $B^2\Sigma \rightarrow A^2\Pi$  (0,0)) strongly exceeds the depicted intensity range in the graph. The strong emission from CN can still be observed if only CO<sub>2</sub> is injected, suggesting a high inward diffusion rate of N<sub>2</sub> from the ambient air into the plasma. This is in agreement with a previous paper of JONKERS *et al.* about the influence of ambient air [16].

The OH radical arises from the dissociation of H<sub>2</sub>O, which is always present at trace level as a contamination in argon or as water vapor in the ambient air.

Excited diatomic association molecules are most likely created by 3-body association:



In this reaction the heavy particles A and B associate in the presence of a spectator S.

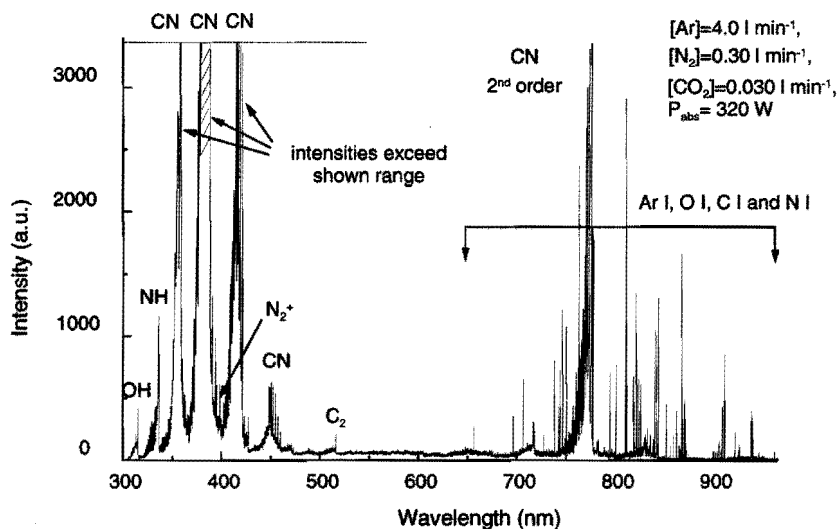
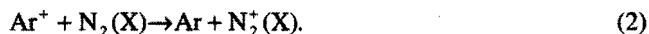
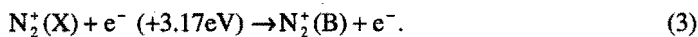


Figure 5. Emission spectrum between 300 and 965 nm of an argon plasma sustained by the TIA in which small amounts of CO<sub>2</sub> and N<sub>2</sub> are introduced, measured at 1 cm above the nozzle. The spectrum is dominated by emission of association products. The CCD camera is strongly over-exposed at those wavelengths where the band heads of the violet system of CN are present. It should be noted that there is no emission from CO nor from the original analytes CO<sub>2</sub> and N<sub>2</sub>.

Emission of CO or CO<sub>2</sub> has never been observed after the introduction of CO<sub>2</sub> into an argon TIA discharge, despite the wide range of experimental conditions ([Ar]=1-6 l·min<sup>-1</sup>, P=0.15-2.0 kW). Introduction of N<sub>2</sub> sometimes yields emission of the first and second positive system of the N<sub>2</sub> molecule, especially of the  $\Delta v=0$  and  $\Delta v=-1$  transitions. The reproducibility of spectra showing the first and second positive system however, is rather limited and normally emission of the first negative system of the molecular ion N<sub>2</sub><sup>+</sup> (B<sup>2</sup>Σ<sub>u</sub><sup>+</sup> → X<sup>2</sup>Σ<sub>g</sub><sup>-</sup>) is much more intense. Especially when no additional CO<sub>2</sub> is introduced, emission of this system is very dominant. This strong emission might indicate that deliberately introduced nitrogen or nitrogen introduced from the ambient air is involved in the charge transfer (CT) reaction:



The charge transfer given by Eqn 2 is quasi-resonant due to the comparable ionization energies for argon and molecular nitrogen (E<sub>i</sub>=15.76 and 15.58 eV respectively). The ground state N<sub>2</sub><sup>+</sup> molecules created in this reaction can be excited towards the B<sup>2</sup>Σ<sub>u</sub><sup>+</sup> state by electron impact, for which only 3.17 eV is needed:



Radiative decay towards the molecular ion ground state will generate spectra of the so-called "first negative system" of  $\text{N}_2^+$ , cf. figure 6.

A possible destruction channel for molecular nitrogen ions is the dissociative recombination reaction (DR), given by:



This reaction could provide the nitrogen atoms that are needed for association reactions as the production of CN and NH. At least one of the nitrogen atoms created in the dissociative recombination process is in the  $^2\text{D}^0$  or  $^2\text{P}^0$  level. Dissociation leading to the ground state limit of both nitrogen neutrals ( $^4\text{S}^0$  and  $^4\text{S}^0$ ) is not expected to play any role [18,19]. The creation of excited nitrogen atoms due to dissociative recombination of  $\text{N}_2^+$  is supported by the observed strong emission lines of atomic nitrogen.

The second positive system of  $\text{N}_2$  ( $\text{C}^3\Pi \rightarrow \text{B}^3\Pi$ ) which is sometimes observed is probably due to excitation transfer (ET) from argon metastables towards ground state molecular nitrogen and due to the association of the nitrogen atoms created by the dissociative recombination of  $\text{N}_2^+$ , cf. figure 6 [20].

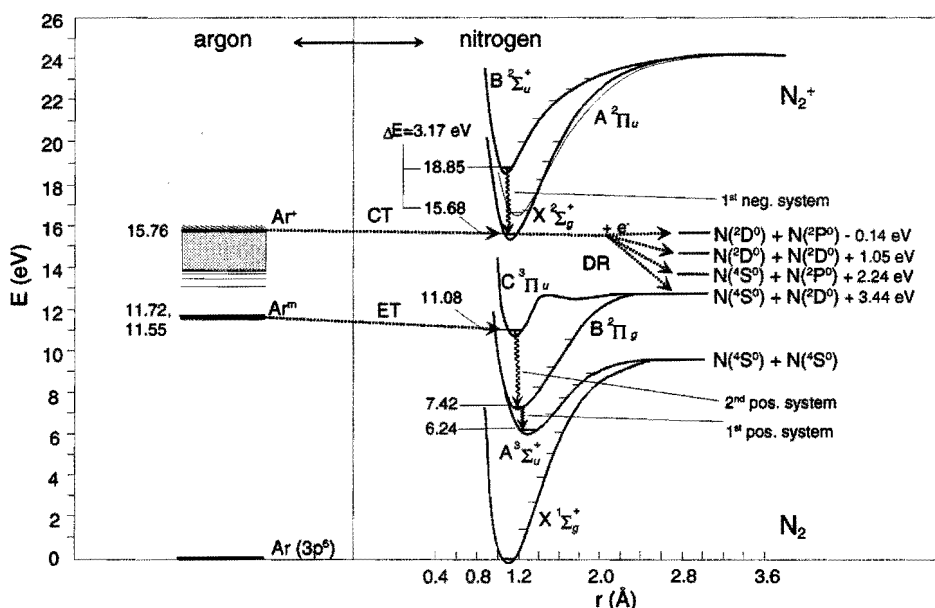


Figure 6. Energy diagrams of argon and the nitrogen molecule compared. Possible charge transfer (CT), excitation transfer (ET) and dissociative recombination (DR) processes are depicted in the figure. On the right the energy levels of the separated neutral nitrogen atoms are shown. The energies given along with the separated atoms represent the kinetic energy releases involved in the dissociative recombination of  $\text{N}_2^+$ .

Measurements with the molecular species SF<sub>6</sub> and H<sub>2</sub>O have been performed in order to investigate whether these molecules are dissociated as well (P=0.5-1.5 kW, [Ar]=2-4 l·min<sup>-1</sup>). Introduction of SF<sub>6</sub> into argon discharges did not lead to emission spectra of molecules containing S or F atoms. Instead, several emission lines of S I were clearly observable (most intense lines at 921.3, 922.8 and 923.8 nm), especially at high powers, indicating that this molecule is at least partly dissociated. Experiments with water injection only resulted in strong OH and atomic oxygen and hydrogen emission. It is not clear whether the OH radical is a dissociation product of water or due to three-body association processes of atomic oxygen, hydrogen and a spectator, cf. Eqn 1.

In order to investigate the influence of the argon carrier gas, also measurements with purely molecular gases have been performed. This can be done using the CT or HT nozzle. It is found that stable discharges in N<sub>2</sub>, CO<sub>2</sub> and air can be sustained when P>300 W and the gas flow exceeds 2 l·min<sup>-1</sup> (to ensure a sufficient cooling of the tip). However, comparable to the argon plasmas produced with the CH nozzle, only emission from dissociation and association products can be seen, again with an exception for nitrogen.

From a discharge in pure CO<sub>2</sub> expanding into the ambient air (using the CT nozzle), very intense emission of CN can be observed. Furthermore, atomic carbon and oxygen lines (most intense lines at 247.9 and the triplet around 777 nm respectively) and NO bands (210-270 nm) are present. Emission from the Swan System of C<sub>2</sub> can hardly be observed, despite the large amount of C atoms present in the discharge.

When the HT nozzle is used, the same diatomic molecules can be observed. The main difference with the CT nozzle is that emission from CN bands can be decreased if argon is used as shielding gas and consequently contact with the ambient air is reduced. Furthermore, the central sample injection ensures a good penetration of the analyte into the plasma. This nozzle therefore is probably most suitable for atomic emission spectroscopy, which however is not the topic of this study. For molecular gas analysis however, also the studied plasmas produced by the HT nozzle have their limitations due to dissociation and association processes.

As a preliminary result we can state that from the four studied molecular gases (CO<sub>2</sub>, N<sub>2</sub>, SF<sub>6</sub> and H<sub>2</sub>O), only nitrogen sometimes has yielded emission of the non-dissociated molecule. It is not likely however, that the detection of nitrogen will have practical applications with respect to molecular gas analysis. Moreover, due to the broad and sometimes strong emission bands, the first and second positive system might easily overgrow weaker bands of other molecules. This is not a favorable perspective since N<sub>2</sub> is present in many molecular gas samples, e.g. in flue gases.

Although emission of CO<sub>2</sub> itself cannot be observed, detection is maybe possible indirectly, e.g. via CN or C I<sup>a</sup> emission. Therefore experiments have been done in which the concentration of CO<sub>2</sub> has been varied systematically (cf. section 3.3).

---

<sup>a</sup> "I" refers to the atomic system. Ion lines ("II") are not observed for Ar, C, O, N or other atomic species.



### 3.3. TIA spectra for different CO<sub>2</sub> flows

In this section the influence of a varying amount of carbon dioxide introduced into discharges produced by the TIA is discussed. In figure 7 the intensities of several atomic and molecular species are depicted as a function of the amount of CO<sub>2</sub> injected into an Ar/N<sub>2</sub> plasma. Intensities have been scaled to unity for the measurement performed with the smallest amount of CO<sub>2</sub> injection ( $2.3 \cdot 10^{-2} \text{ l} \cdot \text{min}^{-1}$  versus  $3.0 \text{ l} \cdot \text{min}^{-1}$  of argon and  $0.05 \text{ l} \cdot \text{min}^{-1}$  of nitrogen). It should be noted that the growth of O I is significantly less than the growth of C I or CN (band head  $B^2\Sigma \rightarrow A^2\Pi (0,0)$ ) and that N I and NH (band head  $A^3\Pi \rightarrow X^3\Pi (1,1)$ ) decrease if the CO<sub>2</sub> increases. The decrease of N I and NH, which is accompanied by an increasing rate of CN association, shows that the introduction of C-atoms (via CO<sub>2</sub>) forces a significant part of the present nitrogen atoms into a CN bond. The question is what happens with the two oxygen atoms created after the complete dissociation of a CO<sub>2</sub> molecule. The figure shows an increase of the O I emission. The fact that this increase is rather small can be explained by an increasing rate of NO association. Another reason for the only moderate increase of O I emission might be the high excitation level of the observed oxygen line (12.08 eV). The excitation energy of the observed carbon line on the other hand, is only 9.00 eV. Introduction of molecules will affect the electron energy distribution function (EEDF) and reduce the number of fast electrons and consequently the population rate of levels with high excitation energy by electron impact.

One can observe that the increase of all species is (far) less than proportional. This might also be related the loss of fast electrons. The excitation power of the plasma decreases due to energy losses involved in dissociation processes. It therefore can be concluded that also the indirect detection of CO<sub>2</sub>, i.e. by monitoring dissociation or association products, will be difficult as well.

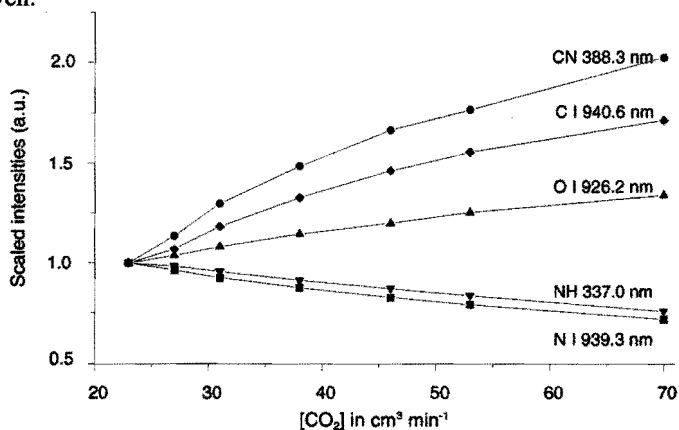


Figure 7. The intensity of several atomic and molecular species as a function of the amount of CO<sub>2</sub> added to the argon/nitrogen mixture ( $[Ar]=3.0 \text{ l} \cdot \text{min}^{-1}$ ,  $[N_2]=0.05 \text{ l} \cdot \text{min}^{-1}$ ,  $P=320 \text{ W}$ ). Measurements are performed at 1 cm above the nozzle.

### 3.4. TIA spectra at different heights in the plasma

The emission of dissociation and association products has been studied at different positions in the plasma. In figure 8 the intensities of several emission lines from an argon discharge in which a constant amount of carbon dioxide is introduced, are given as a function of the height above the nozzle. Maximal intensities are scaled to unity. In the active zone (approximately the first 10 mm above the nozzle), it can be seen that all lines show a comparable behavior. Since C I and CN is readily observed just above the nozzle, dissociation of  $\text{CO}_2$  apparently is an almost instantaneous process. The maximum emission of CN is found just 2 mm further downstream than the maximum of the C I emission and corresponds to the maximum of N I emission.

In the recombination zone of the plasma (i.e. further downstream) we observe a relatively fast decay of C I and Ar I emission whereas CN and N emission drop much slower. It is likely that in the recombination zone of the plasma nitrogen plays an increasing role due to the turbulent mixing with air from the environment.

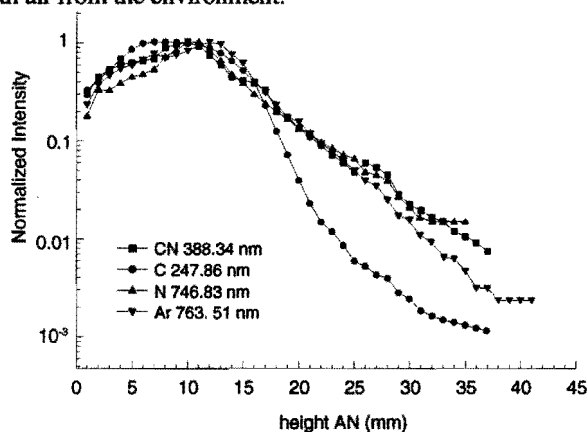


Figure 8. Normalized intensities of several species as a function of the height above the nozzle (AN) in an argon carbon dioxide discharge ( $[\text{Ar}] = 2.0 \text{ l}\cdot\text{min}^{-1}$ ,  $[\text{CO}_2] = 0.30 \text{ l}\cdot\text{min}^{-1}$ ,  $P = 1.0 \text{ kW}$ ). It should be noted that for the first 15 mm AN, intensities of dissociation and association products show a similar response as argon, suggesting an almost instantaneous dissociation of the carbon dioxide. Measurements have been integrated over the total plasma diameter.

### 3.5. Plasmas expanding in gases other than air

The results presented so far are all obtained from TIA plasmas expanding into the surrounding air. To investigate the role of the plasma environment, also measurements have been performed on plasmas expanding into other ambient gases. The surrounding gas in which the plasma is created has been controlled by making use of a column-like quartz vessel (i.d.  $\varnothing$  12 cm, height 70 cm). This vessel is attached to the waveguide structure and surrounds the upper part of the TIA including the plasma. A gas inlet close to the bottom of the vessel can be used to

supply the ambient gas. Exhaust plasma and ambient gases can escape through an aperture of  $\varnothing$  1 cm on top of the vessel. Due to the absence of a pump and the relatively small exhaust aperture, a strong interaction of the plasma with the ambient gas inside the vessel is ensured. If a pure argon plasma expands into a mixture of carbon dioxide and air (ratio 1:1), spectra are strongly dominated by CN emission, similar to a pure CO<sub>2</sub> plasma expanding into open air, cf. section 3.2. However, if the air (and thus the nitrogen) is removed from the vessel and the argon plasma expands into a pure CO<sub>2</sub> environment, the C<sub>2</sub> Swan system becomes very intense and CN emission drops to a negligible level, cf. figure 9. From this it can be concluded that CN association is preferred above C<sub>2</sub> association and that C<sub>2</sub> association is only dominant if no nitrogen atoms are present in the discharge.

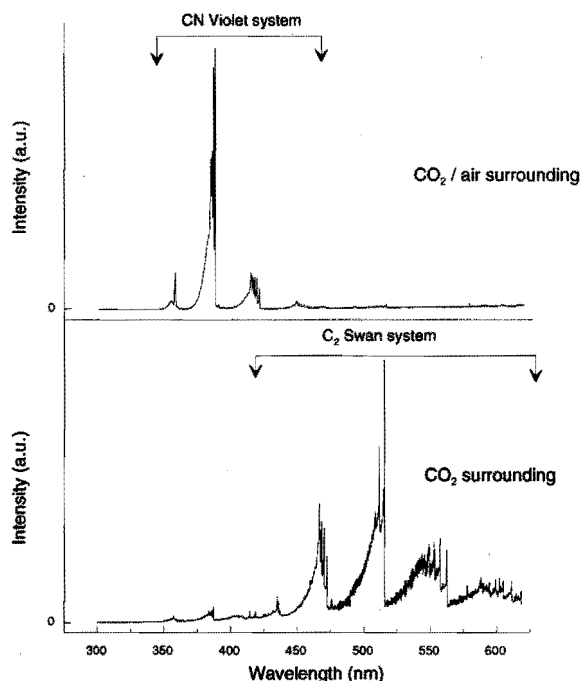


Figure 9.

*Spectra of argon plasmas created with a CH nozzle, expanding into different ambient gases ( $P=1.0$  kW,  $[Ar]=5.0$  l·min<sup>-1</sup>).*

*The upper spectrum is from an argon plasma expanding into a mixture of air and carbon dioxide whereas the lower spectrum is from an argon plasma expanding into a pure carbon dioxide environment. In the upper spectrum CN emission is dominant whereas in the lower spectrum apparently C<sub>2</sub> emission is dominant. Measurements are performed at 1 cm above the nozzle.*

### 3.6. Plasmas produced by the guide-surfatron

Finally the guide-surfatron has been studied with respect to its possible use for the analysis of molecules. The main difference between the previously studied TIA plasmas and the plasmas produced by the guide-surfatron is that the latter plasmas are confined in a quartz tube and thus have no interaction with the ambient gas.

The effect of molecular gas introduction is much more dramatic for the confined GS plasmas than for TIA plasmas. The injection of some H<sub>2</sub>O e.g., by primarily flushing the argon gas over a water surface, increases  $T_{rot}$  from  $1.7 \cdot 10^3$  to  $3.2 \cdot 10^3$  K close to the launching gap and decreases the plasma length from 12 cm to about 3 cm. The injection of a few percent CO<sub>2</sub>, N<sub>2</sub> or SO<sub>2</sub> easily leads to melting of the plasma tube.

Similar to plasmas created by the TIA, the injection of CO<sub>2</sub> and N<sub>2</sub> results in the emission of the violet system of CN (major band head at 388.3 nm). However, if only CO<sub>2</sub> is added, the dominant molecular emission bands in the spectrum arise from the C<sub>2</sub> radical (Swan system, A<sup>3</sup>Π<sub>g</sub>→X<sup>3</sup>Π<sub>u</sub> (0,0) with the major band head at 516.52 nm). This is in contrast to the free expanding torch plasma, in which the CN radiation is always dominant after CO<sub>2</sub> injection, but is comparable with the results from a pure argon TIA plasma expanding into a CO<sub>2</sub> environment. So again it appears that the association of CN is dominant over the association of C<sub>2</sub> if N atoms are present in the discharge.

Due to the absence of a cathode and the plasma confinement in a fused silica tube, experiments can be performed with aggressive gases, e.g. sulfur dioxide. Injection of 0.04 l·min<sup>-1</sup> of SO<sub>2</sub> (E<sub>dis</sub>=5.66 eV) into an argon discharge (3.0 l·min<sup>-1</sup>, P=260 W) results in emission of S I and O I lines, showing that this molecule is dissociated (at least partly) as well. However, emission bands from molecules containing sulfur atoms, are not found in the spectral range of 300-1000 nm.

Together with previous results this strongly indicates that the different kind of molecules which can be observed by emission spectroscopy in the studied microwave induced plasmas at atmospheric pressure is very limited. Especially for larger molecules, only diatomic association molecules or atomic dissociation products will be visible in emission.

Although plasmas created in a capillary column are better shielded than plasmas created by the TIA, the same kind of association products is observed after the introduction of molecular gases. However, the intensities of molecular bands in argon plasmas created by the GS are relatively low due to the absence of interaction with ambient air. Therefore a capillary plasma is to be preferred for the detection of impurities containing other elements than present in the carrier gas (e.g. H or OH emission for the determination of the concentration of H<sub>2</sub>O in Ar). In this case it is required that there are no other molecules present which contain these elements, since this would lead to the formation of similar dissociation and association products. This demand however, will scarcely be fulfilled in practice and for the analysis of complex gas mixtures, both the TIA and the guide-surfatron seem to be unsuited, at least for the studied power range and gases.

Probably at low pressure association of molecules will be less since three-body association strongly depends on collision rates and therefore on the pressure. It therefore is very likely that at reduced pressure three-body association can be reduced. Moreover, dissociation of molecules due to heavy-heavy collisions will decrease. This will be investigated in the next chapter [21].

#### 4. Conclusions

Atmospheric microwave induced plasmas produced by the TIA and a guide-surfatron have been studied with respect to their possible use as excitation sources for the analysis of molecular gases. For this purpose several molecular species have been introduced into various plasmas and the resulting emission has been studied.

The only introduced molecule that under some conditions could be observed with optical emission spectroscopy is nitrogen (emission of the first and second positive system). It is not likely however, that detection of nitrogen will have practical applications. Further, atomic fragments and association products as  $C_2$ , CN, NH, OH and NO are present in the spectrum. CN emission is dominant if  $CO_2$  is introduced into a plasma containing nitrogen atoms or molecules while  $C_2$  emission is dominant if these species are absent, e.g. in an Ar/ $CO_2$  discharge in a capillary tube.

From the results it can be concluded that the studied atmospheric pressure plasmas are very difficult to use as excitation source for the analysis of molecular gas mixtures under the used experimental conditions (argon or molecular carrier gas and an applied power ranging from 150-2000 W). Since most molecules contain elements like N, C, H and O, in general the same diatomic molecules will be created in the plasma. Only in case a few different molecular species are present might it be possible that unambiguous information can be deduced from dissociation or association products, although it is found that matrix effects and non-linearities play an important role in plasmas in which molecular gases are introduced. Preferably a discharge in a capillary tube should be used in order to avoid interaction with molecules from the ambient gas. A disadvantage is that plasmas produced by the GS are very sensitive to molecular gas injection.

Probably, at low pressure dissociation will be less since three-body collisions leading to the association of diatomic molecules will drop to a very low level. This will increase the possibility in finding a regime where excitation of non-dissociated molecules will appear more frequently. Experimental results will be presented in a next paper.

## Acknowledgments

The authors would like to thank Prof. M. Moisan for giving permission to use the TIA design. The plasma torch and large parts of the diagnostics have been constructed by M.J.F. van de Sande and G. ter Plegt.

## References

1. P.W.J.M. Bouwmans, "Inductively Coupled Plasma Emission Spectroscopy", part I & II, John Wiley & Sons, USA (1984).
2. A. Montaser, *CRC Critical Rev. Anal. Chem.* **18**(1), 45 (1987).
3. A.T. Zander and G.M. Hieftje, *Appl. Spectrosc.* **35**, 357 (1981).
4. H. Matusiewicz, *Spectrochim. Acta* **47B**, 1221 (1992).
5. D. Truitt and J.W. Robinson, *Anal. Chim. Acta* **51**, 61 (1970).
6. M. Moisan, G. Sauv e, Z. Zakrewski and J. Hubert, *Plasma Sources, Sci. and Technol.* **3**, 584 (1994).
7. M. Moisan, *Microwave Excitation Plasmas (Chap.V)*. Elsevier Science Publish. B.V., Amsterdam, The Netherlands (1992).
8. A. Ricard, L. St-Onge, H. Malvos, A. Gicquel, J. Hubert and M. Moisan, *J. Phys.* **III**

France 5, 1269 (1995).

9. M. Moisan, M. Chaker, Z. Zakrzewski and J. Paraszczak, *J. Phys. E: Sci. Instrum.* **20**, 1356 (1987).
10. J. Hubert, M. Moisan and A. Ricard, *Spectrochim. Acta* **34B**, 1 (1979).
11. A. Czernikowski and J. Chapelle, *Acta. Phys. Pol.* **63A**, 67 (1983).
12. W.L. Wiese and G.A. Martin, *Wavelengths and transition probabilities for atoms and atomic ions, part 2: transition probabilities*, U.S. Government Printing Office, Washington (1980).
13. G.H. Dieke and H.M. Crosswhite, *J. Quant. Spectrosc. Radiat. Transfer* **2A**, 97 (1962).
14. P.S. Moussounda and P. Ranson, *Spectrochim. Acta* **40B**, 641 (1985).
15. J. Jonkers, J.M. de Regt, J.A.M. van der Mullen, H.P.C. Vos, F.P.J. de Groote and E.A.H. Timmermans, *Spectrochim. Acta* **51B**, 1385 (1996).
16. J. Jonkers, L.J.M. Selen, J.A.M. van der Mullen, E.A.H. Timmermans and D.C. Schram, *Plasma Sources, Sci. and Technol.* **6**, 533 (1997).
17. J. Jonkers, H.P.C. Vos, J.A.M. van der Mullen and E.A.H. Timmermans, *Spectrochim. Acta* **51B**, 457 (1996).
18. D. Kella, P.J. Johnson, H.B. Pedersen, L. Vejby-Christensen and L.H. Andersen, *Phys. Rev. Lett.* **77**, 2432 (1996).
19. S.L. Guberman, *Geophys. Res. Lett.* **18**, 1051 (1991).
20. A. Ricard, "Reactive Plasmas", Société Française du Vide (1996).
21. Chapter 5 of this thesis, E.A.H. Timmermans, J. Jonkers, A. Rodero, M.C. Quintero, A. Sola, A. Gamero, D.C. Schram and J.A.M. van der Mullen, *Spectrochim. Acta* **54B**, 1083 (1999).



# 5

## The behavior of molecules in microwave induced plasmas studied by optical emission spectroscopy: 2. plasmas at reduced pressure

*E.A.H. Timmermans, J. Jonkers, A. Rodero<sup>(†)</sup>, M.C. Quintero<sup>(†)</sup>,  
A. Sold<sup>(†)</sup>, A. Gamero<sup>(†)</sup>, D.C. Schram and J.A.M. van der Mullen*  
published in *Spectrochim. Acta* **54B**, 1083-1096 (1999).

*(†) Departamento de Física Aplicada, Universidad de Córdoba,  
14071 Córdoba (Spain).*



**SUMMARY** - *The emission of various low pressure microwave induced plasmas created and sustained by a surfatron or by a Beenakker cavity has been studied after the introduction of molecular species (i.e. N<sub>2</sub>, CO<sub>2</sub>, SF<sub>6</sub> and SO<sub>2</sub>). Only nitrogen yielded observable emission from the non-dissociated molecule (first and second positive system). Using other gases, solely emission of dissociation and association products has been observed (i.e. atomic species, CN, C<sub>2</sub>, CO, OH and NH). Studies of these intensities have been performed as functions of gas composition, pressure and position in the plasma and have provided insight in molecular processes such as dissociation and association. It is found that parameters such as pressure and gas composition play a very important role with respect to these processes. Since no unambiguous relationship between the observed emission of dissociation or association products and the injected molecules has been found, it is established that it will be difficult to use microwave plasmas at reduced pressure as analytical excitation sources for molecular gas analysis.*

## 1. Introduction

During the last decades Optical Emission Spectroscopy (OES) has been widely used for the analysis of elements in aqueous, solid and gaseous samples [1-4]. In a previous paper [5], the idea was proposed to use emission spectroscopy for the analysis of molecular compounds in gases as well. Although Inductively Coupled Plasmas (ICPs) have been used more frequently as excitation sources in OES, two different Microwave Induced Plasmas (MIPs) were investigated in [5] (cf. chapter 4). The reason is that MIPs generally have a lower heavy particle temperature than ICPs and therefore it can be assumed that dissociation of molecules is less in MIPs than in ICPs. Hence it can be expected that the original molecules, which have to be detected, are less affected by the plasma. However, in the previous study it was found that in the atmospheric microwave discharges produced by the "Torche à Injection Axiale" (TIA) [6] and the "guide-surfatron" (GS) [7], molecules are largely dissociated and that mainly diatomic association products are observable. It was concluded that association due to three particle collisions might be an important channel for the creation of excited diatomic molecules:



with A, B and spectator X being heavy particles. The process given by Eqn 1 could explain the very dominant radiation of association products as CN, NO and NH<sup>a</sup>. However, since only a few different association products were created, it was found that it is difficult, if not impossible, to use emission of these new molecules as a "fingerprint" of the original molecules. As an example, an increased emission of NO and CN might be related to an increase of the amount of CO in the plasma gas, but also to an increase of the amount of CO<sub>2</sub> or some large organic molecules.

It was suggested in the previous study [5] that the low-pressure regime might be more suitable for molecular analysis, because of the negligible role of three particle processes (cf. Eqn 1). Moreover, at low pressure the heavy particle temperature is lower and therefore the

---

<sup>a</sup> Hydrogen atoms are always present in the discharge due to H<sub>2</sub>O impurities in the carrier gas.

dissociation of original molecules less. Another advantage is that due to the absence of air entrainment from the environment, which was clearly present in plasmas created by the TIA that expanded into open air [6], emission of the strongly radiating association products CN, NO and NH will be reduced if the number of nitrogen atoms and molecules present in the discharge gas is limited.

An additional advantage of low-pressure MIPs compared to atmospheric discharges are the lower power requirements. Since low power microwave generators are rather compact and power levels up to 500 W can be transported through coaxial lines, a very compact and modular setup can be used. This facilitates the use of the setup in possible industrial applications, e.g. flue gas analysis.

The aim of this paper is to obtain a deeper insight in the molecular processes occurring in the reduced pressure microwave discharges and to study the feasibility of molecular gas analysis with these plasmas. Two plasma applicators, i.e. the surfatron [8] and the Beenakker cavity [9], have been used to create a widely varying range of plasma conditions (pressure  $p \approx 0.1$ -20 mbar,  $n_e \approx 10^{16}$ - $10^{19} \text{ m}^{-3}$ , heavy particle temperature  $T_h \approx 0.8 \cdot 10^3$ - $1.4 \cdot 10^3 \text{ K}$  and electron temperature  $T_e \approx 1.5 \cdot 10^4$ - $4 \cdot 10^4 \text{ K}$ ).

Spectroscopic measurements have mainly been performed on surfatron plasmas. Discharges have been obtained in different carrier gases (argon, nitrogen and carbon dioxide) in which several different molecular gases (i.e.  $\text{N}_2$ ,  $\text{CO}_2$ ,  $\text{SF}_6$  and  $\text{SO}_2$ ) have been deliberately introduced. The emission has been studied as a function of the gas composition, the pressure and the position in the plasma. Some of the measurements have been repeated for plasmas produced by the Beenakker cavity in order to verify if the results are plasma source independent.

## 2. Experiments and instrumentation

The emission of several low-pressure discharges has been studied after deliberate molecular gas injection. The plasma sources used for our experiments, the surfatron and the Beenakker cavity, will be shortly discussed first<sup>b</sup>:

- The surfatron [8] has been widely used to create surface wave discharges in both noble and molecular gases in the pressure range of  $p \approx 10^{-5}$ -1 bar [10]. The plasma is usually confined by a quartz tube with an inner radius  $r_i \approx 0.7$ -6.0 mm. The surfatron launches EM waves which propagate in the TM ( $m=0$ ) mode along the interface between the plasma and the quartz tube. Due to the characteristic traveling surface wave propagation, long plasma columns can be created. Typical plasma lengths at reduced pressure are  $L_p \approx 5$ -100 cm for power inputs  $P_{in} \approx 30$ -250 W, depending on the carrier gas. In our experiments we created discharges in argon, nitrogen and carbon dioxide. Operational settings are typically  $P_{in} \approx 100$ -150 W, [gas

---

<sup>b</sup> Drawings of the surfatron and Beenakker cavity can be found in chapter 1 ("General introduction") of this thesis.

flow]  $\approx 0.10\text{-}0.15 \text{ l}\cdot\text{min}^{-1}$  and  $p \approx 0.5\text{-}20 \text{ mbar}$ , resulting in plasmas with a length in the range of  $L_p \approx 25\text{-}50 \text{ cm}$  (using argon as plasma gas and a discharge tube with 3 mm inner radius).

- The Beenakker cavity [9] has already extensively shown its potential as excitation source in spectrochemical analysis. Especially the combination of gas chromatography and a Beenakker cavity plasma has been used successfully in the past. The Beenakker cavity is a resonator operating in the  $\text{TM}_{010}$  mode. The plasma is enclosed by a quartz tube with an approximate inner radius between 1.0 and 4.0 mm. The main difference between the Beenakker cavity and the surfatron is the energy-coupling mode into the plasma. Instead of exciting a surface wave whose intensity smoothly decreases along the plasma column, all energy is locally coupled into the plasma inside the resonant cavity<sup>c</sup>. Due to the local energy input, plasmas do not extend far from the cavity and have a relatively high energy density. In our case we used the Beenakker cavity to create discharges in argon, nitrogen or carbon dioxide in the pressure range of  $p \approx 1\text{-}20 \text{ mbar}$ . Typical plasma lengths are  $L_p \approx 5\text{-}10 \text{ cm}$  for power inputs of  $P_{in} \approx 50\text{-}250 \text{ W}$ .

The major components used for the experiments, including the optical setup, which was already elaborately described in [5], are listed in Table 1. With the optics used, measurements in the wavelength range 200-1000 nm could be performed.

<i>Components</i>	<i>Model</i>	<i>Manufacturer</i>
Microwave generator	Microtron 200 Mark II, 2.45 GHz	Electro-Medical Supplies (EMS)
Field Applicators	Surfatron	Laboratory built
	Beenakker cavity	Laboratory built
Monochromator	Monospek 1000, 1200 gr/mm, 420 nm blaze-angle	Jobin Yvon (JY)
CCD camera	ST6-UV, 750 X 242 pixels, each 11.5 X 27 $\mu\text{m}$	Santa Barbara Instrument Group (SBIG)
Mass flow controllers	FC-260 series	Tylan General

*Table 1. Instrumental components.*

### 3. Results and discussion

#### 3.1. General observations from discharges at reduced pressure

The introduction of molecular species into argon plasmas created by the surfatron has two clearly observational effects:

1. The length of the plasma columns strongly reduces; e.g. from 50 cm to 20 cm after introduction of a few per cent of carbon dioxide (at  $\sim 2 \text{ mbar}$ ).

<sup>c</sup> From an electromagnetic point of view, these discharges pertain to different groups according to the widely accepted classifications of HF discharges by MOISAN et al. [11] and MAREC et al. [12].

2. The temperature of the quartz wall increases, which points towards an increased gas temperature and the presence of wall association processes.

Theoretically it can be expected that the introduction of molecules into an initially pure Ar discharge will change the plasma in the following ways:

- The energy transfer from the electrons to the heavy particles will improve due to electron induced vibrational excitation of molecular species.
- Processes like charge transfer followed by dissociative recombination will reduce the electron density whereas the molecular or atomic products created by this dissociative recombination often are released with high kinetic energy.

Consequences of these internal plasma changes are an increase of the heavy particle temperature (and thus of the wall temperature) and a reduction of the electron density. Because it is well known that for surface wave discharges at low pressure a nearly linear relationship exists between the maximum electron density and the length of the plasma column [11], also the observed decrease in the plasma length can easily be understood.

After the introduction of molecules, the emission spectra of the plasmas are dominated by molecular bands. In general these bands are just as in the case of atmospheric pressure MIPs [5] originating from diatomic association products. Table 2 lists the various molecular species that have been observed. It should be noted that the choice of the plasma gas and the plasma operating conditions impose which molecules are observed (see Table 3). The listed molecules are largely similar to those observed in atmospheric microwave discharges produced by the TIA (Torche à Injection Axiale) and the Guide-surfatron using similar gas mixtures [5]. The main differences are the often much stronger emission of the first and second positive system of nitrogen ( $B^3\Pi \rightarrow A^3\Sigma$  and  $C^3\Pi \rightarrow B^3\Pi$ , respectively) and the presence of emission of the Ångström, the fourth positive and the third positive system of CO ( $B^1\Sigma \rightarrow A^1\Pi$ ,  $A^1\Pi \rightarrow X^1\Sigma$  and  $b^3\Sigma \rightarrow a^3\Pi$ , respectively), observed under some conditions when CO<sub>2</sub> is used as discharge gas. Emission of CO, which is a dissociation product of CO<sub>2</sub>, has not been observed under any experimental condition at atmospheric pressure [5]. Instead, only association products like C<sub>2</sub>, NO and CN were observed. Experiments using other molecular species (SO<sub>2</sub>, SF<sub>6</sub>) have given similar results: emission bands of three-atomic or larger molecules are not observed under any condition.

Measurements on plasmas produced by the Beenakker cavity have been carried out as well. Despite the different microwave energy coupling modes (and power densities), the resemblance of the spectra obtained from the plasmas produced by the surfatron and the Beenakker cavity is remarkable. Usually, the same association and dissociation products can be seen if the experimental conditions such as pressure and gas composition are comparable. This indicates that the shape of the EM-field pattern has only a limited influence on the molecular species created inside the plasma. The only exception was found for the emission of CO in low-pressure CO<sub>2</sub> plasmas, which is more readily observed from surfatron than from Beenakker cavity discharges. Probably due to the higher gas temperature in Beenakker discharges, CO is dissociated at a lower pressure in a Beenakker cavity than in a surfatron discharge (using the same power input), cf. section 3.5.

The difference between surfatron and Beenakker cavity with respect to the energy coupling modes, as discussed in section 2, implies that the length of the plasmas produced by the Beenakker cavity is less affected by molecular gas injection. As a result, the use of the surfatron provides the most clearly perceptible results in the study of the influence of molecular gases on low-pressure microwave discharges. For this reason, the surfatron has been used as excitation source for most of the presented measurements.

<i>molecule</i>	<i>observed system</i>	<i>transition</i>	<i>(major) band heads (nm)</i>
NH	3360 Å system	$A^3\Pi \rightarrow X^3\Sigma$	336.0, 337.0
OH	3064 Å system	$A^2\Sigma^+ \rightarrow X^2\Pi$	306.4, 306.7, 307.8, 308.9
C <sub>2</sub>	Swan system	$A^3\Pi_g \rightarrow X^3\Pi_u$	512.9, 516.5
N <sub>2</sub>	first positive system	$B^3\Pi \rightarrow A^3\Sigma$	891.2, 654.5, 646.9, 580.4
	second positive system	$C^3\Pi \rightarrow B^3\Pi$	337.1, 357.7, 375.5, 380.5
N <sub>2</sub> <sup>+</sup>	first negative system	$B^2\Sigma^+_u \rightarrow X^2\Sigma^+_g$	391.4, 427.8,
NO	γ system	$A^2\Sigma^+ \rightarrow X^2\Pi$	226.9, 237.0, 247.9, 259.6
CN	violet system	$B^2\Sigma \rightarrow A^2\Pi$	359.0, 388.3, 421.6
CO	Å system	$B^1\Sigma \rightarrow A^1\Pi$	451.1, 483.5, 519.8, 561.0
	fourth positive system	$A^1\Pi \rightarrow X^1\Sigma$	219.7, 222.2, 226.2, 246.3
	third positive system	$b^3\Sigma \rightarrow a^3\Pi$	266.5, 283.3, 297.7

Table 2. List of the observed molecular bands, the corresponding transitions and the wavelengths at which the major band heads are found.

<i>plasma gases</i>	<i>Ar<sup>†</sup></i>	<i>Ar/H<sub>2</sub>O</i>	<i>Ar/N<sub>2</sub></i>	<i>N<sub>2</sub></i>	<i>Ar/CO<sub>2</sub></i>	<i>CO<sub>2</sub></i>	<i>Ar/SO<sub>2</sub> or Ar/SF<sub>6</sub></i>
observed molecules	OH (-), NH (-), CN (-), NO (-)	OH (++), NH (+), NO (+), CN (-)	N <sub>2</sub> <sup>+</sup> (+), NO (+), OH (-), NH (-), CN (-)	N <sub>2</sub> (++), NO (+), OH (-)	C <sub>2</sub> (++), CN (+), NO (+), OH (-), NH (-)	p>20 mbar <sup>‡</sup> : see Ar/CO <sub>2</sub> p<20 mbar: CO (+), OH (--), NO (--)	OH (-), NH (-), CN (-), NO (-)

<sup>†</sup>in argon, molecular gases like CO<sub>2</sub>, H<sub>2</sub>O and N<sub>2</sub> are present as pollutants at trace level

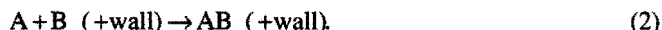
<sup>‡</sup>situation for a surfatron discharge; for a Beenakker cavity discharge the transition from C<sub>2</sub> to CO emission is observed at a lower pressure.

Table 3. Observed molecules from discharges in different gases. In mixtures, argon is the carrier gas and constitutes more than 90% of the plasma gas. The intensities of the observed molecules may vary from very weak (--) to very strong (++)

### 3.2. Association mechanisms for diatomic molecules

As discussed in section 1, at low pressure the rate of three-body association is negligible. However, there are still other routes for the creation of the observed diatomic molecules, namely by:

1. two-body volume association, for which it is required that at least one of the participating heavy particles is a molecule in order to satisfy momentum and energy conservation, and
2. association reactions at the wall, in which both participating heavy particles can be atomic:



It should be noted that the wall acts as a substitute for spectator X given in Eqn 1 in satisfying momentum and energy conservation. The energy released by the association process will be absorbed by the wall so that the molecule is created in the electronic ground state.

As an example, the creation of NO will be discussed. This molecule is easily observed ( $\gamma$  system,  $A^2\Sigma^+ \rightarrow X^2\Pi$ ,  $E_{\text{exc}}=5.47$  eV) if oxygen and nitrogen are present in the discharge and, as we will see, can be produced in the electronic ground state by two-body volume association as well as by wall association. The observed NO emission is a consequence of excitation of the created ground state NO towards the  $A^2\Sigma^+$  level by electron impact or excitation transfer from molecular nitrogen metastables.

The creation of NO is possible via a slightly endothermic volume two-body reaction between molecular nitrogen and oxygen [13]:



for which a total vibrational energy of approximately 2 eV is needed.

Other examples of volume two-body reactions are those between atomic oxygen and molecular nitrogen:

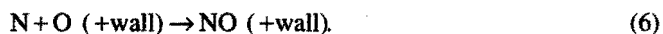


and between atomic nitrogen and molecular oxygen:



These reactions can be rather abundant if the amount of atomic nitrogen and oxygen is high [13]. This is the case when an argon carrier gas is used, because charge transfer between argon ions and molecular nitrogen and oxygen will create molecular ions that are easily subject to dissociative recombination.

An example of a wall process is the creation of NO out of single N and O atoms at the wall of the discharge tube:



Eqn 3-5 suggest that probably only at very low pressures (i.e. in a "collision free" plasma) NO association due to molecular volume processes is negligible. In this case the mean free path is large, so that free radicals will easily reach the quartz wall and as a consequence wall

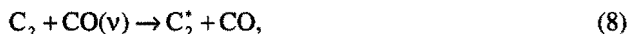
association will become more important (Eqn 6). As a result, it seems virtually inevitable that association products are present in the discharge. Section 3.3 will focus on such an association product: the readily observed  $C_2$  molecule.

### 3.3. Origin of the Swan system emission of the $C_2$ radical

When a small amount of  $CO_2$  (< 5%) is introduced into an argon surfatron discharge, strong emission bands from the  $C_2$  radical ( $\Delta v=0$  branch of the Swan system), atomic oxygen and carbon lines can be observed, whereas emission of  $CO_2$  and its fragments  $CO$  or  $CO^+$  is absent in the studied pressure range (0.5-20 mbar). The typical green  $C_2$  emission, which is also observed from discharges operated in pure  $CO_2$  at a relatively high pressure (cf. section 3.5), is generated by the radiative decay of the  $A^3\Pi_g$  level. Due to the low energy threshold ( $E_{exc}=2.40$  eV), ground state  $C_2$  molecules can easily repeatedly be excited towards this level, either by electron impact:



or by collisions with vibrationally excited  $CO$ :



with  $v \geq 10$ .

At reduced pressure it can be expected that the rate of the 3-body reaction:



is rather low and far inadequate to explain the strong  $C_2$  Swan system emission. We must therefore investigate the role of two-body volume processes and wall reactions.

The association of  $C_2$  is not straightforward, since no two-body volume association processes can be found which energetically allow the creation of  $C_2$  out of two molecular species.

As an example, a reaction such as:



is not likely to occur since, being highly endothermic, it requires an energy input of approximately 10.9 eV.

Since no pure molecular two-body reaction can be found creating  $C_2$ , it is likely that this molecule is created in a reaction in which at least one of the participating heavy particles is a carbon atom.

A reaction in which carbon atoms are involved and which produces emission of the  $C_2$  Swan system was postulated by KUNTZ *et al.* [14]:



in which the ground state C<sub>2</sub>O molecule can be provided by collisions between a ground state and an electronically excited CO molecule [15]:



It should be noted that in Eqn 11 the C<sub>2</sub> radical is directly created in the excited A<sup>3</sup>Π<sub>g</sub> state.

Apart from volume processes in the plasma, C<sub>2</sub> also can be created out of single carbon atoms in a two-particle reaction at the cold quartz tube:



Both Eqn 11 and 13 point out that the presence of atomic carbon is required for the association of C<sub>2</sub>, therefore it is useful to study how C atoms are created in the plasma. The dissociation of CO<sub>2</sub> into CO and O requires only 5.45 eV, whereas the dissociation of CO into C and O requires 11.09 eV. Therefore it is likely that electron impact will dissociate a relative large part of the introduced CO<sub>2</sub> into CO and O. Due to its high dissociation energy it can be expected that CO will hardly be destroyed by electrons. We therefore have to look for other channels leading to the production of C atoms.

Probably, the metastable 4s levels of argon (E<sub>exc</sub>=11.55 and 11.72 eV) play a dominant role. The internal energy of the argon metastables is sufficiently high to quench the CO molecules and create atomic carbon:



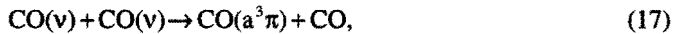
However, other production channels are reported for which a much lower threshold energy is required [16]:



in which v<sub>1</sub> and v<sub>2</sub> represent the principal vibrational quantum numbers, and



In Eqn 15 a total vibrational energy of approximately 5.7 eV is required, which is fulfilled as for instance v<sub>1</sub>=0 and v<sub>2</sub>=26, or when v<sub>1</sub>=11 and v<sub>2</sub>=12. The internal energy metastable a<sup>3</sup>π state in Eqn 16 is 6.01 eV, and thus large enough to produce carbon dioxide and atomic C as well. These metastable CO molecules can either be provided by collisions between two vibrationally excited CO molecules:



or, which at reduced pressure is more likely, by electron excitation from the ground state.

In figure 1 the intensities of an Ar (I)<sup>d</sup> line (935.4 nm, 4p[3/2]<sup>0</sup>→4s'[3/2]<sup>0</sup>, E<sub>exc</sub>=13.15 eV), an O (I) line (926.3 nm, 2p<sup>2</sup>(<sup>4</sup>S<sup>0</sup>)3d→2p<sup>3</sup>3p, E<sub>exc</sub>=12.08 eV) and the most intense band head of the C<sub>2</sub> Swan system (516.5 nm, A<sup>3</sup>Π<sub>g</sub>→X<sup>3</sup>Π<sub>u</sub>, Δv=0 (0,0), E<sub>exc</sub>=2.40 eV) are given as functions of the distance to the surfatron launching gap. Intensities decrease away from the launching gap,

<sup>d</sup> "I" refers to the atomic state. Emission lines of singly ionized elements ("II") are not observed.



as can be expected with the decreasing power flux and electron density  $n_e$ . It should be noted that the intensity drop of  $C_2$  is about twice as fast as that observed for O (I) and Ar (I). Assuming that the intensities of the atomic species are proportional to  $n_e$ , which decreases approximately linearly with the distance to the launching gap [11], this suggests that the  $C_2$  emission is not only due to electron impact of ground state  $C_2$  (Eqn 7) but probably also due to collisions of ground state  $C_2$  with vibrationally excited CO (Eqn 8) or due to the volume association process given by Eqn 11-12, in which  $C_2$  is directly created in the excited  $A^3\Pi_g$  state. Also the involvement of metastable argon atoms in the dissociation of CO could explain the enhanced dependency of the  $C_2$  emission on the electron density.

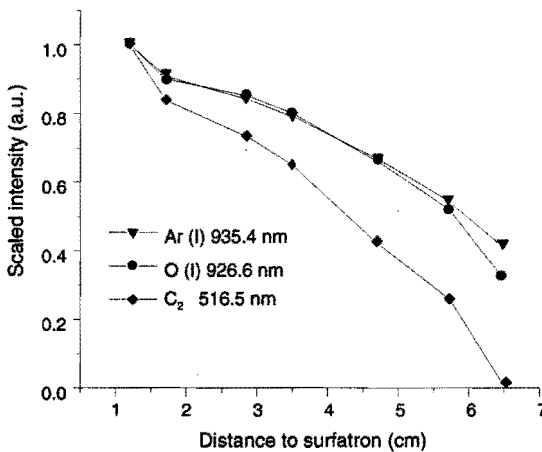


Figure 1.

Scaled intensities of an oxygen line, an argon line and a  $C_2$  band head as a function of the axial position in the plasma column. The intensities decrease further away from the launching gap. This decrease is significantly larger for the  $C_2$  radical than for the atomic lines. Experimental settings are  $[Ar]=0.20 \text{ l}\cdot\text{min}^{-1}$ ,  $[CO_2]=0.025 \text{ l}\cdot\text{min}^{-1}$ ,  $P_{in}=75 \text{ W}$ ,  $p=2.6 \text{ mbar}$  and  $L_{pl}=7 \text{ cm}$ .

### 3.4. Matrix effects

The presence of certain atoms or molecules in the plasma can effect the intensity of the radiation of other species. This so-called matrix effect is of great importance in emission spectroscopy since it limits the accuracy of quantitative measurements, especially when the concentration of the disturbing atoms or molecules is variable or not well-known.

Measurements have been performed on surfatron discharges in order to study matrix effects in low-pressure plasmas as a result of molecular species.

In figure 2 the intensities of  $C_2$  and CN are shown as a function of the amount of  $N_2$  added to an Ar/ $CO_2$  mixture. The intensity of  $C_2$  shows a continuous decrease while CN shows an explosive growth for low nitrogen concentrations, but remains almost constant for higher nitrogen concentrations. The decrease of  $C_2$  is supposed to be mainly caused by the increasing association of CN and shows that the emission of association products is very sensitive to the matrix. The fast stabilization and even decrease of CN is probably due to the energy losses involved in the dissociation processes. This is in agreement with the decreasing plasma length as the concentration of  $N_2$  increases.

The example shown in figure 2 indicates that in molecular emission spectroscopy matrix effects are very strong, especially when the emission of association products is studied. This implies that the use of the emission of association products as quantitative "fingerprints" for the molecular species originally present in the plasma gas is bound to be largely inaccurate.

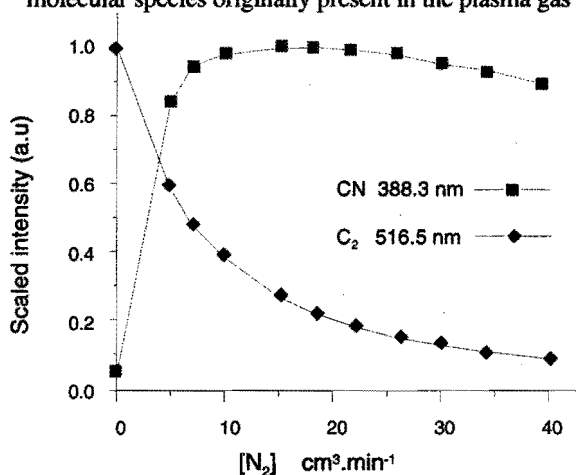


Figure 2.

Scaled intensities of CN and C<sub>2</sub> as a function of increasing [N<sub>2</sub>] while [Ar] and [CO<sub>2</sub>] are kept constant. The maximum intensities are scaled to unity. CN reaches its maximum if [CO<sub>2</sub>]=[N<sub>2</sub>]. The emission of C<sub>2</sub> however, continuously decreases for increasing nitrogen concentrations. Experimental settings are [Ar]=0.50 l·min<sup>-1</sup>, [CO<sub>2</sub>]=5·10<sup>-3</sup> l·min<sup>-1</sup> and p=5 mbar.

### 3.5. Influence of the pressure

At atmospheric pressure it was found that charge transfer between molecular nitrogen and argon ions is an important mechanism [17] in argon plasmas in which nitrogen is introduced:



The charge transfer reaction is quasi-resonant due to the comparable ionization energies for argon and molecular nitrogen ( $E_i=15.76$  and  $15.58$  eV respectively). The presence of this mechanism was supported by the observation of the first negative system of N<sub>2</sub><sup>+</sup> and several atomic nitrogen lines (the latter being a result of the excitation of the atoms created by the dissociative recombination of N<sub>2</sub><sup>+</sup>), whereas emission of N<sub>2</sub>(B) and N<sub>2</sub>(C) is rather weak or not present at all at atmospheric pressure.

At reduced pressure (1-10 mbar), however, rather strong emission of the first and second positive system of N<sub>2</sub> (B<sup>3</sup>Π→A<sup>3</sup>Σ and C<sup>3</sup>Π→B<sup>3</sup>Π, respectively) can be observed from argon discharges in which nitrogen is introduced, while the first negative system of N<sub>2</sub><sup>+</sup> and atomic nitrogen lines are relatively weak or absent. It can therefore be concluded that dissociation of diatomic molecules is indeed less important at reduced pressure.

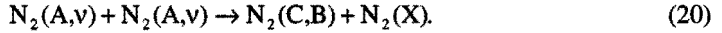
From low-pressure discharges in pure nitrogen, emission of the first and second positive system of N<sub>2</sub> is very intense, while emission of the first negative system of N<sub>2</sub><sup>+</sup> is not present in the pressure range 0.5-10 mbar. Pure nitrogen discharges at atmospheric pressure were characterized by a rather weak emission of N<sub>2</sub> and a relatively strong emission of N<sub>2</sub><sup>+</sup> [5]. The increasing dominance of N<sub>2</sub> emission over N<sub>2</sub><sup>+</sup> emission with decreasing pressure can easily be understood if we consider N<sub>2</sub><sup>+</sup> as the only ion species and only take direct electron excitation

from the (ion) ground state into account. As an example we compare the intensity ratio of the first positive system of  $N_2^+$  ( $E_{exc} \approx 3.2$  eV) and the second positive system of  $N_2$  ( $E_{exc} \approx 11.1$  eV):

$$\frac{N_2^+(B)}{N_2(C)} \propto \frac{n_e N_2^+ \exp(-\frac{3.2}{kT_e})}{n_e N_2 \exp(-\frac{11.1}{kT_e})} \approx \left( \frac{n_e}{N_2} \right) \exp\left(\frac{7.9}{kT_e}\right), \quad (19)$$

with  $n_e$  being the electron density,  $N_2$  and  $N_2^+$  being the densities of the ground state molecules and  $T_e$  the electron temperature. With decreasing pressure the electron temperature will increase so that the exponent in Eqn 19 will decrease and consequently the emission of  $N_2$  will prevail over that of  $N_2^+$ . It should be noted that at very low pressure, excitation towards  $N_2^+(B)$  from the  $N_2$  ground state could become dominant [17] so that Eqn 19 does not hold anymore. However, the high electron temperature required for this direct excitation was not present under our experimental conditions.

The simple consideration given by Eqn 19 does not take into account the role of the metastable  $A^3\Sigma$  level ( $E_{exc} = 6.24$  eV) which has a radiative lifetime of typically 1-3 s. Due to this long radiative lifetime and the low collision frequency at reduced pressure, nitrogen metastables play a significant role and can act as intermediates for excitation towards the radiative B ( $E_{exc} = 7.42$  eV) and C levels by electron impact. Pooling reactions between nitrogen metastables can provide  $N_2(B)$  or  $N_2(C)$  as well [17]:



Both the role of metastables and pooling reactions will lead to a further enhancement of  $N_2(B)$  and  $N_2(C)$  emission in the low pressure regime.

Another remarkable dependence on the pressure can be seen from discharges in which  $CO_2$  is used as carrier gas.

In pure  $CO_2$  discharges the Swan system of  $C_2$  can only be seen at higher pressures. At lower pressures, bands of the Ångström, the third positive and the fourth positive system of CO ( $B^1\Sigma \rightarrow A^1\Pi$ ) can be observed while emission of  $C_2$  has vanished completely, cf. figure 3. The actual transition pressure from CO to  $C_2$  emission, which can easily be observed by a color change of the plasma, depends on tube diameter, power input and power coupling mode. If  $C_2$  emission is observed, it is also accompanied by C (I) and O (I) emission. These atomic lines have largely disappeared at pressures where only CO emission exists.

In  $CO_2$  discharges in a Beenakker cavity the transition from  $C_2$  to CO emission is observed at a lower pressure (app. 5 mbar) than in a surfatron discharge (>20 mbar). This is related to the higher heavy particle temperature in Beenakker cavity discharges under similar experimental settings (power, tube diameter, pressure).

Since at lower pressures, no  $C_2$  or C (I) can be observed, it can be concluded that no atomic carbon is created either (otherwise wall association followed by electron excitation would provide  $C_2$  emission, cf. Eqn 13,7) and that consequently the dissociation of  $CO_2$  is only partial. Apparently, the collision frequency between highly vibrationally excited CO molecules or between ground state CO and  $CO(a^3\pi)$  is negligible (see Eqn 15-17), and CO is only electronically excited by electron impact. At the transition from CO to  $C_2$  emission, the creation

of atomic carbon becomes significant. If atomic carbon is present in the discharge, the production of  $C_2(A)$  will dominate over the excitation of  $CO(X)$  towards  $CO(B^1\Sigma)$  since for the latter reaction an excitation energy of 10.8 eV is required.

The experiments described above show that pressure is an important parameter affecting the molecular processes occurring in plasmas. As a result, in any foreseen application of plasmas for molecular analysis, the pressure should be kept rigorously constant.

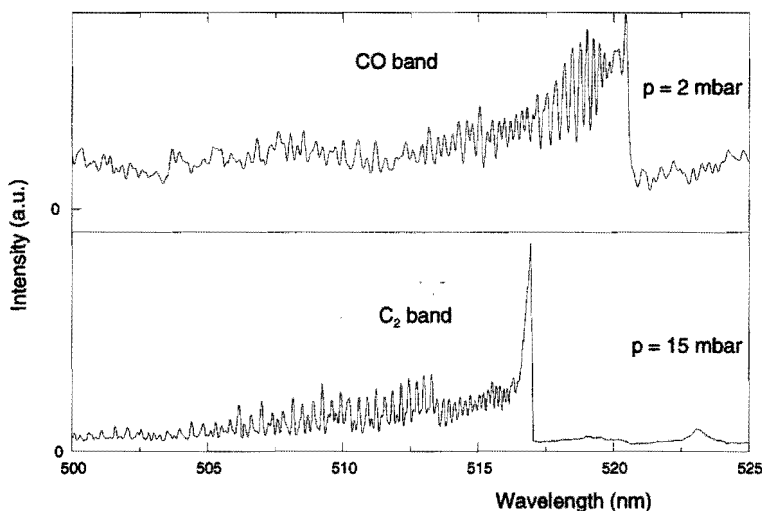


Figure 3. Emission spectra of Beenakker cavity discharges in  $CO_2$  at different pressures. At low pressure (<5 mbar) only emission from  $CO$  is observed whereas at higher pressures (>5 mbar) only  $C_2$  is observed.

### 3.6. Reduced-pressure surfatron discharges for molecular gas analysis

As already concluded in the previous sections, mainly emission of diatomic dissociation and association products and of atomic lines are observed after introduction of molecular gases, a result that is similar to the results which have been previously reported for atmospheric MIPs [5]. Since of all studied molecular gases only  $N_2$  yields emission, any envisaged analytical application (except for  $N_2$ ) has to be based on the detection of emissions of association or dissociation products.

Experiments in which  $SO_2$  is deliberately introduced into argon plasmas created by the surfatron have shown that no (new) molecular emission bands are observed. Only emission from atomic species  $S(I)$  and  $O(I)$  can be seen. The most intense sulfur lines are found at 921.3, 922.8 and 923.8 nm ( $4p5P \rightarrow 4s5S$ ,  $E_{exc}=7.87$  eV), while for oxygen the triplet around 777 nm ( $3p5P \rightarrow 3s5S$ ,  $E_{exc}=10.74$  eV) and the line at 844.64 nm ( $3p3P \rightarrow 3s3S$ ,  $E_{exc}=10.99$  eV) are by far the most intense.

The intensity of the oxygen triplet has been studied after the deliberate introduction of  $\text{SO}_2$  as well as after the introduction of  $\text{CO}_2$ . In figure 4 the normalized intensities are given as functions of the amount of  $\text{SO}_2$  or  $\text{CO}_2$  introduced into argon discharges. If all other parameters are kept constant, the behavior is practically the same, probably due to the similar dissociation energies of  $\text{SO}_2$  and  $\text{CO}_2$  (5.66 and 5.45 eV respectively). It is clear that in this case O (I) emission cannot be used as a "fingerprint" of the molecular gas.

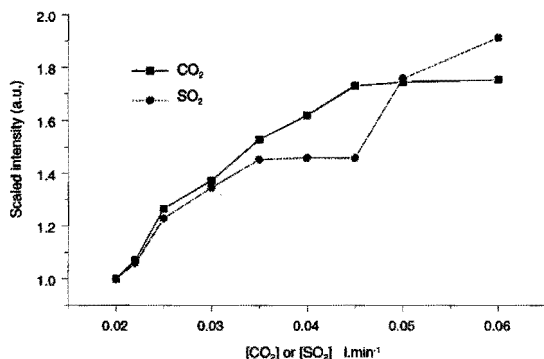


*Figure 4*  
Scaled emission intensities of atomic oxygen in surfatron argon discharges in which carbon dioxide or sulfur dioxide is deliberately introduced. Intensities are scaled to unity for the lowest concentration used. The behavior of the oxygen line is similar for both molecular gases.

Unlike the case of all other gases, it has not been possible to create a discharge in pure  $\text{SF}_6$ , even at a pressure of 1 mbar. Probably due to the high electron affinity of  $\text{SF}_6$ , at least 50% of argon has to be added before a breakdown can be achieved. Under these conditions, no bands of molecules containing S or F atoms have been observed, although rather strong emission lines of S (I) indicate that the  $\text{SF}_6$  is at least partly dissociated.

The introduction of  $\text{N}_2$  into the  $\text{CO}_2$  plasma leads to a decreasing intensity of  $\text{C}_2$  or  $\text{CO}$ . Moreover, emission of the first and second positive system of nitrogen quickly outweighs the emission of the former molecules, to the point that they cannot be detected anymore. Figure 5 shows the second positive system of nitrogen. The spectrum between 300 and 500 nm is dominated by molecular  $\text{N}_2$  bands. Since the emission of the second positive system is rather strong, possible weak bands of other molecules cannot be observed. The first positive system ranges from 550 nm to 1000 nm and is often even more intense. The first and second positive systems are very intense over a wide pressure range ( $p < 20$  mbar) if nitrogen is used as carrier gas. These bands are also present in spectra from discharges in  $\text{Ar}/\text{N}_2$  and  $\text{Ar}/\text{CO}_2/\text{N}_2$  mixtures, but only in case the pressure is lower than 10 mbar.

The vast majority of gases which are of potential interest for molecular analysis, e.g. industrial flue gases, contain high concentrations of nitrogen. Therefore it can be expected that large problems with interfering molecular bands will be encountered during measurements. Moreover, since the kind of observed association products can only to a limited extent be related to the original molecules, it seems very difficult to use emission spectroscopy for molecular gas analysis. The combination of gas chromatography with emission spectroscopy would probably be a feasible alternative, because the molecules are then sequentially introduced

into the plasma. Major drawbacks however, are the loss of the on-line character of the analysis and the sensitivity of gas chromatography to dust.

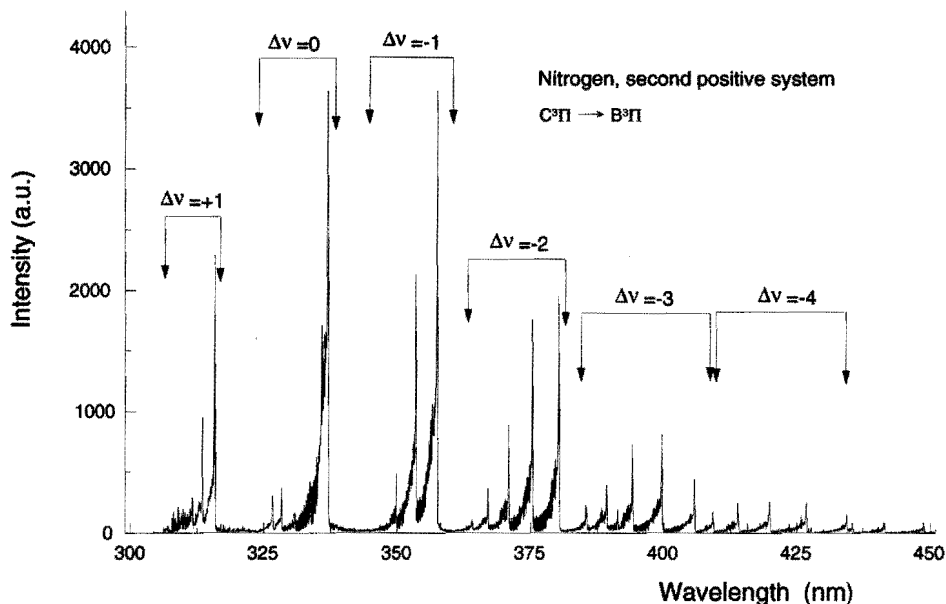


Figure 5. A typical spectrum of the second positive system of nitrogen. The first positive system ranges from 550 to 1000 nm. As a result, a large part of the spectrum is covered with molecular bands when  $N_2$  emission is present.

#### 4. Conclusions

Low-pressure microwave induced plasmas created by the surfatron and the Beenakker cavity have been studied by means of optical emission spectroscopy. The aim of the study was to obtain a deeper insight in molecular processes in the plasma and to investigate the feasibility of low-pressure plasmas as molecular gas analyzers. For these purposes, different molecular gases (i.e.  $N_2$ ,  $CO_2$ ,  $SO_2$ , and  $SF_6$ ) were deliberately introduced into several surfatron and Beenakker cavity discharges and the resulting emission was studied.

As in the case of atmospheric microwave induced plasmas [5], spectra are usually dominated by the emission of association products such as  $C_2$  and  $CN$ , dependent on the gas composition and pressure. At pressures ranging from 0.1 to 20 mbar, nitrogen is the only non-dissociated molecule that has been observed. Introduction of the other gases resulted in the observation of the emission of dissociation and association products only.

It was found that the pressure is an important plasma parameter governing molecular processes. From a discharge in pure  $CO_2$  e.g., only atomic carbon and  $C_2$  emission was observed at pressures above approximately 5-10 mbar (depending on experimental settings), suggesting that the carbon dioxide was (at least partly) dissociated into separate atoms. At a lower pressure,

however, only CO emission was observed, indicating that carbon dioxide is dissociated into CO and O solely.

Several mechanisms have been discussed in order to explain the measured spectra. It was concluded that, also for lower pressure regimes, it seems virtually inevitable to have emission of association products. If the pressure in the discharge tube is reduced to avoid volume association mechanisms due to molecular two-body collisions, the mean free path in plasma increases and (atomic) radicals reach the tube wall more easily where wall association will provide new diatomic species.

The relationship between the observed association and dissociation products and the gas composition was only weak, and moreover, emission of nitrogen was rather intense and extended over a large wavelength range, so that it was concluded that it will be very difficult to use optical emission spectroscopy for molecular gas analysis, except for the case that the detection of nitrogen is the objective. Since the results were similar for both plasma sources, they may probably be generalized to all low-pressure microwave discharges.

## Acknowledgements

The authors would like to thank N. Sadeghi for his fruitful discussions about molecular processes in plasmas and M.J.F. van de Sande, F. Overberg and G. ter Plegt for constructing the plasma sources and diagnostics. Financial support was given by the Dutch Technology Foundation (STW), the Eindhoven Centre Technology for Sustainable Development (TDO) and the European Community Action Scheme for Mobility of University Students Foundation (ERASMUS).

## References

1. P.W.J.M. Boumans, "*Inductively Coupled Plasma Emission Spectroscopy*", part I & II, John Wiley & Sons, USA (1984).
2. A. Montaser, *CRC Critical Rev. Anal. Chem.* **18-1**, 45 (1987).
3. M.D. Calzada, M.C. Quintero, A. Gamero and M. Gallego, *Anal. Chem.* **64-13**, 1374 (1992).
4. Q. Jin, Y. Duan and A. Olivares, *Spectrochim. Acta* **52B**, 131 (1997).
5. *Chapter 4 of this thesis*, E.A.H. Timmermans, J. Jonkers, I.A.J. Thomas, A. Rodero, M.C. Quintero, A. Sola, A. Gamero and J.A.M. van der Mullen, *Spectrochim. Acta* **53B**, 1553 (1998).
6. M. Moisan, G. Sauvé, Z. Zakrewski and J. Hubert, *Plasma Sources, Sci. and Technol.* **3**, 584 (1994).
7. M. Moisan and Z. Zakrewski, *Rev. Sci. Instrum.* **58**, 1895 (1987).
8. M. Moisan and Z. Zakrewski, *J. Phys. D: Appl. Phys.* **24**, 1025 (1991).
9. C.I.M. Beenakker, *Spectrochim. Acta* **31B**, 173 (1977).

10. C.M. Ferreira, *J. Phys. D: Appl. Phys.* **14**, 1811 (1981).
11. M. Moisan and J. Pelletier, "*Microwave Excited Plasmas*", Elsevier Science Pub. B.V. (Plasma Technol. Vol 4), The Netherlands (1992).
12. J. Marec, E. Bloyet, M. Chaker, P. Leprince and P. Nghiem, "*Electrical Breakdown and Discharges in Gases*", Ed. by E.E. Kunhardt and L.H. Luessen, Plenum, USA (1982).
13. N.G. Basov, E.M. Belenov, V.A. Isakov, E.P. Markin, A.N. Oraevskii, V.I. Romanenko and N.B. Ferapontov, *Sov. Phys.-JETP* **41**, 1017 (1975).
14. C. Kuntz, P. Harteck and S. Dondes, *J. Chem. Phys.* **46**, 4177 (1967).
15. F. Gosse, N. Sadeghi and J.C. Pebay-Peyroula, *Chem. Phys. Lett.* **13**, 557 (1972).
16. G. Liuti, S. Dondes and P. Harteck, *J. Chem. Phys.* **44**, 4051 (1966).
17. A. Ricard, "*Reactive Plasmas*", Société Française du Vide (1996).





# 6

## Excitation balances and transport properties studied by power interruption experiments

*E.A.H. Timmermans, I.A.J. Thomas, J. Jonkers and J.A.M. van der Mullen,  
submitted for publication in *Plasma Sources, Sci. and Techn.* (1999).*

**ABSTRACT** - Atmospheric microwave induced argon plasmas with and without analyte injection have been exposed to power interruption experiments in order to study transport processes and to reveal dominant excitation balances. From the time-dependent behavior of line intensities due to electron cooling and quenching during the power interruption, it is found that electron loss channels like diffusion, convection and the dissociative recombination of molecular ions are much larger than for inductively coupled plasmas. It is found that in the ionizing part of the plasma electron dominated mechanisms are responsible for the population of radiative levels. Significant changes in the responses to power interruption are observed when small amounts of molecular compounds are injected (>0.5 %), probably due to a decrease of the electron density. Furthermore it is found that in the recombination zone downstream in the plasma an electron-independent excitation mechanism, probably thermal excitation, is responsible for the population of radiative levels of analytes with relatively low excitation energies. From the downstream propagation of a disturbance created in the ionizing part of the plasma the local axial gas velocity has been determined. In the analyte excitation zone of the plasma typical velocities are around  $25 \text{ ms}^{-1}$ , whereas in the recombining zone velocities of  $12$  to  $18 \text{ ms}^{-1}$  are obtained.

## 1. Introduction

Atomic emission spectroscopy (AES) is nowadays widely used in analytical chemistry for the analysis of analytes, i.e. aqueous or gaseous samples containing unknown elements that have to be determined [1,2]. Aqueous analytes are nebulized in a carrier gas for this purpose and then evaporated in a plasma, usually being an argon plasma. When the elements are excited towards radiative levels, the emission can be used for the analysis of the analyte, both qualitative and quantitative. Apart from the well-known argon Inductively Coupled Plasma (ICP), more and more other plasmas are being used as spectrochemical excitation sources [1,3-5]. This study focuses on two atmospheric microwave-induced plasma sources: the TIA (from Torche à Injection Axiale) and the MPT (Microwave Plasma Torch). Due to their different design features, the much higher operational frequency (2.45 GHz) and the much smaller radial plasma dimensions, argon plasmas produced by the studied plasma torches have characteristics different from ICPs and research is needed in order to study their feasibility as excitation sources.

When plasmas are used as excitation sources, it is obvious that insight in the populating processes of excited radiative levels is of major importance. This paper presents a spectroscopic study that can provide information on these excitation processes. The method that has been used is based on the study of the time dependent behavior of atomic line or molecular band intensities during short interruptions in the power generated by the microwave power supply. These measurements will be referred to as so-called "power interruption (PI) experiments" [6-13]. Apart from insight in excitation balances, the PI experiments can reveal important aspects of transport phenomena such as diffusion processes, heat conduction and convection.

The introduction of aerosols or molecular gases into argon discharges might severely influence the transport phenomena and excitation mechanisms with as consequences that basic

plasma parameters such as electron density and electron and heavy particle temperature are effected [1,14-20]. Moreover, the introduction of easy ionizable elements might lead to matrix effects or non-linearities between concentrations of elements and emission intensities [1,2,20]. Therefore, not only pure argon discharges have been studied by power interruption experiments, but also argon plasmas in which deliberately impurities have been injected, such as aerosols or molecular gases. As will be presented in section 4, the measurements have indeed shown striking differences between pure argon plasmas and argon plasmas with analyte or molecular gas injection.

In the next section the studied plasma sources and the instrumentation used for the power interruption measurements will be discussed. In section 3 the different effects of power interruptions on plasma properties will be discussed. Several excitation balances that can govern the populations of radiative levels will be presented, and moreover, it will be argued that depending on the governing populating balance, different responses of line intensities after a sudden power interruption can be expected. This will be illustrated by some typical power interruption responses as measured from an ICP in the past [12,13]. Experimental results will be presented in section 4. Several experimental results will be compared to results previously obtained from a 100 MHz argon ICP [12,13,21-23]. Conclusions will be given in section 5.

## 2. Experimental set-up

### 2.1 The plasma sources

The atmospheric argon microwave-induced discharges that have been investigated are created by two different plasma sources:

- A plasma torch referred to in literature as the "TIA" (from "*Torche à Injection Axiale*", using the terminology of MOISAN *et al.*, the developers of the torch [24-25]). This waveguide fed torch produces needle-like plasmas (plasma radius  $r_p \approx 0.5$  mm) which expand into the open air [24-30]. Depending on the nozzle geometry discharges in various noble or molecular gases can be created. More detailed information on this topic can be found in a previous paper [30]. In this paper however, we restrict ourselves to plasmas with argon as carrier gas. Typical plasma parameters for such argon discharges are an electron density  $n_e \approx 3 \cdot 10^{21} \text{ m}^{-3}$ , an electron temperature  $T_e \approx 2.2 \cdot 10^4 \text{ K}$  and a heavy particle temperature  $T_h \approx 2 \cdot 10^3 - 4 \cdot 10^3 \text{ K}$  [26-28] at a power input of  $P = 1.0 \text{ kW}$  and an argon gas consumption of  $[\text{Ar}] = 3 \text{ l} \cdot \text{min}^{-1}$ .
- A plasma torch referred to in literature as the "MPT" ("*Microwave Plasma Torch*", developed by JIN *et al.* [31,32] and recently improved by BILGIC *et al.* [33]). The main differences of this plasma torch compared to the TIA are its low power and gas consumption and its separate central gas channel through which analytes can be introduced (comparable with the ICP). Due to the low power requirements, a coaxial feed line is used to power the torch. The flame-like plasma has a diameter  $r_p \approx 2$  mm and is characterized by

$n_e \approx 1 \cdot 10^{21} \text{ m}^{-3}$ ,  $T_e \approx 2.0 \cdot 10^4 \text{ K}$  and  $T_h \approx 3 \cdot 10^3 \text{ K}$  at a power input of  $P=300 \text{ W}$  and a total argon gas flow of  $[\text{Ar}] = 0.5 \text{ l} \cdot \text{min}^{-1}$  [32].

Both plasma sources have been used previously for analytical spectrometry. The MPT features detection limits that are almost comparable to those typically achieved with ICPs [30-39]. Major advantages of the MPT compared to the ICP are the very low power and gas consumption and the compactness of the setup. Detection limits in plasmas produced by the TIA are worse, but since the TIA creates robust plasmas, it was successful for the on-line analysis of combustion gases [40,41].

Most of the presented experimental data in this paper is obtained from plasmas produced by the TIA. Some of the general findings of the power interruption experiments presented in section 4 will be compared to results previously obtained with a 100 MHz inductively coupled plasma [12,13]. This ICP is much more voluminous than the described microwave plasmas and has a radius  $r_p$  of approximately 1 cm and a height of 4 cm. Typical ICP parameters are given by  $n_e = 10^{21} \text{ m}^{-3}$ ,  $T_e = 1 \cdot 10^4 \text{ K}$  and  $T_h = 5 \cdot 10^3 - 7 \cdot 10^3 \text{ K}$  (using a power input  $P=1 \text{ kW}$  and a total argon flow  $[\text{Ar}] = 20 \text{ l} \cdot \text{min}^{-1}$ ) [12,13,21-23].

## 2.2 Instrumentation for the power interruption experiments

The setup used for power interruption experiments is shown in figure 1. The plasma radiation is focused onto the entrance slit of a 1-meter monochromator where an emission line is selected. The current peaks generated by the photo multiplier tube (PMT) due to photons of the selected wavelength are converted into short TTL pulses (15 ns) in order to enable photon counting. By converting only those peaks whose intensities exceed a minimum threshold, dark current pulses of the PMT are filtered out. The TTL pulses are counted by a multi-channel scaler (MCS) which has 4096 channels with a minimum integration time of  $2 \mu\text{s}$  per channel (cf. table 1). When the highest time resolution is used, the MCS thus can monitor approximately 8.2 ms continuously. A computer with a pulse generator is used to synchronize the power interruptions of the microwave generator (with TTL signals) and the data acquisition by the multi-channel scaler (MCS). Measurements are started typically 70  $\mu\text{s}$  before the power interruption.

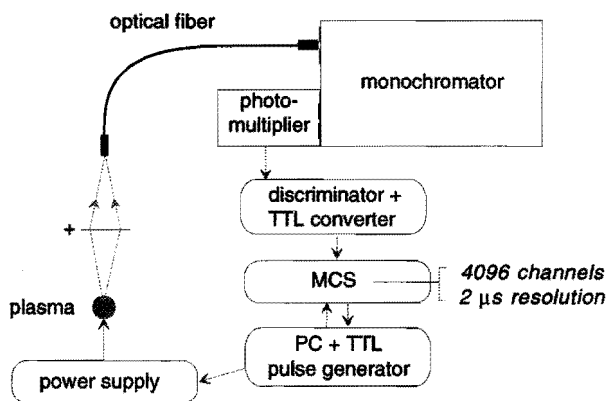


Figure 1.

Set-up used for PI experiments. A computer is used to synchronize the interruptions of the microwave generator and the data acquisition by the multi-channel scaler (MCS). The photo multiplier pulses are converted into TTL signals in order to enable photon counting (cf. table 1).

In order to be able to count a significant number of photons in 2  $\mu$ s, broad entrance and exit slits are used for the monochromator (200-250  $\mu$ m). Moreover, measurements typically have been averaged 5000 times in order to reduce the noise level. The repetition frequency of an on/off cycle of the generator is typically set to 100 Hz.

<i>Components</i>	<i>Model</i>	<i>Manufacturer</i>
Magnetron + power supply <sup>†</sup>	MW-GIR2M130-2K, f=2.46 GHz, P <sub>max</sub> =2 kW	Muegge (Germany)
Plasma sources	Torche à Injection Axiale (TIA) Microwave Plasma Torch (MPT)	Laboratory built Laboratory built
Gas mass flow controllers	FC-260 series	Tylan General
Monochromator	HR1000, 1200 gr/mm, 300-550 nm blazed	Jobin Yvon
Photo multiplier tube	R928, Side-on (Peltier cooled)	Hamamatsu
Discriminator + TTL converter		EG&G
Multi-channel scaler	Ortec ACE-MCS, 24 bits, 4096 channels, 2 $\mu$ s resolution	EG&G
TTL pulse generator	Metabyte CTM05/A	Laboratory built, based on a Keithley Metabyte counter timer PC board

<sup>†</sup> Modified by Muegge in order to enable a fast decay of the output power (<2  $\mu$ s) during the interruption experiments.

*Table 1. Instrumental components used for the spectroscopic measurements and the power interruption experiments.*

### 3. Theory

#### 3.1 Different effects of power interruptions

The balance between power input and transport processes in steady state largely determines plasma parameters like the electron density  $n_e$ , the electron temperature  $T_e$  and the heavy particle temperature  $T_h$ . When the power is interrupted the plasma will be exposed to transport processes only and as a result these parameters will change. A consequence of changing plasma parameters is that the plasma radiation will be affected as well. In the presented power interruption experiments these changes in the emission, which thus can provide information on the transport processes and excitation balances, are studied.

The first power relaxation experiments have been performed on arcs by GUREVICH and PODMOSHENSKII in 1963 [6]. Later experiments on arcs were done by been KAFROUNI *et al.* in 1979 [7]. Power modulations on ICPs were reported by PARISI and HIEFTJE [8] and by OLISEK and BRADLEY [9]. They modulated the plasma power with a sinusoidal or a quasi-rectangular wave. Farnsworth [10] was the first one (in 1985) who completely switched off the ICP

generator (for 200  $\mu\text{s}$ ). All these studies were focused on transport properties and therefore they measured the spatially delay of macroscopic disturbances, what we will refer to as the delayed response (cf. section 3.3). The work of BLYDDER and MILLER [11] and FEY *et al.* [12,13] also focused on the so-called instantaneous responses to power interruptions in ICPs. They were able to determine the ratio between  $T_e$  and  $T_h$ , and moreover, they obtained a lot of information on dominant excitation balances. Some of the results of FEY *et al.* will be given in section 3.3 in order to be able to compare results from the microwave induced plasmas studied in this paper to those obtained from ICPs.

In most laboratory plasmas, such as the microwave induced plasmas studied in this paper, the EM energy is mainly absorbed by free electrons, which on their turn heat the heavy particles. The cold surroundings finally cool these heavy particles. Schematically this energy transport can be depicted as

$$\{\text{EM field}\} \rightarrow \{\text{electrons}\} \rightarrow \{\text{heavy particles}\} \rightarrow \{\text{surroundings}\}.$$

Since the energy transfer from the electrons towards the heavy particles is a relatively inefficient process (due to the large difference in mass) and the cooling by the surroundings is rather efficient,  $T_h$  will remain substantially lower than  $T_e$ . As an example, for typical argon plasmas produced by the Torche à Injection Axiale, one of the plasma sources studied in this paper (cf. section 2.1),  $T_e$  is approximately  $2.2 \cdot 10^4$  K [26], whereas  $T_h$  does not exceed  $4 \cdot 10^3$  K [28].

A consequence of the energy transport balance is that after a power interruption, electrons will be influenced first. Within a very short time ( $< 1 \mu\text{s}$ ) they will largely thermalize with heavy particles and will therefore be significantly cooled down [12,13,22].

On different time scales, electrons will be quenched due to convection, diffusion and recombination processes and heavy particles will be cooled by the surroundings. Measurements performed on ICPs have shown that the electron density decay time due to recombination and diffusion is approximately 150  $\mu\text{s}$  [12]. For the MIPs discussed in this paper however, the decay time is expected to be significantly smaller due to the much smaller radial dimensions of the plasmas. By measuring the decay time of the plasma radiation after a power removal, more insight in the diffusion and convection processes can be obtained (cf. section 4.1).

Both electron cooling and electron quenching will induce changes in the plasma radiation that will be referred to as the *instantaneous response* to power interruption, since these changes occur within a few hundreds of  $\mu\text{s}$  after the PI. This in contrast to the so-called delayed response, which typically starts after 1 ms (cf. section 3.3).

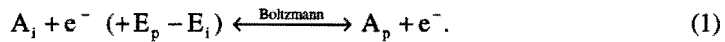
As will be discussed in section 4, electron quenching can provide information on transport processes as diffusion and convection, whereas electron cooling can give insight in excitation processes. In section 3.2 various excitation mechanisms will be given, which depend differently on  $T_e$  and  $T_h$ . By studying the time dependent behavior of atomic line or molecular band head intensities during power interruptions information can be obtained about the excitation mechanisms dominantly governing the atomic state distribution function (ASDF).

### 3.2 Excitation balances

There are several ways in which electronically excited species can be created as a result of interactions with other particles [12,13]. In this section we will concentrate on the creation of atomic species A or molecular species AX in the (radiative) electronic p-state (denoted as "A<sub>p</sub>" and "AX<sub>p</sub>" respectively). Considering power interruption experiments, especially the influence of T<sub>e</sub> on the production mechanisms of excited species is important, cf. section 3.2.3. Therefore, we distinguish between excitation mechanisms in which free electrons are involved and mechanisms that are completely governed by heavy particle interactions. In general the electron-induced balances show a strong dependence on T<sub>e</sub>, whereas heavy particle controlled mechanisms show (almost) no dependence on T<sub>e</sub>. The most dominant excitation mechanisms in both categories will be discussed separately.

#### 3.2.1 Electron governed excitation balances

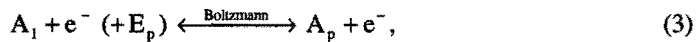
One of the most important population channels of A<sub>p</sub> is the excitation from a lower state i by electron collisions. Together with its inverse process this can be depicted as:



This will be referred to as the *Boltzmann* balance of excitation (to the right) and de-excitation (to the left). The energy that is required in the excitation process is equal to the difference between E<sub>p</sub> and E<sub>i</sub>, the excitation energies of the p- and i-level from the ground state. Since the kinetic energy of electrons is directly related to the electron temperature, this balance clearly is electron temperature dependent. If the Boltzmann balance is in equilibrium, the density n<sub>p</sub> of a heavy particle in the p-state is related to that of the density in the i-state n<sub>i</sub> by:

$$\frac{n_p^B}{g_p} = \frac{n_i^B}{g_i} \exp\left(-\frac{E_p - E_i}{kT_e}\right) \quad (2)$$

where g<sub>p</sub> and g<sub>i</sub> are the statistical weights of the levels in question and k the Boltzmann constant. For several analytes, e.g. Na and Zn, by far the most intense emission is coming from radiative levels that have rather low excitation energies with respect to the ground state and only direct excitation from the ground state needs to be considered. In this case Eqn 1 can be written as:

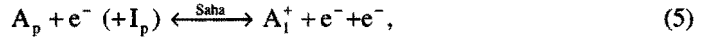


and Eqn 2 becomes:

$$\frac{n_p^B}{g_p} = \frac{n_1}{g_1} \exp\left(-\frac{E_p}{kT_e}\right) \quad (4)$$

A second important electron-controlled process is three-particle recombination. Especially highly excited (argon) levels that are close to the ion ground state are often populated by three-body recombination. Together with the corresponding inverse process of ionization this can be depicted as:





with  $A_1^+$  being a (ground state) ion and  $I_p$  the ionization energy from level  $p$ . This balance will be referred to as a *Saha* balance. If this balance is in equilibrium, and under the assumption that only neutral and singly ionized species are present (so that  $n_e = n_i$  with  $n_i$  being the ion density), the density of a level  $p$  will be given by:

$$\frac{n_p^s}{g_p} = \frac{n_e^2}{2g_+} \left( \frac{h^2}{2\pi m_e kT_e} \right)^{3/2} \exp\left( \frac{I_p}{kT_e} \right) \quad (6)$$

with  $g_+$  being the statistical weight of the ion ground state,  $n_e$  the electron density,  $m_e$  the mass of an electron and  $h$  Planck's constant. Obviously, also this balance is electron temperature dependent. As an example, the Thomson rate coefficient [39] is given, showing the strong dependence of 3-body recombination rate on  $T_e$ :

$$k_{\text{rec}}^{\text{Thomson}} \sim 3.3 \times 10^{-21} n_e^2 T_e^{-3/2} [\text{m}^6 \text{s}^{-1}]. \quad (7)$$

A third process in which electrons play a direct role is the *dissociative recombination* (DR) of molecular ions, which often results in at least one electronically excited particle:

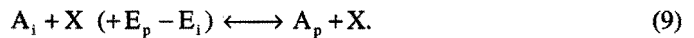


It is well known that certain excited states of some elements can be rather effectively populated by DR. In general cross-sections for DR (weakly) decrease with increasing electron temperature.

### 3.2.2 Heavy particle governed excitation balances

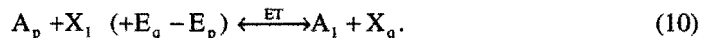
Several excitation balances can be distinguished which are ruled by heavy particle interactions. Although these balances have a varying dependence on the heavy particle temperature  $T_h$ , they have in common that they are (almost) independent of  $T_e$ .

Similar to the electron-ruled Boltzmann balance given in Eqn 1, particles can also be excited due to inelastic collisions with other (ground state) heavy particles. This so-called *Thermal excitation* by heavy particle  $X$  and the reverse process of de-excitation can be depicted as:



It should be noted that the internal energy difference between  $A_i$  and  $A_p$  should be overcome by changes in the kinetic energy of particles  $A$  and  $X$ , similar as for electrons in excitation processes ruled by the Boltzmann balance. If we consider excitation from  $A_1$ , thermal excitation will especially be important for high  $T_h$  and low  $E_p$  (i.e.  $<$  a few eV) and can be found in plasma regions with a low degree of ionization.

Another well-known excitation balance is the so-called *excitation transfer* (ET) balance:

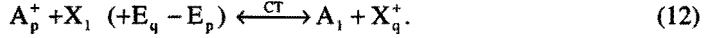


In practice this balance can only be relevant if the excitation energies of  $A_p$  and  $X_q$  are comparable. In case excitation transfer is the dominant populating mechanism of  $A_p$ , and the plasma is relatively close to equilibrium, the relevant densities will be related according to:

$$\frac{n_{A_p} n_{X_1}}{g_{A_p} g_{X_1}} \approx \frac{n_{A_1} n_{X_q}}{g_{A_1} g_{X_q}} \exp\left(\frac{E_q - E_p}{kT_h}\right), \quad (11)$$

in which all symbols have their usual meaning.

Comparable to the ET balance is the so-called *charge transfer* (CT) balance, given by:



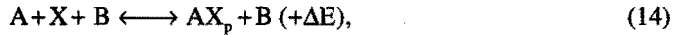
Obviously this balance can only be meaningful if the concerned p-state is an ion level.

Similar to Eqn 9, the relevant densities would be related as:

$$\frac{n_{A_p^+} n_{X_1}}{g_{A_p^+} g_{X_1}} \approx \frac{n_{A_1} n_{X_q^+}}{g_{A_1} g_{X_q^+}} \exp\left(\frac{E_q - E_p}{kT_h}\right) \quad (13)$$

in case CT is the only relevant mechanism.

When molecular species are considered, there are several additional routes to populate excited levels. Except by the mechanisms discussed before, molecules can directly be created in an electronically excited state as well. Excited molecules can be created in 3-body volume association processes [42]:



but also due to chemical reactions. A well-known example is the chemiluminescence radiation of  $\text{NO}_2$ , which can be directly created in an excited state [43].

Moreover, similar to Eqn 8, the dissociation of molecular complexes (possibly formed in chemical reactions) can directly create elements in excited states. Since dissociation can be induced both by heavy particles and electrons it is rather difficult to predict the influence of  $T_e$  on this mechanism.

### 3.2.3 The responses to PI-induced electron cooling

As discussed in section 3.2.2 processes like thermal excitation, excitation transfer and charge transfer are (almost) independent of  $T_e$ . Therefore, emission of levels that are populated by these mechanisms show (almost) no instantaneous response due to electron cooling. Only on a larger time scale changes will be observed due to heavy particle cooling.

However, if we compare the responses of levels that are populated by the electron-ruled Boltzmann balance and Saha balance, a remarkable difference can be observed.

First we will discuss the response of levels governed by the Boltzmann balance. If we consider direct excitation from the ground state (cf. Eqn 3) and the presence of Boltzmann equilibrium, the density of level p after the electron cooling will be given by (cf. Eqn 4):

$$\frac{n_p^{B*}}{g_p} = \frac{n_1^*}{g_1} \exp\left(-\frac{E_p}{kT_e^*}\right), \quad (15)$$

in which the parameters marked with an asterisk represent the situation after the cooling. Introducing  $\gamma = T_e/T_e^*$  and dividing the density before the temperature drop with the density immediately after the temperature drop, it can be derived that:

$$\ln \frac{n_p^B}{n_p^S} = -\frac{(\gamma-1)}{kT_e} E_p + \ln \frac{n_1^*}{n_1}, \quad (16)$$

in case of Boltzmann equilibrium. Since  $\gamma > 1$  and  $n_1^* \approx n_1$ , it can be seen that the density of excited state p will decrease due to the electron cooling. As a result, emission from level p will decrease as well.

Using the same procedure, it can be shown that for levels governed by the Saha balance, the relationship for densities after and before cooling is given by:

$$\ln \frac{n_p^{S^*}}{n_p^S} = \frac{(\gamma-1)}{kT_e} I_p + \frac{3}{2} \ln \gamma + \ln \frac{n_e^{*2}}{n_e^2} \quad (17)$$

If we assume that  $n_e^* \approx n_e$ , we obtain  $n_p^{S^*} > n_p^S$ . Opposite to levels that are populated by the Boltzmann balance, levels populated by 3-particle recombination therefore will show an increase of the emission as a result of electron cooling.

Similar, it is to be expected that intensities of excited species created by dissociative recombination processes will increase as well, since the cross-sections for DR increase when  $T_e$  drops. However, this trend has not been found in this study due to the absence of radiative levels that are dominantly populated by DR.

It should be noted that in general several mechanisms contribute to the population of a certain level. For instance, a temporary increase of the emission after the power removal due to 3-body recombination by no means indicates that the Saha-balance is the only population balance. Such a response we will therefore be referred to as "Saha-like" since the upward jump of the line intensity as a response to electron cooling, shows that the Saha-balance is significantly contributing to the population concerned level (immediately) after the power removal. Identically we will call an instantaneous decrease in intensity after PI a Boltzmann-like response.

### 3.3 Typical ICP responses explained

As mentioned in section 1, results will be compared to results that have been obtained from an ICP in the past [12,13]. Some typical power interruption responses of an ICP are given in figure 2. The Saha-like upward jump after power removal (at  $t=0$ ) of highly excited levels of argon (cf. figure 2a) can be attributed to Eqn 17. After this response due to electron cooling a gradual decay of the intensity can be observed, which is caused by diffusion and recombination of electrons. Typical decay times as a result of electron quenching are  $\tau_q(\text{ICP}) \approx 150 \mu\text{s}$ . When the power is switched on again (in this case after  $80 \mu\text{s}$ ), a sudden drop in the emission can be observed due to electron heating. This intensity drop can also be explained by Eqn 17, using  $\gamma < 1$ .

The Mg analyte on the other hand, shows a Boltzmann-like response to power interruptions (cf. figure 2c). The emission drop due to electron cooling (at “power-off”) and the upward jump due to electron heating (at “power-on”) are in agreement with Eqn 16. It should be noted that after electron cooling the emission remains almost constant during the power-off period, cf. figure 2c. In contrast to levels that are governed by the Saha-balance, populations of levels that are governed by the Boltzmann balance are only weakly dependent on the electron density. Moreover, since after the PI-induced cooling the electrons have a temperature of  $T_e^* \approx T_h$ , the more or less constant emission of Mg indicates that  $T_h$  remains constant during the time interval in which the power is switched off (approximately 80  $\mu$ s). Apparently, transport processes are rather slow in an ICP and typical time scales are significantly larger than 80  $\mu$ s.

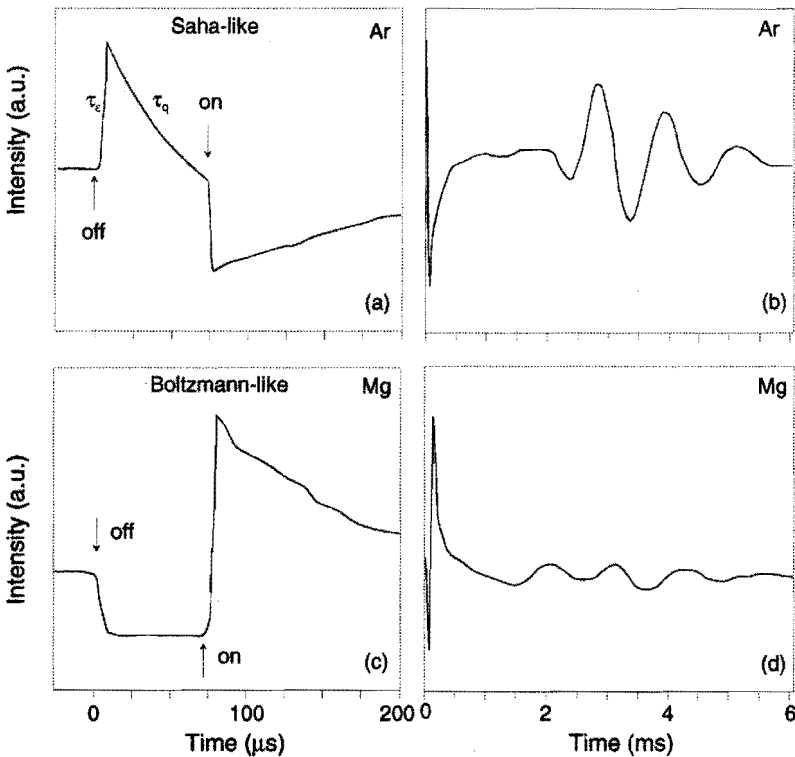


Figure 2 The instantaneous (a,c) and delayed (b,d) responses of two lines to power interruption as measured from an ICP. Graphs a and b show the response of an Ar 6-4p line at 549.6 nm whereas graphs c and d show the response of a Mg 3p3s $\rightarrow$ 3s3s line at 285.2 nm. The differences between a Saha-like (a) and a Boltzmann-like response (c) can clearly be distinguished. In figure 2a the time of the increase in line intensity due to electron cooling is two orders of magnitude smaller than the time constant reflecting the emission decay due to electron quenching ( $\tau_e \approx 1 \mu$ s and  $\tau_q \approx 150 \mu$ s respectively). This implies that electron cooling and quenching can easily be distinguished from each other. As we will see in section 4.1 this is not the case for plasmas produced by the TIA and MPT.

Apart from the instantaneous responses, on a larger time scale oscillations in the intensities can be observed (cf. figure 2b, 2d). These so-called delayed responses typically start a few ms after the power is switched on again and are believed to be caused by local disturbances in the plasma-generating zone in the vicinity of the induction coil. Since they travel downstream the plasma, the time of arrival of the delayed response varies in axial direction. By measuring the time of arrival at different axial positions in the plasma, the local drift velocity can be determined. Typical experimentally found values are  $10\text{--}12\text{ ms}^{-1}$ , which agree quite well with velocities obtained by studying the propagation of small gas pulses [13].

## 4. Experimental results

### 4.1 General findings from the power interruption measurements

The first series of power interruption experiments are performed on pure argon discharges created by the TIA. An example of a typical response of an argon line ( $4p \rightarrow 4s$ ) is given in figure 3 on the left. It gives the response to PI at a height of 2 mm above the nozzle (AN). When the power is switched off, a steep Saha-like upward jump can be distinguished, immediately followed by a decay of the emission due to electron diffusion, recombination and/or convection losses. Thus, the Saha-like upward jump due to electron cooling as described by Eqn 17 is just as in ICPs [12] clearly present in the pure Ar-TIA.

The decay time of the argon radiation is in the order of  $2\text{--}5\ \mu\text{s}$ , which is much faster than typical decay times in ICPs ( $\tau_q(\text{ICP}) \approx 150\ \mu\text{s}$ ). This is largely due to the significantly smaller radial dimensions of the TIA. As a result, diffusion, recombination and convection losses are much larger in the TIA. It should be noted that in contrast to the ICP, the time scales for electron cooling and electron quenching are comparable and that a separate study of both effects is hardly possible. Moreover, it should be realized that the decay time of the microwave generator (i.e. the time elapsed between "power off" and reaching 10% of the original power) is  $1\text{--}2\ \mu\text{s}$  and will contribute to the measured emission decay time  $\tau_q(\text{TIA})$ . In order to perform measurements with a higher accuracy and possibly obtain more information on differences in the time scales of electron cooling and quenching, therefore a MCS with a better time resolution (currently  $2\ \mu\text{s}$ ) and the generator with a faster decay should be used.

A sharp increase of the argon line intensity can be observed at the re-ignition of the power. This Boltzmann-like electron heating jump is totally different from the Saha-like downward heating jump that was observed for argon lines in the ICP (cf. figure 2a). As can be seen from figure 3a, the emission intensity, and thus the electron density in TIA plasmas drops towards a very low level during the "power off" state, and therefore the plasma has to be ignited again when the power level is restored. This process is dominated by electron excitation and therefore Boltzmann-like. In the experiments performed on the ICP however, argon line emission was still rather strong when the power was switched on again.

The oscillations that can be observed in figure 3a when the power is restored are probably caused by internal impedance changes of the plasma and are not yet fully understood. These

oscillations should not be confused with the delayed responses that will be discussed in section 4.5.

In a pure argon plasma, all argon lines show a Saha-like response to power interruption. However, when an aerosol is introduced into the argon plasma with a cross-flow nebulizer [1], the Saha-like response has completely disappeared and the response has become Boltzmann-like (cf. figure 3 on the right). Obviously, the introduction of an aqueous analyte induces measurable changes in the excitation mechanisms. More power interruption measurements on argon discharges with analyte injection will be presented in the next sections.

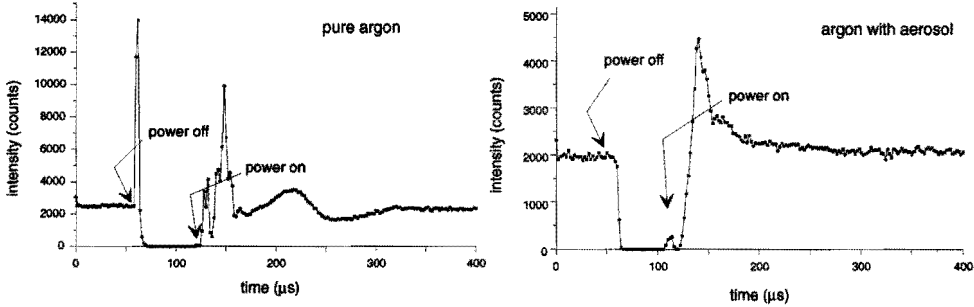


Figure 3. Typical emission intensities of an argon line during power interruption experiments (763.51 nm,  $4p \rightarrow 4s$ ) measured at 2 mm above the nozzle (AN) in the ionizing part of the TIA. On the left the response from a pure argon discharge, on the right from a plasma with aerosol injection.

As already noted, the fast emission decay times in the TIA suggest high electron diffusion, recombination or convection losses rates (at least just above the nozzle in the ionizing part of the plasma, where the responses given in figure 2 are measured).

If diffusion will be the main loss channel for electrons, the time scale  $\tau$  in which the plasma decays can be approximated by:

$$\tau = \frac{\Lambda^2}{D_a}, \quad (18)$$

with  $\Lambda$  being the plasma gradient length and  $D_a$  the diffusion rate. Plasmas produced by the TIA have a hollow profile and as a consequence, the gradient length is rather small. Experimentally it is found that the gradient length is in the order of  $\Lambda = 1 \cdot 10^{-4}$  m [28]. Using  $D_a = 1 \cdot 10^{-3}$  m<sup>2</sup>s<sup>-1</sup> [26], we obtain  $\tau = 1 \cdot 10^{-5}$  s, which is somewhat larger than the decay time that can be obtained from figure 3. Therefore it can be expected that convection or recombination play an important role as well. This is in agreement with the work of JONKERS *et al.* [26,28], who suggest that the dissociative recombination of  $N_2^+$ , being created by charge transfer of  $N_2$  with  $Ar^+$ , is an effective electron loss channel for plasmas created by the TIA.

#### 4.2 Transport properties derived from responses of different species

In analytical chemistry, usually plasmas are used in which aqueous aerosols are injected. As discussed in the previous section, the injection of water changes the response of argon lines from partly Saha-like to completely Boltzmann-like. It is interesting to investigate the responses of other species, especially analytes, as well. Studies have been performed on argon discharges produced by the TIA in which aerosols containing zinc and sodium were injected. The responses of the 8 lines listed in table 2 have been measured at three different heights in the plasma (cf. figure 4):

1. In the ionizing part just above or at 2 mm above nozzle (AN), where it is known from the experiments of JONKERS *et al.* [26,28] that for pure argon plasmas  $n_e$  and  $T_e$  are high ( $3 \cdot 10^{21} \text{ m}^{-3}$  and  $2.2 \cdot 10^4 \text{ K}$ ), whereas  $T_h$  is rather low ( $< 10^3 \text{ K}$ ).
2. In the central part of the plasma at 10 mm AN, which is found to be optimum excitation zone for most analytes [32,39]. For pure argon plasmas it was found that  $T_e \approx 1.8 \cdot 10^4 \text{ K}$ ,  $T_h \approx 4 \cdot 10^3 \text{ K}$  and  $n_e \approx 10^{20} \text{ m}^{-3}$ .
3. In the recombining part at 20 mm AN, where the electron density is very low (below our detection limit of the  $H\beta$  emission line broadening method, approximately  $10^{18} \text{ m}^{-3}$ ), whereas the heavy particle temperature exceeds  $4 \cdot 10^3 \text{ K}$ .

Results are given in figure 5.

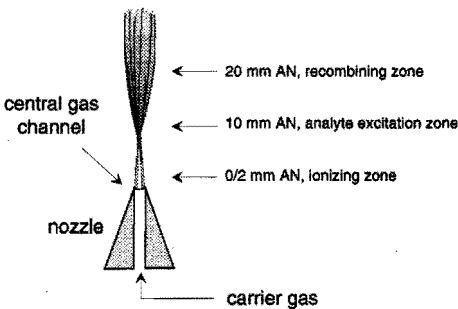
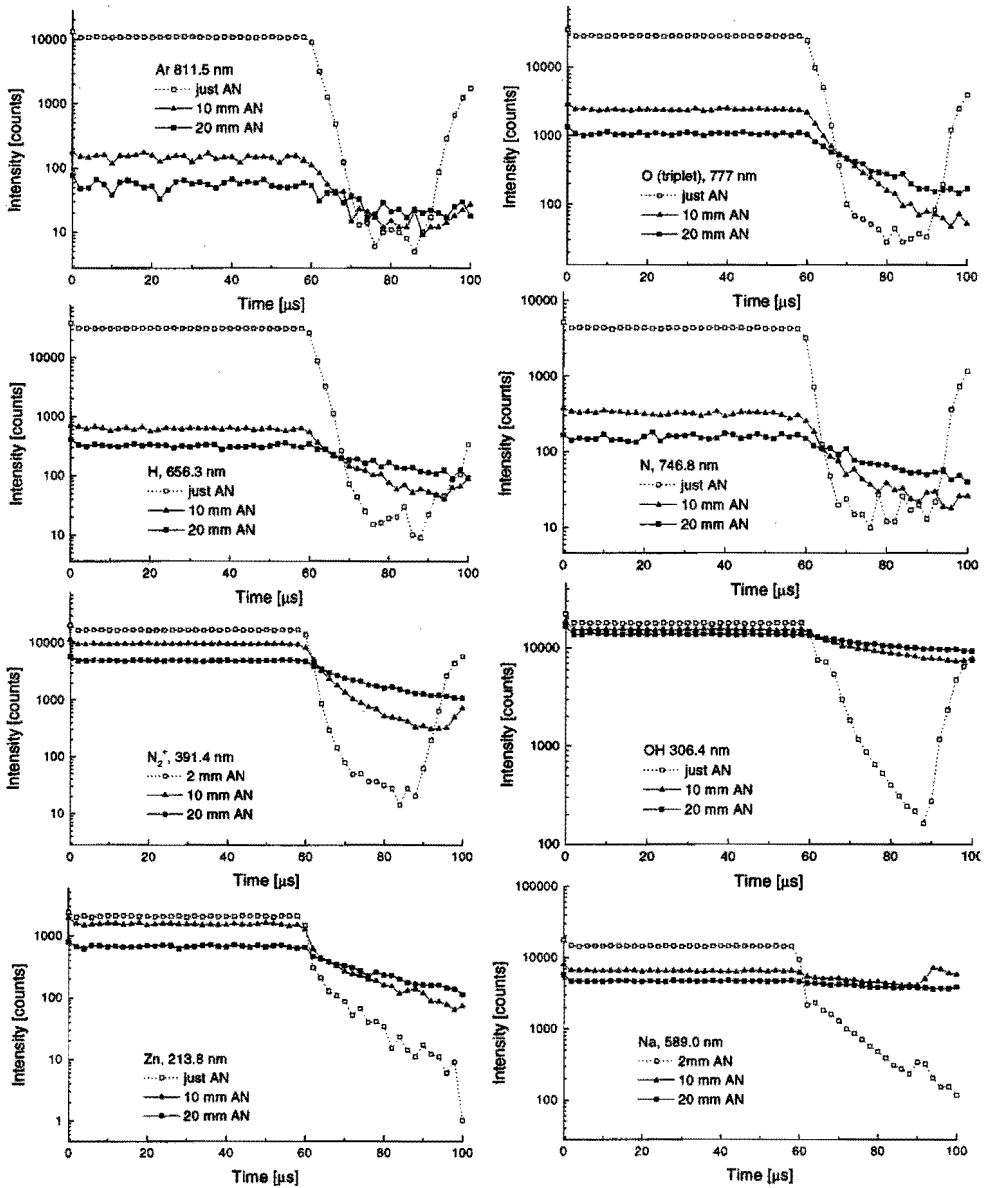


Figure 4.

The three different axial positions at which the measurements presented in figure 5 have been obtained (0 or 2 mm AN, 10 mm AN and 20 mm AN). As can be seen, the measurements have been performed in different plasma zones.

element	wavelength [nm]	transition	energy [eV]
Ar	811.53	4p → 4s	13.08 → 11.55
O	777.44	3p → 3s	10.74 → 9.14
H	656.28	3d → 2p	12.09 → 10.20
N	746.83	3p → 3s	11.99 → 10.34
N <sub>2</sub> <sup>+</sup>	391.44	B <sup>2</sup> Σ <sub>v</sub> <sup>+</sup> → X <sup>2</sup> Σ <sub>g</sub> <sup>+</sup>	3.17 → 0
OH	306.36	A <sup>2</sup> Σ <sup>+</sup> → X <sup>2</sup> Π	4.46 → 0
Zn	213.86	4p → 4s	5.80 → 0
Na	589.00	3p → 3s	2.10 → 0

Table 2. Observed lines during PI measurements with water or aqueous analyte introduction.



**Figure 5.** Responses of emission lines from argon, oxygen, hydrogen, nitrogen, the OH radical,  $N_2^+$ , zinc and sodium, measured at three different heights in the TIA (just or 2 mm AN, 10 mm AN and 20 mm AN). A zinc- and sodium-containing aerosol has been introduced into the argon plasma during all measurements. It should be noted that the intensities of different elements cannot be compared mutually.

From figure 5 it can be seen that power interruption has the strongest influences in the ionizing part of the plasma, resulting in the shortest decay times and relatively strongest drops



in the emission. These decay times significantly increase in the analyte excitation zone and increase even further in the recombining part of the plasma. It should be noticed that for all measurements (except for the zinc measurements) the power was switched on again at  $t=90 \mu\text{s}$ . This explains the upward Boltzmann-like jump after  $90 \mu\text{s}$  for the measurements just above the nozzle. At the more downstream positions however, the re-ignition hardly has any instantaneous influence.

Some striking differences can be observed between elements with relatively high excitation energies (Ar, O, N, H) and elements with lower excitation energies (OH, Zn, Na). From the steady state emission (i.e.  $t < 60 \mu\text{s}$ ) it can be seen that the population of levels with high excitation energies rapidly decreases outside of the ionizing zone. For levels with low excitation energies (including  $\text{N}_2^+$ ) this sharp decrease in intensity as function of the axial position is not present. Since  $\text{H}_\beta$  emission line broadening measurements have shown that even in pure argon plasmas electron densities are below  $10^{18} \text{ m}^{-3}$  at 20 mm AN, this suggests that these species are downstream excited by an electron-independent excitation mechanism. Moreover, if the responses are compared at all axial positions separately, at all heights highly excited levels show a relatively strong PI response. Apparently, these levels are mainly populated by electron-dominated processes. Levels with low excitation energies show hardly any or even no response to power interruptions in the central plasma part and in the recombining zone. This indicates once more that these levels are being populated by heavy particles dominated mechanisms.

The decay time of the heavy particle temperature  $\tau_{T_h}$  when the power is interrupted can be estimated numerically from the conduction and convection losses.

The decay time due to conduction ( $\tau_{\text{cond}}$ ) can be estimated from:

$$\lambda \nabla^2 T_h = -C \frac{\partial T_h}{\partial t} = -\frac{3}{2} n_1 k \frac{\partial T_h}{\partial t}, \quad (19)$$

with  $\lambda$  being the heat conductivity coefficient and  $C$  the heat capacity.

From Eqn 19 it can be derived that:

$$\tau_{\text{cond}} \approx \frac{3}{2} n_1 k \Lambda^2 \lambda^{-1}, \quad (20)$$

with  $\Lambda$  the characteristic plasma radius.

When considering the situation at 10 mm AN, typical values are given by  $\Lambda=2.5 \cdot 10^{-3} \text{ m}$ ,  $\lambda=1 \text{ Wm}^{-1}\text{K}^{-1}$  and  $n_1=2 \cdot 10^{24} \text{ m}^{-3}$  (calculated from the equation of state for a pressure of  $p=1 \cdot 10^5 \text{ Pa}$  and a gas temperature of  $4 \cdot 10^3 \text{ K}$  [28]), so that a conduction time constant of  $\tau_{\text{cond}} \approx 3 \cdot 10^{-4} \text{ s}$  is found.

The convection term is given by:

$$\nabla \cdot \left( \frac{5}{2} n_1 k T_h v \right), \quad (21)$$

with  $v$  being the axial velocity, so that:

$$\nabla \cdot \left( \frac{5}{2} n_1 k T_h v \right) = -\frac{3}{2} n_1 k \frac{\partial T_h}{\partial t}, \quad (22)$$

and the convection time constant ( $\tau_{\text{conv}}$ ) can be estimated by :

$$\tau_{\text{conv}} \approx \frac{3 \Lambda_z}{5 v} \quad (23)$$

At 10 mm AN the axial velocity is typically given by  $v=15-20 \text{ ms}^{-1}$ . The characteristic length  $\Lambda_z$  is more difficult to determine, but if we assume that  $\Lambda_z$  is in the order of a few mm, we find that  $\tau_{\text{conv}} \approx 2 \cdot 10^{-4} \text{ s}$ , which is of the same order as the heavy particle decay time due to conduction.

The heavy particle temperature decay time  $\tau_{\text{Th}}$  will be a combination of these decay times and will approximately be given by:  $\tau_{\text{Th}} \approx 2 \cdot 10^{-4} \text{ s}$ .

If we assume that in the central part and in the recombining zone of the plasma the upper levels of the measured Zn and Na transitions are populated by thermal excitation, cf. Eqn. 9, the emission decay times can be related to the decay time constant of  $T_h$ .

In the case that thermal excitation prevails and the corresponding balances equilibrate (cf. Eqn 9), the density of excited species  $n^*$  can be written as:

$$n^* = \frac{g^*}{g_1} n_1 \exp\left(-\frac{\Delta E}{kT_h}\right) \quad (24)$$

so that:

$$\ln n^* = C - \frac{\Delta E}{kT_h}, \quad (25)$$

with  $C = \ln\left(\frac{g^*}{g_1} n_1\right)$  being constant.

Differentiation with respect to time gives:

$$\frac{\partial(\ln n^*)}{\partial t} = \frac{\Delta E}{kT_h^2} \frac{\partial(T_h)}{\partial t} = \frac{\Delta E}{kT_h} \frac{\partial \ln(T_h)}{\partial t}, \quad (26)$$

so that the following approximate relationship between the heavy particle cooling time and the emission decay time can be established:

$$\tau_n \approx \frac{kT_h}{\Delta E} \tau_{\text{Th}}, \quad (27)$$

If we again consider the emission at 10 mm AN (and thus  $kT_h \approx 0.4 \text{ eV}$ , see below Eqn 20), we find  $\tau_{\text{Na}^*} \approx 38 \mu\text{s}$  and  $\tau_{\text{Zn}^*} \approx 14 \mu\text{s}$ , using  $\Delta E = 2.1 \text{ eV}$  for Na and  $\Delta E = 5.8 \text{ eV}$  for Zn.

Since both approximated decay times are in reasonable agreement with the measurements, as can be seen from figure 5, thermal excitation indeed seems a possible mechanism for low excited levels in the analyte excitation zone and recombining part of the plasma.

Apart from thermal excitation there are a few other mechanisms which are rather insensitive to power interruptions that may contribute to the rather intense analyte emission the recombining zone of the plasma. Charge transfer will not have a significant influence

since the electron density (and thus the ion density) is very low in the recombining zone. The excitation transfer balance (cf. Eqn 10) is a better candidate. Due to the low electron density in this zone only metastable levels are possibly highly populated. The most likely metastable species present in the afterglow are Ar(4s), having an internal energy of 11.55 or 11.71 eV, N<sub>2</sub>(A) at 6.18 eV, N(<sup>2</sup>P) at 2.38 and N(<sup>2</sup>D) at 3.57 eV. The metastable nitrogen atoms or molecules can result from air entrainment, which recently has been demonstrated to be important for argon plasmas created by the TIA [28,30]. The radiative lifetimes of the given metastable levels are typically 1 s and once created in the active zone of the plasma they can be transported downstream provided that they are not being quenched by collisions with electrons or heavy particles. However, due to the presence of active quenching species (like atomic oxygen) and the short mean free path of heavy particles in atmospheric microwave discharges the penetration depth of at least argon metastables probably will be negligible. Moreover, since excitation transfer from metastables cannot explain the different decay times for the various elements during PI, also the influence of atomic and molecular nitrogen seems limited. In addition, the agreement of the measurements with the relationship between the heavy particle temperature decay time given by Eqn 27 and the emission decay times of Na and Zn strongly suggests that a heavy particle temperature governed balance as thermal excitation is the dominant process

Another process that may contribute to the strong analyte emission is excitation by vibrationally excited molecules. It is likely that in the recombining plasma zone the so-called vibrational temperature (that can be determined from the population distribution of vibrational states) equals the gas temperature due to the high pressure. Therefore thermal excitation and excitation by vibrationally excited molecules cannot be distinguished by the power interruption experiments and additional research would be necessary to study the contribution of vibrationally excited molecules.

### **4.3 Influence of molecular gas additives**

As was discussed in section 4.1, in case of aerosol injection, even just above the nozzle responses of all studied lines were Boltzmann-like. A typical aerosol injection rate used for the TIA is 5 ml·hr<sup>-1</sup> of liquid, which corresponds to a molecular gas flow of approximately 0.1 l·min<sup>-1</sup>. It is interesting to investigate plasmas with a smaller molecular load, in order to study the transition from a Saha-like to a Boltzmann-like response. Therefore power interruption measurements have been performed on mixtures of argon with small carbon dioxide additives. No analyte or aerosol has been introduced during these measurements.

In figure 6 the ratio of the maximum height of the Saha-like upward jump versus the steady-state emission is depicted for various emission lines as a function of the additional CO<sub>2</sub> flow (ranging from 0 - 0.05 l·min<sup>-1</sup>) as measured at 4 mm AN. It should be noted that if this ratio becomes unity this corresponds to the situation that the Saha-like behavior has disappeared (cf. the sketches in the figure). Emission from levels with a relatively low excitation and high ionization energy (e.g. levels of C and CN) show no or hardly any Saha-like upward jump. Apparently these levels are mainly ruled by the Boltzmann balance.

Species with high excitation energies and which are relatively close to the ionization potential (e.g. levels Ar and O) only show a significant Saha-jump when no additional CO<sub>2</sub> is added. After the addition of CO<sub>2</sub> the height of the Saha-jump rapidly decreases and even if only 0.5% of the plasma gas is carbon dioxide, the Saha-like jump has already vanished completely and the response to power interruption becomes fully Boltzmann-like. Since the rate of recombination processes (and thus the height of the Saha-like jump) depends on  $n_e$ , this might indicate that the electron density is significantly lower with molecular gas injection. A possible extra loss channel for electrons is dissociative recombination of molecular ions created by charge transfer with argon ions.

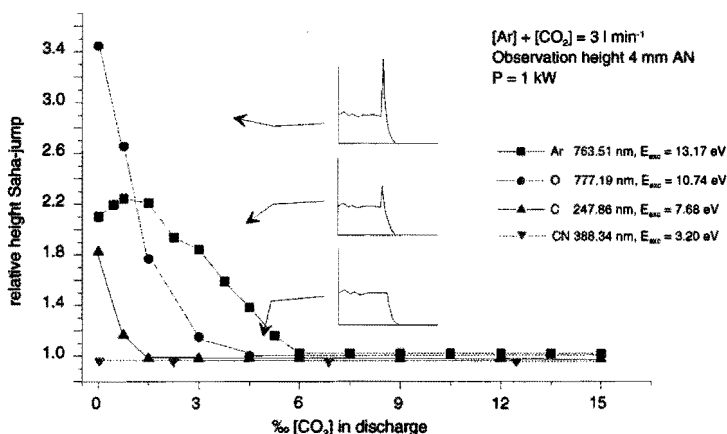


Figure 6. The relative height of the Saha-jump for an argon, an oxygen and a carbon line and a CN band head as a function of the amount of CO<sub>2</sub> added to the argon discharge. It should be noted that if this height equals unity the response to power interruption is Boltzmann-like.

#### 4.4 The TIA and the MPT compared

There are two major differences between the two plasma sources under study, TIA and the MPT:

- The MPT contains two separate gas channels: similar to the ICP analytes are introduced through the central channel whereas pure argon is supplied through the outer channel. The TIA only has one channel and the argon and analyte are mixed before entering the plasma.
- The MPT typically consumes only 0.5 l·min<sup>-1</sup> of argon whereas the TIA typically consumes 3 l·min<sup>-1</sup>. At these latter high gas flows the plasma usually is turbulent, which induces a strong inward flux of ambient air [28]

It is interesting to study whether power interruption experiments on plasmas produced by both torches lead to significantly different observations. It can be expected that the above differences lead to lower diffusion, conduction and convection rates in the MPT than in the TIA.

In figure 7 typical instantaneous hydrogen responses are given from a MPT argon discharge with a small water load injection. As can be seen, the response changes from Saha-like close to the nozzle to Boltzmann-like further downstream.

Typical  $1/e$  emission decay times are comparable to times found for the TIA and are largely determined by the resolution of the MCS ( $2 \mu\text{s}$ ) and the decay time of the generator. However, since this decay time is also partly determined by diffusion and other electron loss processes and no significant differences in the decay times between the TIA and the MPT are measured, this suggests that both plasmas are comparable with respect to these loss processes. This can be understood from considerations with respect to the skin depth  $\delta$ , given by:

$$\delta = \sqrt{\frac{2}{\mu_0 \mu_r \omega \sigma}}, \quad (28)$$

with  $\mu_0$  and  $\mu_r$  the relative and vacuum magnetic permeability,  $\omega$  the angular frequency and  $\sigma$  the conductivity. Typical parameters are given by  $\mu_r \approx 1$  and  $\sigma \approx 10^4 \Omega^{-1}\text{m}^{-1}$  (for argon discharges with  $n_e \approx 3 \cdot 10^{21} \text{ m}^{-3}$  and  $T_e \approx 2.2 \cdot 10^4 \text{ K}$  [44]). Because both plasmas are operated at the same frequency (2.45 GHz), the skin depths are comparable and given by  $\delta \approx 0.1 \text{ mm}$ . This small skin depth is one of the main reasons for the small plasma diameter and strong gradients in both plasmas and largely determines the fast electron density quenching after PI.

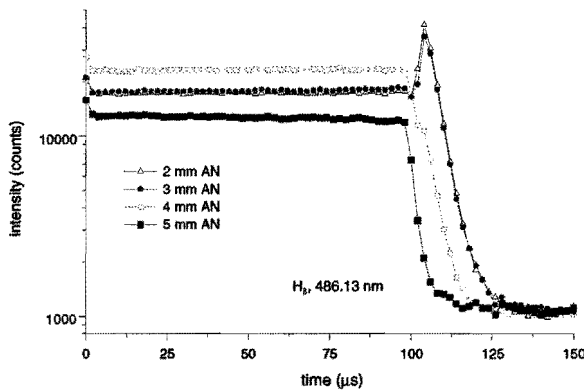


Figure 7.

*The decay of hydrogen emission at different heights in the MPT. A small water load was supplied to the plasma in order to enhance  $H_{\beta}$  emission. It can be observed that the response to electron cooling changes from Saha-like close to the nozzle to Boltzmann-like further downstream.*

#### 4.5 Determination of the axial flow velocity

Apart from the instantaneous responses discussed in the previous sections due to electron cooling and quenching, often a delayed response can be distinguished that very likely is caused by strong local disturbances in the ionizing part of the plasma during power interruptions. These disturbances are transported downstream the plasma with the (local) average axial gas velocity and cause deviations in the plasma emission. As discussed in section 3.3, the time arrival of the delayed response therefore can be used to determine the gas velocity. An example of some responses of Na emission measured at different axial positions of the TIA is given in figure 8. On the right the deduced gas velocities from these and additional responses are given. It should be noted that in the ionizing plasma part it is hardly

possible to determine the velocity since here the “delayed” and instantaneous responses coincide.

The axial gas velocities have been determined from the delayed responses of other elements (Zn, H and O) and the OH radical as well. In the recombining zone velocities between 12 and 18  $\text{ms}^{-1}$  are found, which is in reasonable agreement with the values given in figure 8. In the ionizing zone, the velocities seem substantially higher, although usually the delayed responses cannot be resolved from the instantaneous responses with satisfactory precision in this region. An exception has to be made for  $\text{H}_\alpha$  emission, from which velocities are deduced of approximately 29  $\text{ms}^{-1}$  at 5 mm AN and 26  $\text{ms}^{-1}$  at 7 mm AN.

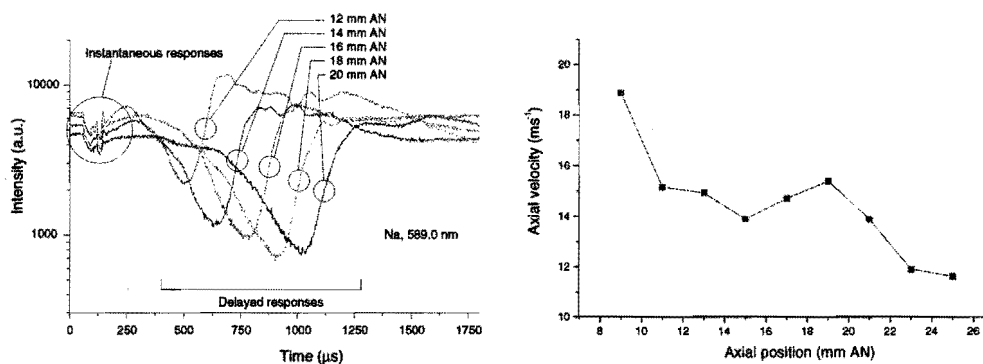


**Figure 8.** *On the left the delayed responses of a sodium analyte line at five different axial positions of a plasma produced by the TIA. The times of arrival of these responses can be used to calculate the local average flow velocities. Deduced velocities (from the shown examples on the left and some additional responses) are given in the figure on the right. It should be noted that in the ionizing part of the plasma this method cannot be used since the instantaneous and delayed responses overlap, whereas far downstream ( $>22$  mm AN) large error margins are induced by spreading and weakening of the shape of the responses.*

The delayed responses from argon are too weak for velocity determinations, but it can be expected that they correspond to the values as found for other elements. The experiments were done with an argon flow of 3  $\text{l}\cdot\text{min}^{-1}$  and a nozzle diameter of 1.8 mm so that the initial flow velocity was 20  $\text{ms}^{-1}$ , which is more than the typical axial gas velocities found downstream, but lower than the axial velocities in the ionizing zone. The large velocity difference between the ionizing and recombining part is probably due to an increasing (outward) radial gas flow. This outward flux can also explain the strong increase of the plasma diameter from typically 1 mm in the ionizing zone to approximately 1 cm in the recombining zone.

It should be mentioned that, unlike for the ICP, in the studied microwave discharges a delayed response is not always observed [20]. Moreover, sometimes the shape of the delayed responses has changed during the propagation to such an extent that it was not possible to obtain any useful information from them. So far, we have no conclusive explanation for these phenomena.

## 5. Conclusions

Atmospheric microwaves induced argon plasmas with and without analyte injection produced by the TIA (Torche à Injection Axiale) and the MPT (Microwave Plasma Torch) have been exposed to so-called power interruption experiments. By studying the intensities of emission lines during a short temporary power removal, information has been obtained on transport properties and excitation mechanisms of radiative levels.

In the ionizing part of the plasmas, intensities of highly excited (argon) levels dropped very fast towards a negligible level (typically in 3-6  $\mu\text{s}$ ), which is in sharp contrast to earlier measurements performed on an ICP ( $\tau \approx 150 \mu\text{s}$ ). This shows that diffusion and convection losses are much larger in the investigated microwave discharges, probably mainly due to the smaller plasma dimensions and the larger gradients. Despite the differences in dimensions and operational settings between the TIA and the MPT no major differences between these two plasma sources have been observed during power interruption experiments.

From calculations of the conduction and convection losses in the plasma, a decay time of the heavy particle temperature  $T_h$  in the order of  $2 \cdot 10^{-4}$  s is estimated. From a simple model a relationship has been established between this decay time and the emission decay time of radiative levels that are populated by thermal excitation. Since the measured emission decay times of Na and Zn in the recombining zone are in reasonable agreement with the decay times predicted by the model, it is likely that thermal excitation is the dominant analyte excitation process in those plasma regions with intense analyte emission and low electron density.

It is found that after the introduction of small amounts of molecular gases into argon discharges (i.e. more than 0.5% of  $\text{CO}_2$  compared to the argon carrier gas) the instantaneous responses of line intensities due to electron cooling are Boltzmann-like for all species, even for the argon lines. In argon discharges without molecular gas or aerosol introduction on the other hand, the responses to electron cooling of emission lines with high excitation energies are clearly Saha-like. This suggests that the presence of molecular species reduces the electron density in steady state operation.

During the (short) power interruptions the plasma is severely disturbed in the ionizing part of the plasma. This disturbance travels downstream the plasma with the axial gas velocity and causes a delayed response of the emission intensity in the central and recombining zone. From the time of arrival of this delayed response the local axial velocity can be determined. Typical results are 12-18  $\text{ms}^{-1}$  in the recombining zone and higher values ( $\sim 25 \text{ms}^{-1}$ ) more upstream.

## Acknowledgements

The authors would like to thank Prof. D.C. Schram for his fruitful discussions. Financial support was given by the Eindhoven Centre Technology for Sustainable Development (TDO) and by the Dutch Technology Foundation (STW).

## References

1. P.W.J.M. Boumans, "Inductively coupled plasma emission spectroscopy", part 2: "Applications and fundamentals", John Wiley & Sons, New York (1987).
2. A. Montaser, *CRC Critical Rev. Anal. Chem.* **18**(1), 45 (1987).
3. R.E. Sturgeon, S.N. Willie and V.T. Luong, *Spectrochim. Acta* **46B**, 1021 (1991).
4. H. Matusiewicz, *Spectrochim. Acta* **47B**, 1221 (1992).
5. Q. Jin, Y. Duan and J.A. Olivares, *Spectrochim. Acta*, **52B**, 131 (1997).
6. D.B. Gurevich and I.V. Podmoshenskii, *Opt. Spectrosc.* **15**, 319 (1963).
7. H. Kafrouni, J.M. Bagneux, A. Gleizes and S. Vacquie, *J. Quant. Spectrosc. Radiat. Transfer* **21**, 457 (1979).
8. A.F. Parisi and G. M. Hieftje, *Appl. Spectrosc.* **40**, 181 (1986).
9. J.W. Olesik and K. R. Bradley, *Spectrochim. Acta* **42B**, 377 (1987).
10. P. B. Farnsworth, *Appl. Spectrosc.* **39**, 1078 (1985).
11. E.L. Bydder and G.P. Miller, *Spectrochim. Acta* **43B**, 819 (1988).
12. F.H.A.G. Fey, W.W. Stoffels, J.A.M. van der Mullen, B. van der Sijde and D.C. Schram, *Spectrochim. Acta* **46B**, 885 (1991).
13. F.H.A.G. Fey, "Excitation balances and transport in an inductively coupled plasma", Ph.D. Thesis, Eindhoven University of Technology, The Netherlands (1993).
14. D.S. Hanselman, N.N. Sesi, M. Huang and G.M. Hieftje, *Spectrochim. Acta* **49B**, 495 (1994).
15. S. Long, R. Browner, *Spectrochim. Acta* **43B**, 1461 (1988).
16. S. Nowak, J.A.M. van der Mullen, A.C.A.P. van Lammeren and D.C. Schram, *Spectrochim. Acta* **44B**, 411 (1989).
17. J.F. Alder, R.M. Bombelka and G.F. Kirkbright, *Spectrochim. Acta* **35B**, 163 (1980).
18. B.L. Caughlin and M.W. Blades, *Spectrochim. Acta* **42B**, 353 (1987).
19. P.S. Moussounda and P. Ranson, *Spectrochim. Acta* **40B**, 641 (1985).
20. E.A.H. Timmermans, I.A.J. Thomas, J. Jonkers, J.A.M. van der Mullen and D.C. Schram, *Fresenius J. Anal. Chem.* **362**(5), 440 (1998).
21. J.A.M. van der Mullen and J.M. de Regt, *Fresenius J. Anal. Chem.* **355**, 532 (1996).
22. J.M. de Regt, "Fundamentals of inductively coupled plasmas: a spectroscopic study", Ph.D. Thesis, Eindhoven University of Technology, The Netherlands (1996).
23. J.M. De Regt, J.A.M. van der Mullen and D.C. Schram, *Phys. Rev. E* **52**, 2982 (1995).
24. M. Moisan, G. Sauvé, Z. Zakrzewski and J. Hubert. *Plasma sources, Sci. and Techn.* **3**, 584 (1994).
25. A. Ricard, L. St-Onge, H. Malvos, A. Gicquel, J. Hubert and M. Moisan, *J. Phys. III France* **5**, 1269 (1995).
26. J. Jonkers, L.J.M. Selen, J.A.M. van der Mullen, E.A.H. Timmermans and D.C. Schram, *Plasma Sources, Sci. and Techn.* **6**, 533 (1997).
27. J. Jonkers, J.M. De Regt, J.A.M. van der Mullen, H.P.C. Vos, F.P.J. de Groot and E.A.H. Timmermans *Spectrochim Acta* **51B**, 1385 (1996).
28. J. Jonkers, "Excitation and transport in small scale plasmas", Ph.D. Thesis, Eindhoven University of Technology, The Netherlands (1998).



29. A. Rodero, M.C. Quintero, A. Sola and A. Gamero, *Spectrochim. Acta*, **51B**, 467 (1996).
30. *Chapter 4 of this thesis*, E.A.H. Timmermans, I.A.J. Thomas, J. Jonkers, A. Rodero, M.C. Quintero, A. Sola, A. Gamero and J.A.M. van der Mullen, *Spectrochim. Acta* **53B**, 1553 (1998).
31. Q. Jin, F. Wang, C. Zu, D.M. Chambers and G.M. Hieftje, *J. Anal. At. Spectrom.* **5**, 487 (1990).
32. Q. Jin, C. Zhu, M.W. Borer and G.M. Hieftje, *Spectrochim. Acta* **46B**, 417 (1991).
33. A.M. Bilgic, C. Prokisch, J.A.C. Broekaert and E. Voges, *Spectrochim. Acta* **53B**, 773 (1998).
34. Y. Duan, Y. Li, X. Tian, H. Zhang and Q. Jin, *Anal. Chim. Acta* **295**, 315 (1994).
35. Y.X. Duan, X.G. Du, Y.M. Li and Q.H. Jin, *Appl. Spectrosc.* **49**, 1079 (1995).
36. D.M. Ye, H.Q. Zhang and Q.H. Jin, *Talanta* **43**, 535 (1996).
37. Q. Jin, H.Q. Zhang, F. Liang, W.J. Yang and Q.H. Jin, *J. Anal. At. Spectrom.* **11**, 331 (1996).
38. Q. Jin, W. Yang, F. Liang, H. Zhang, A. Yu, Y. Cao, J. Zhou and B. Xu, *J. Anal. At. Spectrom.* **13**, 377 (1998).
39. C. Prokisch and J.A.C. Broekaert, *Spectrochim. Acta* **53B**, 1109 (1998)
40. E.A.H. Timmermans, J. Jonkers, J.A.M. van der Mullen and D.C. Schram, "Microwave induced plasmas for the analysis of molecular compounds in incinerator gases", Progress in Plasma Processing of Materials 1997, Proceedings of the TPP4 conference, July 15-18 1996 Athens, Begell House inc., 299 (1997).
41. *Chapter 3 of this thesis*, E.A.H. Timmermans, F.P.J. de Groote, J. Jonkers, D.C. Schram and J.A.M. van der Mullen, "Atomic emission spectroscopy for the on-line monitoring of incinerator processes", *submitted for publication in J. Anal. At. Spectrom.* (1999).
42. L.M. Biberman, V.S. Vorob'ev and I.T. Yakubov, *Soviet Phys. Usp.* **15**, 292 (1973).
43. J.C. Greaves and D. Gravin, *J. of Chem. Phys.* **34**, 348 (1961).
44. J. Aubreton, C. Bonnefoi and J.M. Mexmain, *Rev. Phys. Appl.* **21**, 365 (1986).

# 7

## The behavior of argon $4s^3P_2$ metastables in the TIA studied via diode laser absorption

*E.A.H. Timmermans, M.J. van de Sande, D.C. Schram and J.A.M. van der Mullen,*

**ABSTRACT** – Diode laser absorption experiments have been performed on atmospheric microwave induced argon plasmas produced by the “Torche à Injection Axiale” in order to study the  $4s^3P_2$  metastables densities. It is found that the density is maximal in the active plasma zone ( $\sim 1.5 \cdot 10^{18} \text{ m}^{-3}$ ) and rapidly decreases in the recombining plasma zone. In strongly ionizing atmospheric plasmas the  $4s$  population can be used to estimate the electron temperature. The obtained value (1.3 eV) is considerably lower than the temperature found with Thomson scattering in a previous study ( $\sim 2.0$  eV). The very strong scattering of the laser spot on the plasma in the expansion zone just above the nozzle suggest that in this region the plasma is filamentary. Above this zone lateral measurements have been Abel-inverted. Hollow profiles, like those that were determined for the electron density in previous studies, have not been observed for the  $4s$  distribution. It is found that the plasma zone with high  $4s$  density is extended further downstream with increasing gas flow whereas the introduction of typically a few percent of  $\text{CO}_2$  already results in a significant quenching of the metastables. The width of the absorption profile varies from typically 10 GHz in the active zone, where Van der Waals broadening is dominant to 4 GHz in the recombining zone, where Doppler becomes significant. The position of the central absorption frequency is found to be dependent on among others the position in the plasma. If this shift is attributed to the Stark effect it is obtained that the maximum electron density is within  $2\text{--}4 \cdot 10^{21} \text{ m}^{-3}$ . Since this latter value is rather high, it must be concluded that the Van der Waals effect induces a shift as well. The width and shift have been used to study trends in plasma properties (i.e. gas temperature and electron density) as a function of various parameters (i.e. position in the plasma, gas flow and gas composition). Observed tendencies are in agreement with findings in previous studies.

## 1. Introduction

In the past five years, several studies on atmospheric microwave induced argon and helium plasmas produced by the “TIA” (from “Torche à Injection Axiale” [1,2]) have been reported by JONKERS *et al.* [3,4], RODERO *et al.* [5,6] and TIMMERMANS *et al.* [7,8]. Topics they describe include transport properties and chemical processes such as excitation, dissociation and association mechanisms [8]. Apart from that, studies on plasma parameters such as electron temperature [3], electron density [3,5] and gas temperature [4], were reported as well. These plasma parameters and properties form the basis of the discussion on the potential of these plasmas as excitation sources in analytical chemistry [7]. Compared to the widely investigated argon ICP (Inductively Coupled Plasma), TIA plasmas are characterized by their large deviations from LTE (Local Thermal Equilibrium). Large discrepancies between the electron temperature  $T_e$  and heavy particle temperature  $T_h$  were found. In the active zone of an argon discharge for instance, typical values are given by  $T_e \approx 22 \cdot 10^3 \text{ K}$  and  $T_h \approx 2 \cdot 10^3 \text{ K}$ . Severe deviations from the Saha-Boltzmann relation for the population of excited states were found as well. The Atomic State Distribution Function (ASDF) points towards a highly ionizing system in the active zone, where the plasma has a (hollow) cone-like shape with steep gradient lengths for the electron density and temperature ( $\sim 10^{-4} \text{ m}$ ), which among others is related to the short skin depth (also  $\sim 10^{-4} \text{ m}$ ) of the microwave radiation (2.45 GHz) which is used to sustain the discharge. As a consequence, diffusion and convection play an important

role in the plasma kinetics and moreover, mixing with (cold) ambient air is readily observed [4,7].

Apart from the fact that these sharp gradients create a strongly non-equilibrium shape of the ASDF, as already shown in [3], it might be possible that the Electron Energy Distribution Function (EEDF) is distorted as well and has a non-Maxwellian shape. In order to reveal non-equilibrium properties of the EEDF more information on the ASDF is needed. Moreover, this information can improve the general perception of the plasma.

In this study we focus on the ASDF of argon discharges produced by the TIA. The density  $n_1$  of argon  $3p^1S_0$  ground state atoms can easily be calculated from the equation of state ( $p=n_1kT_h$ ), provided that  $T_h$  is known and that the total pressure  $p$  is determined by the partial pressure of argon ground state neutrals. With optical emission spectroscopy (OES) only  $4p \rightarrow 4s$ ,  $4d \rightarrow 4p$ ,  $5p \rightarrow 4s$ ,  $5d \rightarrow 4p$ ,  $6s \rightarrow 4p$  and  $6d \rightarrow 4p$  transitions can be measured and consequently only concentrations of the upper levels of these transitions can be determined if the line intensities are measured in an absolute way. However, using OES no information can be obtained about the population of the four  $4s$  levels, being the lowest excited states of argon. The  $4s^3P_2$  and  $4s^3P_0$  states are metastable whereas the  $4s^3P_1$  and  $4s^1P_1$  states are resonant so that the plasma is optically thick for emission from the radiative decay of these levels. Moreover, the concerned radiation is in the far VUV (106.7 and 104.8 nm respectively) and cannot be detected with equipment commonly used for OES [9].

Spatially resolved information on the  $4s$  population would be of great importance. Argon  $4s$  atoms constitute a large reservoir of energy so that these levels can be responsible for the excitation and ionization of analytes in spectrochemical analysis (Penning-ionization) [10] and the excitation of molecular states. Moreover, the population of the  $4s$  state is a decisive intermediate step for the stepwise excitation and ionization of argon, and thus largely influences the plasma kinetics [11,12].

In this paper we have studied the population of the metastable  $4s^3P_2$  level (excitation energy  $E_{exc}=11.55$  eV) with laser absorption experiments. For this purpose a tunable laser diode is modulated around the central wavelength of the  $4s^3P_2 \rightarrow 4p^3D_3$  transition  $\lambda_0=811.531$  nm. The  $4s^3P_2$  and  $4p^3D_3$  states will be referred to as "4s" and "4p" throughout the remainder of this paper. Densities of the  $4s$  state are determined with a spatial resolution of approximately  $10^{-4}$  m, which is sufficient to reveal whether the  $4s$  distribution has a (hollow) cone-like structure close to the nozzle, as is the case for the electron density  $n_e$ . In previous papers it was found that the deliberate addition of molecular gases through the central argon gas channel leads to a significant decrease of the argon emission. In this work it is studied whether deliberate molecular gases injection ( $CO_2$ ) quenches the  $4s$  population as well. Furthermore, the influences of the microwave power and the total argon gas flow on the  $4s$  density are investigated. From calculations it can be found that the plasma jet becomes turbulent at a flow of approximately  $2 \text{ l}\cdot\text{min}^{-1}$ . Using optical emission spectroscopy however, no anomalous changes in the emission of higher excited levels could be observed when the flow changed from laminar to turbulent [13]. Here we will investigate whether the transition from laminar to turbulent flow affects the  $4s$  density.

From the broadening of the  $4s^3P_2 \rightarrow 4p^3D_3$  absorption profile information can be obtained on the particle interactions and the heavy particle temperature [14-16]. Therefore, in

many cases the shape and the width of the measured absorption profiles have been analyzed as well. In contrast to the resonant  $4s^3P_1$  and  $4s^1P_1$  levels, the studied  $4s$  level has no optical coupling to another level with a significant population (i.e. the ground state), so that resonance broadening is not present [15]. Van der Waals and Stark broadening are the only significant collisional broadening mechanisms for the studied transition, whereas the Doppler broadening is related to the thermal motion of the argon atoms (and thus to  $T_h$ ). The measured absorption profile will have a maximum at a frequency that slightly differs from  $\nu_0$ . In principle, this shift can be used to determine the electron density  $n_e$  [9,15].

In the next section the theoretical principles of the absorption experiments will be given and estimations will be made for the contributions of the different broadening mechanisms of the absorption profile. In section 3 the plasma source and the set-up for the laser absorption experiments will be discussed. Experimental results and their significance for the general perception of argon plasmas produced by the TIA will be presented in section 4. Finally, in section 5 the conclusions will be given.

## 2. Theory

### 2.1. The principles of absorption measurements

The intensity change of a beam of radiation (e.g. produced by a laser), propagating through a plasma, i.e. a both absorbing and emitting medium, can be represented by the differential equation [17]:

$$\frac{dI_\nu(s)}{ds} = -\kappa(\nu,s)I_\nu(s) + j_\nu(s), \quad (1)$$

with  $I_\nu(s)$  the spectral intensity of the beam (in  $\text{W}\cdot\text{m}^{-2}\cdot\text{sr}^{-1}\cdot\text{Hz}^{-1}$ ),  $j_\nu(s)$  the plasma emission coefficient (in  $\text{W}\cdot\text{m}^{-3}\cdot\text{sr}^{-1}\cdot\text{Hz}^{-1}$ ) and  $\kappa(\nu,s)$  the absorption coefficient (in  $\text{m}^{-1}$ ) for frequency  $\nu$  at location  $s^a$ . The plasma emission coefficient represents the intensity increase of the radiation due to spontaneous emission. From Eqn 1 it can be derived that for a beam with an initial intensity  $I_\nu(a)$  at frequency  $\nu$  before penetrating into the plasma at location  $a$ , the intensity  $I_\nu(b)$  after leaving the plasma at location  $b$  can be written as:

$$I_\nu(b) = I_\nu(a)e^{-\tau_{ab}(\nu)} + S_\nu(1 - \exp^{-\tau_{ab}(\nu)}), \quad (2)$$

with  $S_\nu$  the plasma source term of (in  $\text{W}\cdot\text{m}^{-2}\cdot\text{sr}^{-1}\cdot\text{Hz}^{-1}$ ) and  $\tau_{ab}(\nu)$  the optical depth, i.e. the absorption coefficient  $\kappa(\nu,s)$  integrated over the "line-of-sight" through the plasma:

$$\tau_{ab}(\nu) \equiv \int_a^b \kappa(\nu,s)ds. \quad (3)$$

<sup>a</sup> It should be noted that  $I_\nu(s)$  and  $j_\nu(s)$  depend on  $\nu$  as well and should therefore be written as  $I_\nu(\nu,s)$  and  $j_\nu(\nu,s)$ . However, in order to simplify the notation, this parameter is usually omitted in the remainder of this paper.

Under well-considered experimental conditions, e.g. by positioning the detector at a large distance from the plasma or, as we did, by using a pinhole between plasma and detector, the contribution of  $j_v(v,s)$  on the measured intensity can be ignored. In this case the second term at the right of Eqn 2 can be neglected so that it can be reduced to:

$$I_v(b) = I_v(a) e^{-\tau_{ab}(v)} \tag{4}$$

In order to be able to interpret the absorption measurements, it is necessary to obtain an expression linking the absorption coefficient  $\kappa(v,s)$  to the density of the considered absorbing level. This relationship will be derived by considering the radiation processes of:

- spontaneous emission:  $Ar(p) \rightarrow Ar(q) + h\nu_{pq}$ ,
- absorption:  $Ar(q) + h\nu_{pq} \rightarrow Ar(p)$ ,
- and stimulated emission:  $Ar(p) + h\nu_{pq} \rightarrow Ar(q) + h\nu_{pq} + h\nu_{pq}$ ,

with the corresponding transition probabilities  $A_{pq}$ ,  $B_{qp}$  and  $B_{pq}$  respectively. In these processes p and q represent electronic argon levels at energies  $E_p$  and  $E_q$  from the ground state, h is Planck's constant and  $\nu_{pq}$  the emitted or absorbed photon, with  $h\nu_{pq} = E_p - E_q = E_{pq}$

We first consider Thermodynamic Equilibrium (TE), in which Detailed Balancing (DB) is present, which means that the number of forward processes equals that of the corresponding backward processes. For the radiative transitions between levels p and q this means that [18]:

$$n_p A_{pq} + n_p B_{pq} \rho_v(v, T) = n_q B_{qp} \rho_v(v, T), \tag{5}$$

with  $n_p$  and  $n_q$  the densities of the corresponding states and  $\rho_v(v, T)$  the spectral energy density (in  $W \cdot m^{-3} \cdot Hz^{-1}$ ), which in TE is given by Planck's radiation law [14]:

$$\rho_v(v, T) = \frac{8\pi h v^3}{c^3 (e^{\frac{h\nu}{kT}} - 1)}, \tag{6}$$

with k is Boltzmann's constant and T the temperature.

From Eqn 5 and 6 and using the Boltzmann distribution, which is also present under TE conditions:

$$\frac{n_q}{g_q} = \frac{n_p}{g_p} \exp\left(-\frac{E_{pq}}{kT}\right) \tag{7}$$

and  $E_{pq} = E_p - E_q = h\nu_{pq}$ , the so-called "Einstein Relations" can be derived:

$$B_{pq} = \frac{g_q}{g_p} B_{qp} = \frac{c^3}{8\pi h \nu_{pq}^3} A_{pq} \tag{8}$$

Although the presented derivation is based on the assumption of the presence of TE, it can be shown that Eqn 8 is valid for non-TE conditions as well [18].

The absorption coefficient  $\kappa(v,s)$  in the plasma is determined by the probabilities for absorption and stimulated emission:

$$\kappa(\nu, s) = \frac{h\nu}{c} (B_{qp} n_q(s) - B_{pq} n_p(s)) \phi_\nu, \quad (9)$$

with  $\phi_\nu$  being the line shape function, giving the dependence of the absorption coefficient on the frequency  $\nu$ . The frequency integral of the line shape function equals unity,  $\int \phi_\nu d\nu = 1$ .

When  $B_{pq}$  and  $B_{qp}$  are expressed as functions of  $A_{pq}$  (cf. Eqn 8), it is obtained that:

$$\kappa(\nu, s) = \frac{c^2}{8\pi\nu_{pq}^2} \frac{g_p}{g_q} A_{pq} n_q(s) \left( 1 - \frac{n_p(s)g_q}{n_q(s)g_p} \right) \phi_\nu. \quad (10)$$

For the argon transition between the metastable 4s and the 4p level, the absorption coefficient is thus given by:

$$\kappa(\nu, s) = \frac{c^2}{8\pi\nu_{4p4s}^2} \frac{g_{4p}}{g_{4s}} A_{4p4s} n_{4s}(s) \left( 1 - \frac{n_{4p}(s)g_{4s}}{n_{4s}(s)g_{4p}} \right) \phi_\nu. \quad (11)$$

with  $\nu_{4p4s}$  being the central transition frequency ( $3.6942 \cdot 10^{14} \text{ s}^{-1}$ ),  $A_{4p4s}$  the transition probability for spontaneous emission ( $0.331 \cdot 10^8 \text{ s}^{-1}$  [19]),  $n_{4s}$  the density of the metastable 4s state,  $n_{4p}$  the density of the 4p level and  $g_{4s}$  and  $g_{4p}$  the corresponding statistical weights (5 and 7 respectively). In the presented absorption experiments, the laser frequency is tuned around the  $\nu_{4p4s}$  frequency. In general, the laser irradiation will change the ratio  $n_{4p}/n_{4s}$ , so that via the changing factor between brackets in Eqn 11, the absorption coefficient will change as well (i.e. for high laser powers this leads to saturation). In order to avoid this intrusive behavior of the laser irradiation, the intensity of the laser beam has been strongly attenuated by filters. Now, since in strongly ionizing argon discharges in which the electron temperature is not too high the metastable 4s density is much higher than the 4p density, and thus  $n_{4s}g_{4p} \gg n_{4p}g_{4s}$ , Eqn 11 can be reduced to:

$$\kappa(\nu, s) = \frac{c^2}{8\pi\nu_{4p4s}^2} \frac{g_{4p}}{g_{4s}} A_{4p4s} n_{4s}(s) \phi_\nu. \quad (12)$$

If we integrate both sides of this equation over the line profile we find after some rearrangement that

$$n_{4s}(s) = \frac{8\pi\nu_{4p4s}^2}{A_{4p4s}c^2} \frac{g_{4s}}{g_{4p}} \int \kappa(\nu, s) d\nu. \quad (13)$$

Thus the 4s density at a location 's' can be obtained by a frequency integration of the local absorption coefficient. However,  $\kappa(\nu, s)$  is not a direct observable parameter. It must be deduced from the transmission  $T(\nu)$ :

$$T(\nu) = \frac{I_\nu(b)}{I_\nu(a)}, \quad (14)$$

with  $I_\nu(a)$  the measured intensity before penetrating into the plasma and  $I_\nu(b)$  the measured intensity after passing through the plasma.

Taking the logarithm of  $T(\nu)$ , cf. Eqn 4, we obtain the optical depth  $\tau_{ab}(\nu)$ :

$$\tau_{ab}(\nu) = -\ln(T). \quad (15)$$

Now Eqn 3 shows that  $\tau_{ab}(v)$  is an additive and that the relation between  $\kappa(v,s)$  and  $\tau_{ab}(v)$  is similar to that between the intensity and the emission coefficient for an optically open transition, which implies that the local values of  $\kappa(v,s)$  can be obtained via an Abel inversion of the  $\tau_{ab}(v)$  values, provided that the plasma is rotation symmetric. So in order to obtain the  $n_{4s}(r)$  for the various radial positions the following procedure should be followed:

1. tune the laser to an appropriate frequency  $v_1$ ,
2. measure for a series of lateral positions the transmission  $T(v_1)=I_b(v_1)/I_e(v_1)$  of the plasma,
3. determine for these lateral positions the optical depth  $\tau_{ab}(v_1)=-\ln(T(v_1))$ ,
4. perform the Abel inversion so that for  $v_1$  the radial distribution  $\kappa(v_1,r)$  is obtained,
5. repeat steps 1 to 4 for other frequencies, say  $v_2, v_3, \dots, v_n$ ,
6. construct for each radial position the absorption profile  $\kappa(v,r)$

Integration of this profile will give the local density  $n_{4s}(r)$  whereas the width will give insight in other local plasma properties (cf. section 2.2).

The procedure given above, by which an vast amount of data must be handled, will only be successful for rotation symmetrical plasmas that are very stable. Moreover, even for this category it is difficult to obtain information for central plasma regions if the plasma has a hollow structure [20]. Realizing that a large part of the TIA has a hollow filamentary, sometimes turbulent structure, it is not to be expected that it is useful to perform Abel inversions of the logarithm of the transmission for many separate frequencies. Therefore we applied the following approximations:

- The Abel inversion was applied to the area of the optical depth profile. Apart from that also the height of the optical depth (at central frequency  $v_c$ ) was Abel inverted, so that the local value of the width of the absorption profile  $\kappa(v,r)$ , which is no additive quantity itself, can be obtained from the local area and the local height of  $\kappa(v,r)$ , assuming that the profile has a Lorentzian shape.
- The logarithm of the transmission was not taken. Instead we applied the approximation that

$$\tau_{ab}(v)=-\ln(T)\approx 1-T, \quad (16)$$

which is valid for T values close to unity.

The error created by the second approximation is limited since the minimum value values for the transmission are around 0.85 (and in most cases much closer to unity). The first approximation has more impact on the accuracy of the results. However, it has been found that this technique gives reliable information of the cone-tip region were the plasma radial distribution is more or less Gaussian. Moreover, it is to be expected that the results of this method are sufficiently accurate to get insight in the absolute value of the 4s level occupation and the trends in the behavior of this quantity as a function of the axial position, the power, gas flow and the presence of molecules.



## 2.2. Broadening mechanisms

Because resonance broadening can be neglected for the studied  $4s \rightarrow 4p$  transition (cf. section 1), the remaining broadening mechanisms<sup>b</sup> that mainly determine the shape of the absorption profile  $\phi_\nu$  are Stark, Doppler and Van der Waals broadening:

- Stark broadening, which is due to the interaction between bound and free electrons, results in a Lorentzian absorption profile with a full width at half maximum (FWHM) that (in Hz) is approximated by [9,14,15]:

$$\Delta\nu_s = 2 \cdot 10^{-22} n_e w \frac{v_0^2}{c} \left[ 1 + 5.5 \cdot 10^{-6} \alpha n_e^{1/4} \left( 1 - 6.8 \cdot 10^{-3} n_e^{1/6} T_e^{-1/2} \right) \right], \quad (17)$$

with  $\alpha$  being the dimensionless ion broadening parameter (approximately 0.026 for  $T_e = 2 \cdot 10^4$  K [14]) and  $w$  the electron impact parameter (approximately  $7 \cdot 10^{-12}$  m for  $T_e = 2 \cdot 10^4$  K [14]). Since the term between brackets is close to unity, the Stark broadening depends almost linearly on the electron density and hardly on the electron temperature. For typical conditions inside a TIA argon discharge ( $n_e \approx 3 \cdot 10^{21}$  m<sup>-3</sup> and  $T_e \approx 2 \cdot 10^4$  K) it can be calculated that the Stark broadening is  $\Delta\nu_s \approx 1.9$  GHz.

- Doppler broadening, which is due the thermal motion of the atoms, results in a Gaussian shaped absorption profile with a full width at half maximum (in Hz) given by [15]:

$$\Delta\nu_D = v_0 \sqrt{\frac{8(\ln 2)kT_h}{m_{Ar}c^2}}, \quad (18)$$

with  $T_h$  the heavy particle temperature and  $m_{Ar}$  the mass of an argon atom. For  $T_h = 2 \cdot 10^3$  K it is found that  $\Delta\nu_D \approx 1.9$  GHz, approximately equal to the Stark broadening.

- Van der Waals or pressure broadening, which results from the interaction between neutral heavy particles, leads to a Lorentzian profile of the absorption coefficient. In literature different estimations for the FWHM due to Van der Waals broadening can be found. DE REGT *et al.* [20] used an expression in which the FWHM (in Hz) is linear proportional to the neutral density [21]:

$$\Delta\nu_v = \gamma \frac{v_0^2}{c} n_a, \quad (19)$$

with  $n_a$  the neutral density and  $\gamma$  the Van der Waals broadening coefficient. Using  $\gamma = 5 \cdot 10^{-36}$  m/m<sup>-3</sup> they were able to explain the wide absorption profiles at the edges of an argon ICP. In our case this expression would yield a broadening  $\Delta\nu_v \approx 8.2$  GHz using  $n_a = 3.6 \cdot 10^{24}$  m<sup>-3</sup> (obtained from the equation of state for  $T_h = 2 \cdot 10^3$  K and atmospheric pressure). BAER *et al.* [22] used an expression with a different temperature dependence to estimate the FWHM (in GHz) of the Van der Waals broadening in atmospheric-pressure flow fields consisting of argon and atomic oxygen:

<sup>b</sup> In the expressions for the full width at half maximum, all parameters are in SI units, unless indicated otherwise.

$$\Delta v_v \text{ (GHz)} \approx 760 T_h^{-0.7} (\chi_{Ar} + 1.3 \chi_O), \quad (20)$$

with  $\chi_{Ar}$  and  $\chi_O$  the mole fractions of argon and atomic oxygen in the flow field. Using  $\chi_{Ar}=1$  and  $\chi_O=0$  this would yield a broadening of  $\Delta v_v \approx 3.7$  GHz for  $2 \cdot 10^3$  K, which is significantly less than predicted by Eqn 19.

Combining these three broadening mechanisms shows that it can be expected that in our case ( $n_e \approx 3 \cdot 10^{21}$ ,  $T_h \approx 2 \cdot 10^3$  K) the FWHM of the total absorption profile is maximally between 8 and 12 GHz, dependent on which expression for the Van der Waals broadening is used. The total width is largely determined by this Van der Waals broadening<sup>c</sup>. In principle, Doppler and Van der Waals broadening can be used to determine the heavy particle temperature  $T_h$  (Eqn 19 would yield the neutral density  $n_a$ , which however is related to  $T_h$  by the equation of state), whereas Stark broadening can be used for the determination of  $n_e$ .

### 3. Experimental set-up

#### 3.1. The microwave-induced argon plasma torch

The presented diode laser absorption measurements have been performed on atmospheric argon microwave-induced discharges created by a wave-guide fed plasma torch referred to in literature as the "TIA" (from "*Torche à Injection Axiale*", using the terminology of MOISAN *et al.*, the developers of the torch [1,2]). This torch produces needle-like plasmas (with a maximum plasma radius  $r_p \approx 0.7$  mm) expanding into the open air. In previous papers of JONKERS *et al.* [3,4] and TIMMERMANS *et al.* [7,8], studies on electron temperatures, electron densities, gas temperatures, excitation mechanisms, transport properties and molecular processes in argon plasmas produced by the TIA have been reported. Some typical plasma parameters are given by an electron density  $n_e \approx 3 \cdot 10^{21} \text{ m}^{-3}$ , an electron temperature  $T_e \approx 22 \cdot 10^3$  K and a heavy particle temperature  $T_h \approx 2 \cdot 10^3 - 4 \cdot 10^3$  K at a power input  $P = 1.0$  kW and an argon gas consumption of  $[Ar] = 3 \text{ l} \cdot \text{min}^{-1}$  [3,4]. From previous studies it is known that the plasma has a hollow cone-like shape in the ionizing part close to the nozzle, with steep gradient lengths for the electron density and temperature ( $\sim 10^{-4}$  m).

#### 3.2. Diode laser absorption measurements

In figure 1 the experimental set-up is depicted. The diode laser beam is directed through the plasma and its intensity is measured with a radiation-sensitive detector. The plasma is located on a platform that can be translated in vertical and horizontal direction with high accuracy (resolution in horizontal direction  $\sim 5 \cdot 10^{-5}$  m), perpendicular to the laser beam. The used diode laser (2010 External Cavity Diode Laser, manufactured by Environmental Optical

<sup>c</sup> The laser has a width of approximately 4 MHz, which is much smaller than the measured width (typically 8 GHz), and therefore can be ignored.

Sensors Incorporated) can be tuned between 800 and 820 nm and is thus suitable for studies on the  $4s^3P_2 \rightarrow 4p^3D_3$  transition in argon (811.531 nm). The laser wavelength was modulated using a sawtooth waveform Piezo voltage generated by a frequency generator. This Piezo voltage was typically varied between +5 and -5 V with a 5 Hz duty cycle. A laboratory-built photon-sensitive detector (sensitive for photons in the wavelength range 400-1000 nm), generating a DC voltage output with an amplitude that is linearly proportional to the photon flux, is used to measure the transmission (and thus the absorption as well). A reference signal from the frequency generator is used to synchronize the Piezo modulation (and thus the laser frequency) and the detector output reading, both being monitored on a digital oscilloscope (Tektronix TDS 3014). Measurements are typically averaged 16 times before being stored.

The cross-section of the laser beam has an elliptical shape with a height of 2.5 mm and a width of 0.7 mm, which obviously is too wide to perform spatially resolved measurements on the TIA (which has characteristic gradient lengths for the electron density and temperature of approximately 0.1 mm). This is overcome by focussing the laser beam with a lens ( $f=160$  mm), cf. figure 1. The plasma is positioned in the focal plane, where the laser spot has a radius of 60  $\mu\text{m}$  in horizontal direction, which is sufficiently narrow to reveal the presence of a hollow profile in the metastable densities. In order to avoid saturation effects due to a changing ratio of  $n_{4p}/n_{4s}$  (cf. Eqn 11), the laser beam has been strongly attenuated with filters (approximately by a factor of  $10^4$ ). Absorption measurements with different driver output currents have been performed in order to verify that now saturation effects were absent. All absorption profiles were found to be identical in size and shape so that saturation effects can safely be neglected. Measurements presented in this paper are obtained using driver output currents in the range of 30-50 mA, which correspond to diode laser powers of approximately 7-10 mW. Since the laser beam is strongly scattered on the filamentary plasma, the detector (having a photon-sensitive area of  $4 \times 4 \text{ mm}^2$ ) has to be placed in the vicinity of the plasma. A pinhole (with a diameter of approximately 2 mm) is used to shield the detector from the plasma. With this pinhole, the background detector voltage due to plasma light is negligible and as a result, measurements do not have to be corrected for the plasma radiation.

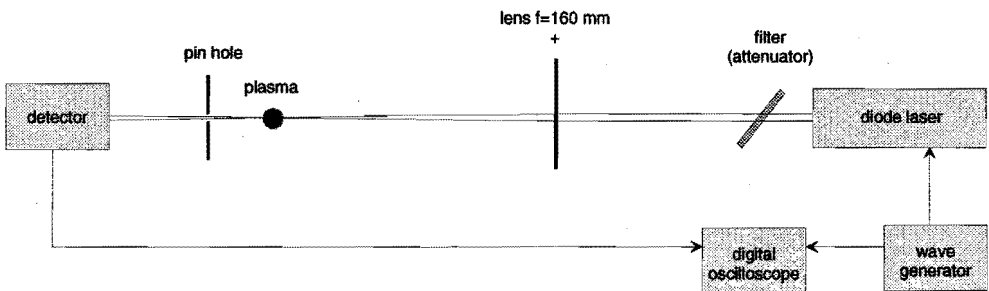
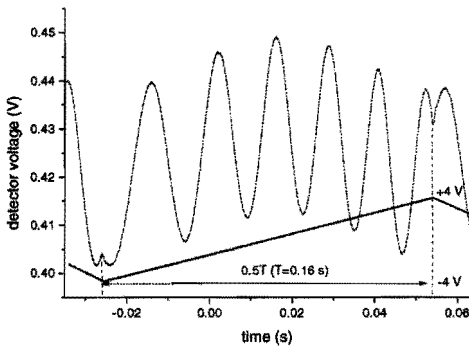


Figure 1. The experimental set-up used for the diode laser measurements. The plasma is located in the focal plane of the lens in order to improve the radial resolution of the measurements. A sawtooth waveform produced by the frequency generator is both used to modulate the frequency of the laser and to trigger the detector signal acquisition.

### 3.3. Frequency calibration

Measurements provide the detector signal (in V) versus the sweep time elapsed in the sawtooth waveform Piezo voltage (in s), cf. figure 2. However, the relationship between Piezo voltage and laser wavelength  $\lambda$  (or frequency  $\nu$ ) is not linear and hence has to be calibrated. The dispersion relation has been obtained with the interference pattern created by a transparent glass plate placed perpendicularly between the laser diode and the detector. Dependent on the diode laser wavelength, constructive or destructive interference is observed and, as a result, a sinusoidal signal is measured, cf. figure 2. The frequency difference between two maxima (or two minima) is given by  $\zeta\nu=c/2nd$ , with  $n$  the refractive index and  $d$  the thickness of the glass plate. Using a plate with  $n=1.511$  (at 810 nm) and  $d=14.55$  mm, it is obtained that  $\zeta\nu=6.818$  GHz.



The laser frequency is a non-linear function of the Piezo voltage so that the spacing between the maxima in figure 2 is not constant. Using fitting procedures including all minima and maxima present in the calibration measurements, this non-linearity has been accounted for. In the example given in figure 2, twelve extrema are present on the rising slope of the Piezo voltage, so that the laser is tuned over a frequency range of more than 40 GHz during the modulation.

Figure 2. Typical example of a calibration measurement. The fringes in the detector signal are induced by interference in a transparent plate (with known thickness and refractive index).

It should be noted that this calibration procedure provides relative frequencies only, i.e. no information on the absolute wavelength (or frequency) is obtained.

## 4 Experimental results

### 4.1. Introduction

Absorption is readily observed in the active part of argon plasmas. The line-of-sight value is typically in the order of 5-12%, using normal operational conditions (power input  $P=1$  kW and argon flow  $[\text{Ar}]=4$  l·min<sup>-1</sup>, no molecular gas additives). A typical example of a measured transmission profile  $T(\nu)$  is given in figure 3. The measured Voigt profile is rather

well approximated by a Lorentzian fit so that, like estimated in section 2.2, the addition of Stark and pressure broadening is dominant over Doppler broadening. The deviations from the Lorentz fit at the edges of the graph are mainly induced by correcting for the dependence of the laser output power on the frequency.

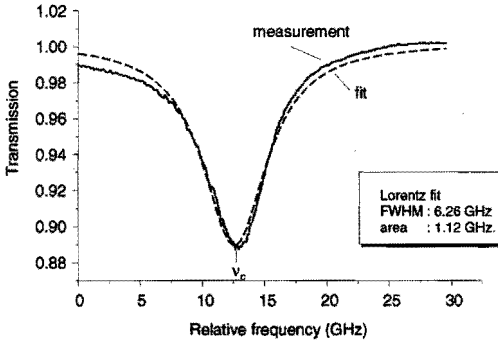


*Figure 3*

*A typical example of a measured transmission profile  $T(\nu)$ , obtained at 4 mm AN (above nozzle),  $P=1$  kW,  $[Ar]=3$  l·min<sup>-1</sup>. The frequency scale is calibrated from the interference pattern created by a transparent plate (cf. section 3.3). The obtained relative frequency values are sufficient to determine the area, height and width of the transmission profile.*

The transmission profile has been used to determine the absolute value of the 4s level occupation. The trends in the behavior of this quantity have been studied as a function of the axial position, the power, gas flow and the presence of molecules. It is observed that apart from the area of the absorption profile, its shape and central frequency  $\nu_c$  vary as well as a function of the position in the plasma and experimental conditions. These changes give information on changes in plasma parameters and therefore have been studied as well.

#### 4.2. Frequency shift

The central frequency  $\nu_c$  of the transmission profile  $T(\nu)$  is not constant. Significant shifts (in the order of 1 GHz) are observed when comparing different lateral or axial positions. The introduction of molecular gases induces a shift in the central frequency as well. This shift can be (partly) attributed to the Stark effect, which apart from a profile broadening (cf. Eqn 17) leads to a shift, so that the observed central frequency  $\nu_c$  of the absorption coefficient is no longer the same as the theoretical central absorption frequency  $\nu_0$  of the undisturbed atom. This Stark shift  $\delta\nu_s$  is given by [14]:

$$\delta\nu_s = \nu_c - \nu_0 = 2 \cdot 10^{-22} n_e w \frac{\nu_0^2}{c} \left[ \frac{d}{w} \pm 6.3 \cdot 10^{-6} \alpha n_e^{1/4} \left( 1 - 6.8 \cdot 10^{-3} n_e^{1/6} T_e^{-1/2} \right) \right], \quad (21)$$

with  $d/w$  the dimensionless relative electron impact shift, being approximately 1.0 for the studied transition at  $T_e=2$  eV. The Stark shift can be used to determine the electron density, cf. Eqn 21. Since in our case  $d/w$  is much larger than the other term between brackets in the expression for the Stark shift,  $\delta\nu_s$  is in good approximation linear proportional to  $n_e$ .

In figure 4 the shifts in the central position of the optical depth are depicted as a function of the lateral position of an argon discharge at 4 and 8 mm AN (above nozzle), using  $P=800$  W and  $[Ar]=3$  l·min<sup>-1</sup>. We assumed  $\nu_c$  to be equal to  $\nu_0$  at the edges of the plasma. A large uncertainty is induced by this approximation since the absorption profile is rather weak in this

region so that the determination of its maximum is difficult. The electron density that is found when the shift is totally attributed to the Stark effect is also given in figure 4. The small gradient lengths at the edge of the plasma should be noted. They are comparable with those found with Thomson scattering [3]. Moreover, the (non-Abel inverted) data indicate that  $n_e$  has a hollow profile at 4 mm AN, whereas the distribution is Gaussian-like at 8mm AN, again in agreement with Thomson scattering experiments.

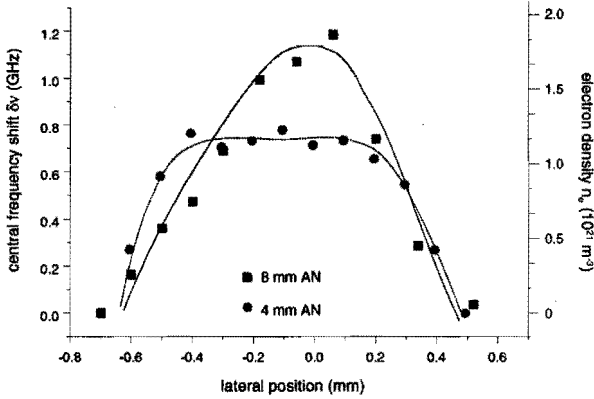


Figure 4. The central frequency shift  $\Delta\nu$  of the optical depth measured at two different heights in the plasma and the corresponding electron density if this shift is attributed to the Stark effect solely ( $[Ar]=3 \text{ l}\cdot\text{min}^{-1}$ ,  $P=800 \text{ W}$ ).

In figure 5 the shift of the measured central peak frequency in the transmission is given as a function of the height for two different gas flows. The profile that just could be detected in the recombining zone has now been taken as reference since it can be expected that in this region Stark effects can be neglected. In this case the total shift is approximately 3 GHz, which would yield an electron density of  $4.5 \cdot 10^{21} \text{ m}^{-3}$  in the active plasma zone. This value is higher than those obtained from  $H\beta$  broadening and Thomson scattering experiments.

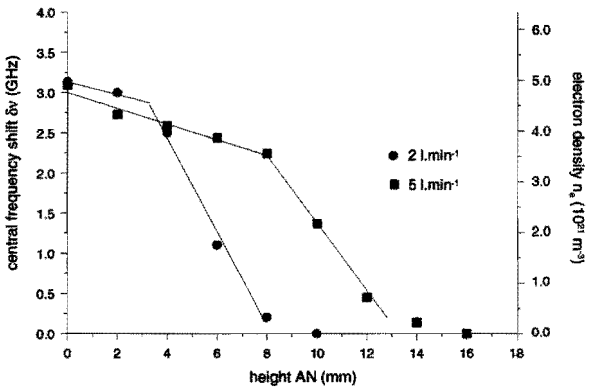


Figure 5. The central frequency shift  $\Delta\nu$  of the optical depth and the corresponding electron density at various axial heights in the plasma for two different argon gas flows (2.0 and 5.0  $\text{l}\cdot\text{min}^{-1}$  respectively,  $P=1 \text{ kW}$ )

It should be noted that when the active zone is approached sideways, a frequency shift  $\Delta\nu \approx 1 \text{ GHz}$  is observed (cf. figure 4), whereas approaching the active zone along the plasma axis in upstream direction gives  $\Delta\nu \approx 3 \text{ GHz}$  (cf. figure 5). This means that the measured shift cannot be attributed to the Stark effect solely. The observed shift is most likely a combination of Stark shift and Van der Waals shift [22]. When approaching the ionizing plasma zone in

upstream direction along the plasma axis the contribution of the Van der Waals shift will increase due to the lower gas temperature and thus higher neutral density close to the nozzle, compared to the recombining zone. However, when approaching sideways, the Van der Waals contribution will decrease due to the higher gas temperature in the plasma center, compared to the plasma surroundings. This mechanism is supported by the fact that the electron density as found with Thomson scattering ( $\sim 3 \cdot 10^{21} \text{ m}^{-3}$ ) is intermediary the two maximum densities given in figures 4 and 5.

More study will be needed for a better interpretation of the measured shift in absorption profile. Moreover, for a more accurate determination of  $\delta v$  a reference signal should be used, e.g. obtained from the transmission profile in a low-pressure argon lamp [23]. A consequence of the shift in  $v_c$  is that a line-of-sight measurement is a summation of absorption profiles with different central peak positions. This implies that the width of the optical depth profile is larger than in virtue of the broadening mechanisms discussed in section 2.2. This complicates the Abel inversion and line shape analysis.

### 4.3. Abel inversion

In order to obtain the radial distribution of the 4s densities, the areas of the lateral optical depths have been Abel inverted. As an example, in figure 6a and 6b the areas of the optical depth profiles measured from an argon discharge at 4 and 8 mm AN respectively ( $[\text{Ar}] = 4 \text{ l} \cdot \text{min}^{-1}$ ,  $P = 1 \text{ kW}$ ) are given as a function of the lateral position  $x$  (with respect to plasma axis  $x=0$ ). In order to include all data points in the Abel inversion, data for negative lateral positions are mirrored (i.e.  $x \rightarrow \text{abs}(x)$ ). A polynomial function with a derivative that is close to zero at the plasma axis has been fitted through the data points (strictly speaking the derivative should equal zero at the plasma axis). These polynomial fits and their Abel inverted profiles are given in figure 6c and 6d. It should be realized that in our case the fit that has been Abel inverted might be rather inaccurate due to the limited number of data points in the profile and the diameter of the laser beam ( $\sim 0.12 \text{ mm}$ ), which is of the same order of typical gradient lengths. Moreover, as discussed in the previous section, line-of-sight measurements are a convolution of shifted profiles, which introduces additional errors.

Thomson scattering (TS) experiments by JONKERS *et al.* [3] have shown that the electron density has a pronounced hollow profile close to the nozzle. Unfortunately we were not able to investigate the 4s distribution in this plasma region (0-3 mm AN) since the accuracy of the measurements was too poor as a result of scattering of the laser beam on the unstable plasma filaments. The electron density distribution as found by TS still has a slightly hollow profile at 4 mm AN, the lowest measurable position for radially resolved absorption measurements. The radial 4s density distribution on the other hand, has no hollow structure, cf. fig.6. However, due to problems with Abel inversion on such small-scale, often turbulent, plasmas with steep gradients it is not to be expected that such fine details can be resolved.

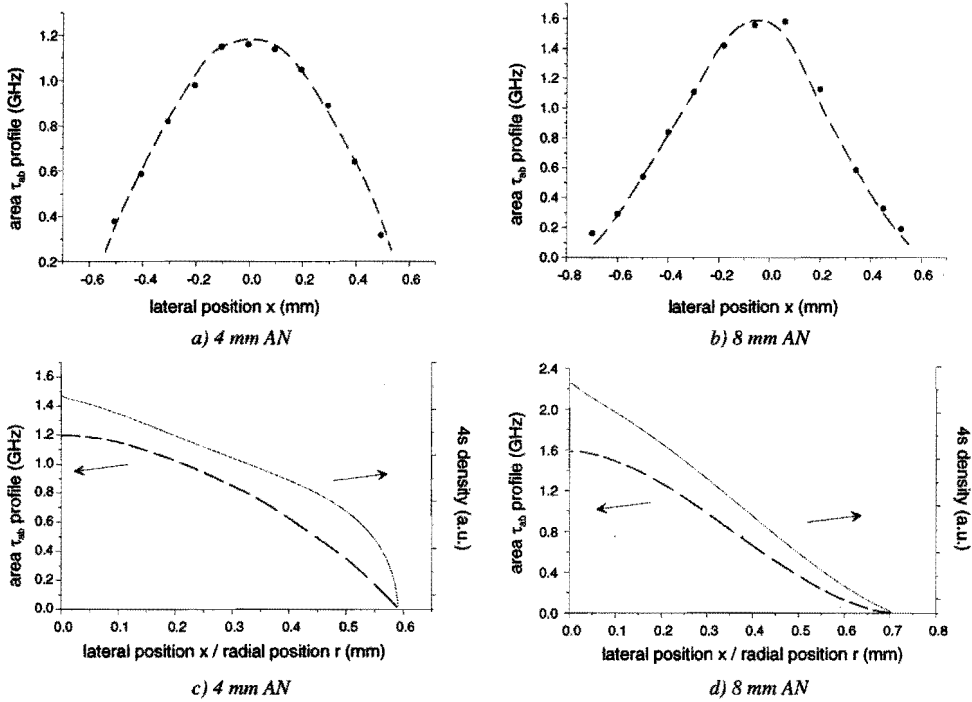


**Figure 6.** Example of Abel inverted  $4s$  distribution profiles measured at two different axial heights. Figure 6a) and 6b) show the areas of the lateral optical depth profiles at 4 and 8 respectively ( $[Ar]=4.0 \text{ l}\cdot\text{min}^{-1}$ ,  $P=1 \text{ kW}$ ). Through the set of data points obtained in a lateral scan a polynomial has been fitted that is Abel inverted. These polynomials and the corresponding Abel inverted profiles are depicted in 6c) and 6d). The Abel inverted profiles are linear proportional to the local  $4s$  density (cf. the right y-axis).

#### 4.4. The argon ASDF

To get an estimation of the  $4s$  density we assumed a uniform  $4s$  distribution in radial direction. The  $4s$  density can then easily be derived from the absorption profile and the absorption length that (in an approximate way) has been obtained from the Abel inversion procedure. In figure 7 a typical  $4s$  density is included in the argon ASDF. This density ( $n_{4s}=1.5 \cdot 10^{18} \text{ m}^{-3}$ ) is obtained at 4mm AN using an area of the optical depth of 1.5 GHz and an absorption length of 0.8 mm. The ground state density is determined from the equation of state, using  $T_h=2 \cdot 10^3 \text{ K}$ . The  $4p$ ,  $5d$ ,  $6s$  and  $6d$  densities are found from absolute line intensities [24].



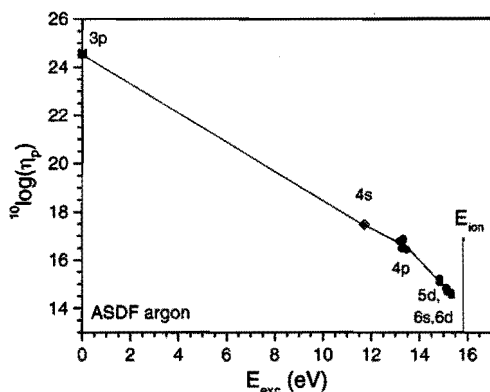


Figure 7.

The ASDF of argon. The 3p ground state density has been determined from the equation of state, the 4s density follows from the absorption measurements and the 4p, 5d, 6s and 6d densities are taken from JONKERS *et al.* [24] and are determined from absolute line emission intensities.

In argon TIA discharges it can be expected that the plasma is strongly ionizing and that the 4s population therefore is coupled to that of the ground state via the relation:

$$\frac{n_{4s}}{g_{4s}} = r_{4s}^1 \frac{n_1}{g_1} \exp\left(-\frac{\Delta E}{kT_e}\right), \quad (22)$$

with  $r_{4s}^1$  a coefficient that can be calculated from a collisional radiative model (CRM) and  $\Delta E=11.71$  eV, the excitation energy of the 4s level. From Eqn 22 it can be seen that the 4s density can be used to determine the electron temperature. The  $r_{4s}^1$  coefficient is more or less independent of the electron density and slightly depends on the electron temperature. For typical TIA conditions CRM calculations showed that  $r_{4s}^1 \approx 5 \cdot 10^{-4}$ . Using this value, it is found that the electron temperature  $T_e \approx 1.3$  eV. This temperature is significantly smaller as obtained by Thomson scattering (typically 2.0 eV), but is in good agreement with the temperature of 1.1 eV that has been found by VAN DER MULLEN *et al.* [25] from solving the particle balance. In the active zone of atmospheric small-scale plasmas with small electron density gradient lengths, ambipolar diffusion (of which SCHOTTKY already recognized the importance in 1924 [26]), is a much more important electron loss channel than electron recombination processes. Consequently VAN DER MULLEN *et al.* neglected these processes and supposed that ionization was balanced by outward diffusion.

#### 4.5. Profile broadening

It is found that the width of the optical depth  $\tau_{ab}(\nu)$  strongly varies as a function of position and gas composition (cf. section 4.8). As an example, the FWHM of the optical depth as measured along the plasma axis is given in figure 8 ( $[Ar]=5.0$  l·min<sup>-1</sup>,  $P=1$  kW). As discussed in section 2.2, mainly three broadening mechanisms will contribute to the total broadening of the absorption coefficient  $\kappa(\nu, s)$ . The Stark broadening  $\Delta\nu_S$  will be maximal in the region with the highest values for the electron density, i.e. approximately between 0 and 8 mm AN. Using  $n_e \approx 3 \cdot 10^{21}$  m<sup>-3</sup> it is obtained that  $\Delta\nu_S \approx 1.9$  GHz, cf. Eqn 17. Further downstream a fast decrease of  $\Delta\nu_S$  can be expected. Doppler broadening  $\Delta\nu_D$  will be especially important

in regions with a high gas temperature. Rayleigh scattering measurements have shown that the plasma has a low gas temperature close to the nozzle (less than  $1 \cdot 10^3$  K). This temperature increases towards a maximum value of typically  $4 \cdot 10^3$  K at approximately 20 mm above nozzle (AN) and decreases further downstream [4]. This implies that  $\Delta\nu_D \approx 1.3$  GHz close to the nozzle and increases towards  $\Delta\nu_D \approx 2.7$  GHz at 20 mm AN, cf. Eqn 18.

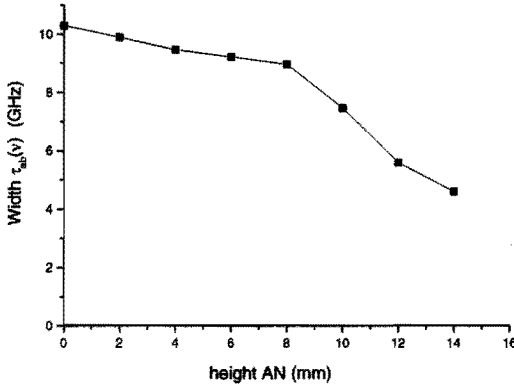


Figure 8.  
The FWHM of the optical depth  $\tau_{ab}(\nu)$  as measured along the plasma axis ( $[Ar]=5.0$  l·min $^{-1}$ ,  $P=1$  kW).

Van der Waals broadening will be the dominant broadening mechanism in large parts of the plasma. According to Eqn 19 and Eqn 20, this broadening decreases with increasing gas temperature (or decreasing neutral density), so that it can be expected that the width of the absorption profile steadily decreases between 0 and 20 mm AN. This diminution is indeed observed between 0 and 14 mm AN, cf. figure 8 (above 14 mm AN the absorption became too weak for an accurate width determination). It should be noted that in figure 8 the width of  $\tau_{ab}(\nu)$  instead of  $\kappa(\nu, s)$  is plotted. Consequently, an error is induced by the shift in the central frequencies of absorption coefficient profiles along a line-of-sight, cf. section 4.2. After correcting for the approximate Doppler and Stark contribution to the overall width, the Van der Waals broadening is typically 6 GHz at 2 mm AN, much smaller than predicted by Eqn 19, giving a Van der Waals broadening of 16 GHz (using  $T_h \approx 1 \cdot 10^3$  K [4] and the broadening coefficient  $\gamma \approx 5 \cdot 10^{-36}$  m/m $^{-3}$  as found by DE REGT *et al.* for an argon ICP). Since the ICP has a much higher gas temperature we must conclude that this broadening coefficient is valid for a small temperature range only. Using a broadening of 6 GHz, Eqn 19 would yield  $\gamma \approx 2 \cdot 10^{-36}$  m/m $^{-3}$  in our case. However, using Eqn 20, like BAER *et al.* did, a Van der Waals broadening of 6.0 GHz is found, which is in good agreement with our measurements. Also further downstream (where the broadening decreases due to a decrease of the neutral density) this equation provides reasonable estimations for the broadening.

#### 4.6. Influence of the gas flow

Axial measurements have been performed for a laminar gas flow (2.0 l·min $^{-1}$ ) and a turbulent gas flow (5.0 l·min $^{-1}$ ). For  $[Ar]=2.0$  l·min $^{-1}$ , absorption is visible between 0 and 10

mm AN, whereas for  $5.0 \text{ l}\cdot\text{min}^{-1}$  this length has been elongated till 16 mm AN, cf. figure 9, in which the line-of-sight integrated 4s density or column density ( $\text{m}^{-2}$ ) is given. This figure shows a large resemblance with the line-of-sight integrated intensity of emission lines from the TIA (among others argon  $4p \rightarrow 4s$ ) [13] by TIMMERMANS *et al.* who found that the line emission generating plasma zone extends with increasing argon flow (cf. chapter 2).

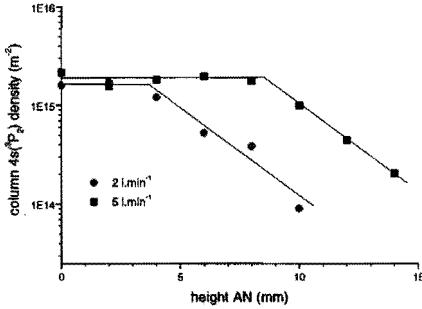


Figure 9.

The column density of the 4s level for two different argon flows ( $2.0$  and  $5.0 \text{ l}\cdot\text{min}^{-1}$ ) as a function of the height.

#### 4.7. Influence of the power input

Within the normal range of applied power levels (600-1200 W) no anomalous changes in the 4s density have been observed. Since within this power range the plasma dimensions are relatively unaffected, it can be expected that with increasing power density especially  $n_e$  will increase and that  $T_e$  will be relatively constant. Since in the ionizing plasma region  $n_{4s}$  is (almost) independent of  $n_e$  and exponentially dependent on  $T_e$ , cf. Eqn 22, it can be understood that the power only has a limited influence. However, if the power is strongly reduced (to typically 100 W, approximately the minimum power to sustain the discharge), the plasma shrinks significantly in size and only one filament remains. In this case the absorption profile has become very wide (up to 20 GHz, i.e. much wider than observed in any other experiment discussed in this study), which points towards a very low gas temperature (and thus large Van der Waals broadening). Since the depth of the line-of-sight transmission is typically 8-10% this means that the column 4s density is comparable to normal conditions. However, since the absorption path is much shorter, this means that the 4s density has significantly increased.

As discussed by VAN DER MULLEN *et al.* [25], in the active zone of atmospheric small-scale plasmas electrons are dominantly lost by ambipolar diffusion and losses due to recombination processes can be neglected (cf. section 4.4). Due the structure of argon, which has a rather large energy gap between the ground state and the first excited level ( $\sim 12 \text{ eV}$ ) and a much smaller energy gap between this first excited level and the ionization level ( $\sim 4 \text{ eV}$ ) the ionization rate is for TIA argon plasmas in good approximation equal to the rate coefficient  $K(1,2)$  (in  $\text{m}^3\text{s}^{-1}$ ) for excitation from the ground state to the first excited (4s) state. Substituting  $K(1,2)$  for the ionization coefficient in the particle balance gives [25]:

$$n_e n_1 K(1,2) = \frac{n_e D_a}{\Lambda^2}, \quad (23)$$

so that

$$K(1,2) = \frac{D_a}{n_1 \Lambda^2}, \tag{24}$$

with  $D_a$  the ambipolar diffusion coefficient ( $m^2 s^{-1}$ ),  $\Lambda$  the radial gradient length (m) and:

$$K(1,2) \propto T_e^{1/2} \exp\left(-\frac{\Delta E_{12}}{kT_e}\right) \tag{25}$$

If we compare a filamentary low-power TIA plasma to a plasma sustained at a higher power level, it can be expected that the relative decrease of  $\Lambda^2$  is (much) larger than the relative increase of  $n_1$ , so that  $K(1,2)$  will increase, cf. Eqn 24. From Eqn 25 it follows that this must imply that  $T_e$  has increased as well, which will also contribute to an increase of  $n_{4s}$ , cf. Eqn 22.

#### 4.8. Quenching by molecular gas additives ( $CO_2$ )

Experiments with  $CO_2$  have been done in order to investigate the quenching of metastables. It is found that a  $CO_2$  addition of approximately 4% leads to an almost total disappearance of the absorption profile. Another result is that the plasma diameter is reduced as well. The radial absorption length at 4 mm AN is approximately 1.2 mm in pure argon discharges (cf. figure 10), and reduces to approximately 0.9 mm when 0.4% of  $CO_2$  is added. This is a relatively small change compared to the change in the optical depth ( $\sim$  a factor 3), so that it can be concluded that  $CO_2$  effectively quenches the  $4s$  density. This is also supported by measurements of the optical depth in plasmas without and with  $CO_2$  injection (20 sccm in  $4.0 \text{ l}\cdot\text{min}^{-1}$  argon) at different axial positions. In case of  $CO_2$  injection, only between 0 and 10 mm AN absorption can be observed, whereas for pure argon discharges this is between 0 and 18 mm AN.

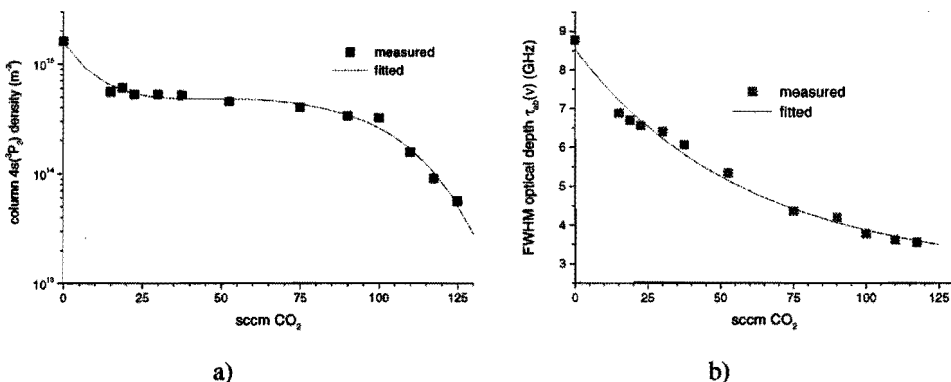


Figure 10. The line-of-sight integration of the  $4s$  density (figure a) and the FWHM of the optical depth (figure b) as a function of  $CO_2$  added to an argon discharge ( $[Ar]=4.0 \text{ l}\cdot\text{min}^{-1}$ ,  $P= 1.0 \text{ kW}$ , measured at 4.0 mm AN).

In figure 10a the column density of the 4s level is given as a function of CO<sub>2</sub> added to the discharge. It should be noted that after the introduction of 15 sccm (i.e. less than 0.4% of the total gas flow), the column density is reduced by a factor of 3.

From figure 10b it can be seen that the introduction of molecular gases also considerably reduces the width of the absorption profile. De-convolutions of the measured Voigt profiles show that the width of the Lorentz broadening (being a result of the Stark and Van der Waals effect) decreases. This means that the electron density decreases and the gas temperature increases cf. Eqn 17 and Eqn 19. This is in agreement with previous studies, e.g. power interruption experiments [27], in which also was found that the electron density in argon discharges was significantly reduced after a few percent of molecular gas. Optical emission spectroscopy performed on atmospheric surface wave sustained argon discharges had shown that the introduction of CO<sub>2</sub> led to a higher gas temperature [8] (cf. chapter 4).

For CO<sub>2</sub> flows above 100 sccm the profile of the optical depth is clearly Gaussian. If we contribute this width to the Doppler effect, it can be used to determine the gas temperature, cf. Eqn 18:

$$T_h = \frac{m_{Ar} c^2}{8(\ln 2)k} \left( \frac{\Delta v_D}{v_0} \right)^2, \quad (26)$$

which yields  $T_h \approx 7 \cdot 10^3$  K for  $\Delta v_D \approx 3$  GHz (cf. figure 10b). It should be realized that this is a rough approach only and that it provides an upper limit for the gas temperature, since Stark and Van der Waals broadening are totally neglected. However, de-convolution of the measured Voigt profiles show that with increasing CO<sub>2</sub> flow the Gauss width increases (apart from the sharply decreasing Lorentz width), which again demonstrates that  $T_h$  increases.

## 5. Conclusions

Diode laser absorption has been used to determine the density of the metastable 4s<sup>3</sup>P<sub>2</sub> level of argon discharges produced by the Torche à Injection Axiale. It is found that in the ionizing part this density is given by  $n_{4s} \approx 1.5 \cdot 10^{18} \text{ m}^{-3}$ . Further downstream in the recombining plasma zone this density rapidly decreases. In strongly ionizing atmospheric plasmas the 4s population is coupled to the 3p<sup>1</sup>S<sub>0</sub> ground state density via an expression that is dependent on the electron temperature  $T_e$ , so that  $n_{4s}$  can be used to estimate  $T_e$ . The obtained value (~1.3 eV) is lower than the temperature found with Thomson scattering in a previous study (~2.0 eV), but in good agreement with the temperature that VAN DER MULLEN *et al.* found by solving the particle balance. Abel-inverted data have shown that the distribution of metastables has a smooth profile with weak gradients. No hollow profile has been observed for the  $n_{4s}$  distribution for heights of 4 mm above the nozzle and further downstream. Closer to the nozzle, laser scattering on the plasma was too large to perform radially resolved measurements. This strong scattering points towards a filamentary plasma in this region. It has been observed that with increasing argon flow the plasma part with high  $n_{4s}$  is extended further downstream. The introduction of small amounts of CO<sub>2</sub> (typically a few percent) on the other hand results in significant quenching of metastables.

From the central frequency and the broadening of the absorption profile information on various plasma parameters is obtained. The central frequency is Stark and Van der Waals shifted and therefore is gas temperature and electron density dependent. It is found that, like for the  $4s$  distribution, the plasma zone with high electron density is extended further downstream with increasing argon flow whereas the electron density decreases after  $CO_2$  injection. These trends were in agreement with previously obtained results from optical emission spectroscopy and power interruption experiments. The width of the absorption profile typically varied between 10 GHz close to the nozzle, where due to a low gas temperature Van der Waals broadening is dominant, to typically 4 GHz in the recombining zone, where Doppler broadening becomes most significant. The width was reduced to typically 3 GHz close to nozzle after the injection of a few percent of  $CO_2$ . By attributing this broadening entirely to the Doppler effect, an upper limit of  $7 \cdot 10^3$  K for the gas temperature was found.

## Acknowledgements

The authors would like to thank H.M.M. de Jong and A.B.M. Hüsken for their technical assistance and A. Hartgers for the CRM calculations. Financial support was given by the Eindhoven Centre Technology for Sustainable Development (TDO) and the Dutch Technology Foundation (STW).

## References

1. M. Moisan, G. Sauvé, Z. Zakrzewski and J. Hubert, *Plasma sources, Sci. and Techn.* **3**, 584 (1994).
2. A. Ricard, L. St-Onge, H. Malvos, A. Gicquel, J. Hubert and M. Moisan, *J. Phys. III France* **5**, 1269 (1995).
3. J. Jonkers, L.J.M. Selen, J.A.M. van der Mullen, E.A.H. Timmermans and D.C. Schram, *Plasma Sources, Sci. and Techn.* **6**, 533 (1997).
4. J. Jonkers, A. Hartgers, L.J.M. Selen, J.A.M. van der Mullen and D.C. Schram, *Plasma Sources, Sci. and Techn.* **8**, 49 (1999).
5. A. Rodero, M.C. García, M.C. Quintero, A. Sola and A. Gamero, *J. Phys. D: Appl. Phys.* **29**, 681 (1996).
6. A. Rodero, M.C. Quintero, A. Sola and A. Gamero, *Spectrochim. Acta* **51B**, 467 (1996).
7. E.A.H. Timmermans, I.A.J. Thomas, J. Jonkers, J.A.M. van der Mullen and D.C. Schram, *Fresenius J. Anal. Chem.* **362(5)**, 440 (1998).
8. Chapter 4 of this thesis E.A.H. Timmermans, J. Jonkers, I.A.J. Thomas, A. Rodero, M.C. Quintero, A. Sola, A. Gamero, J.A.M. van der Mullen and D.C. Schram, *Spectrochim. Acta* **53B**, 1553 (1998).
9. D.S. Baer and R.K. Hanson, *J. Quant. Radiat. Transfer*, **46(6)** 455 (1992).
10. P.W.J.M. Boumans, "Inductively coupled plasma emission spectroscopy", part 2:

- "Applications and fundamentals"*, John Wiley & Sons, New York (1987).
11. A. Montaser and D.W. Golightly, *"Inductively coupled plasmas in analytical atomic spectrometry"*, second edition VCH Publishers, Inc., New York (1992).
  12. L.S. Polak and Y.A. Lebedev, *"Plasma Chemistry"*, Cambridge International Science Publishing, Cambridge (1998).
  13. *Chapter 2 of this thesis*, E.A.H. Timmermans, I.A.J. Thomas, D.C. Schram and J.A.M. van der Mullen, "Spectrochemical characteristics of microwave induced plasma torches", *to be submitted for publication* (1999).
  14. H. Griem, *"Plasma spectroscopy"*, McGraw-Hill Book Company, New York (1964).
  15. H. Griem, *"Spectral line broadening by plasmas"*, Academic Press, New York (1974).
  16. H. Griem, *"Principles of plasma spectroscopy"*, Cambridge University Press, Cambridge (1997).
  17. M. Mitchner and C.H. Kruger, *"Partially ionized gases"*, Wiley-Interscience, New York (1973).
  18. A.C.G. Mitchell and M.W. Zemansky, *"Resonance radiation and excited atoms"*, Cambridge University Press, Cambridge (1971).
  19. W.L. Wiese and G.A. Martin, *"Wavelengths and transition probabilities for atoms and atomic ions"*, part 2: *"Transition probabilities"*, U.S. Government Printing Office, Washington (1980).
  20. J.M de Regt, R.D. Tas and J.A.M. van der Mullen, *J. Phys. D: Appl. Phys.* **29**, 2404 (1996).
  21. V.W. Lelevkin, D.K. Otorbaev and D.C. Schram, *"Physics of non-equilibrium plasmas"*, North-Holland, Amsterdam (1992).
  22. D.S. Baer, H.A. Chang and R.K. Hanson, *J. Quant. Radiat. Transfer* **50(6)**, 621 (1993).
  23. K. Tachibana, H. Harima and Y. Urano, *J. Phys. B: At. Mol. Phys.* **15**, 3169 (1982).
  24. J. Jonkers, H.P.C. Vos, J.A.M. van der Mullen and E.A.H. Timmermans, *Spectrochim. Acta* **51B**, 457 (1996).
  25. J.A.M. van der Mullen and J. Jonkers, *Spectrochim. Acta* **54B**, 1017 (1999).
  26. W. Schottky, *Physik. Zeitschr.* **XXV**, 635 (1924).
  27. *Chapter 6 of this thesis*, E.A.H. Timmermans, I.A.J. Thomas, J. Jonkers and J.A.M. van der Mullen, "Excitation balances and transport properties in atmospheric microwave induced plasmas studied by power interruption experiments", *submitted for publication in Plasma Sources, Sci. and Techn.* (1999).

# 8

## General conclusions



In this thesis spectroscopic studies on several microwave induced plasmas that are used as spectrochemical excitation sources (i.e. the "torche à injection axiale" (TIA), the microwave plasma torch (MPT), the Beenakker cavity, the surfatron and the guide-surfatron) have been presented. Topics as analyte excitation, molecular dissociation and association, transport processes and metastable distributions have been discussed. Each chapter focuses on specific aspects of the study and is presented in an isolated way. Consequently, each chapter contains the conclusions relevant to the subject of that chapter. In this chapter a survey of general conclusions will be given.

- The large variety of microwave induced plasmas and the often easy changeover from argon to helium operation makes them interesting candidates as excitation sources for spectrochemical analysis. In this study plasmas produced by the TIA and the MPT have been studied with respect to this application. It is found plasmas produced by the latter torch have better detection limits, due to a more effective sample penetration into the hot plasma zone.
- Plasmas produced by the TIA show a high tolerance to the introduction of molecular gases, which points towards a high potential as excitation source for the elemental analysis of gaseous samples. Accordingly, this torch has been used successfully for the on-line monitoring of metals (like zinc, lead, sodium and magnesium) in combustion gases in the secondary combustion chamber of AVR-Chemie, a large hazardous waste incinerator in The Netherlands. The potential of this robust torch for measurements under very rough experimental conditions, where (generally) commercially available laboratory equipment is not usable, has been clearly demonstrated. A constant combustion gas sampling has been realized with a plasma operated at under-pressure whereas the maximum intensity of analyte emission is observed from discharges in mixtures of argon and combustion gases (in a ratio of approximately 3:2)
- Since both atmospheric and reduced-pressure microwave induced plasmas usually have a high tolerance for molecular gas injection, they can be used very well for the study of molecular plasma processes.
- At atmospheric pressure no emission is observed from deliberately introduced 3-atomic or larger molecules (i.e.  $\text{H}_2\text{O}$ ,  $\text{CO}_2$ ,  $\text{SO}_2$ ,  $\text{SF}_6$ ). Instead, atomic emission and the emission of diatomic association products (i.e.  $\text{C}_2$ ,  $\text{CN}$ ,  $\text{NO}$ ,  $\text{OH}$ ,  $\text{NH}$ ) is frequently observed. It is found that at atmospheric pressure 3-body association processes play an important role. Moreover, it seems that in free expanding torches molecular emission bands are inevitable as a result of air entrainment.
- At reduced pressure (~1-10 mbar) the importance of 3-body processes is limited. However, it is found that in this pressure regime association at the wall of the discharge tube is important (which is a process with two atoms or molecules and the wall as a substitute for the third body), so that basically the same association products are observed.

Unlike for the atmospheric discharges, under some conditions emission of the dissociation product CO is observed after the injection of CO<sub>2</sub>.

- The analysis of molecular gas mixtures with plasma techniques will be very complex, since both at reduced and atmospheric pressure no conditions are found in which originally injected molecules are observed in emission (except for nitrogen). Moreover, matrix effects are readily observed, i.e. changes in the concentration of a certain element/molecule affect the emission of another element/molecule.
- Microwave induced plasmas have a high tolerance for molecular gases with respect to the maximum load that can be introduced before they are extinguished. However, it is shown by passive optical emission spectroscopy, power interruption experiments and laser absorption spectroscopy that the introduction of small amounts of molecular gas (typically 1%) already introduces large changes in the plasma kinetics. In general the electron density decreases whereas the gas temperature increases.
- Power interruption experiments have been used to study excitation and transport processes in freely expanding plasma torches. The fast decay times of line intensities that result from electron excitation (typically a few  $\mu\text{s}$ , compared to 150  $\mu\text{s}$  for inductively coupled plasmas) show that the plasma is out of equilibrium as a result of processes as diffusion and convection. From the experiments insight in these processes is obtained. Moreover, it has been possible to determine the axial gas flow velocity from the propagation of disturbance that is created in the active zone of the plasma.
- From the power interruption experiments it is found that in the active zone radiative levels of analytes are mainly populated by electron dominated processes. In the recombining zone however, thermal excitation is found to be responsible for the population of low-lying radiative levels (e.g. for Na).
- Spatially resolved diode laser absorption measurements on argon discharges produced by the TIA have shown that especially in the active zone the density of the metastable  $4s^3P_2$  level is high. However, the distribution is less steep than that of the electron density. It is found that molecular gas injection leads to quenching of the metastables .
- Densities of the  $4s$  level in a pure argon discharge point towards a relatively low electron temperature ( $\sim 1.3$  eV). This is close to the temperature that can be deduced from solving the particle balance ( $\sim 1.1$  eV), but is significantly lower than the temperature found by Thomson scattering ( $\sim 2.0$  eV).
- The width and the shift of the central frequency of the optical depth as measured via laser absorption provide information on plasma parameters such as the gas temperature and the electron density.

## Summary

Plasmas nowadays play an essential role in many industrial processes and laboratory applications. Some well-known examples are deposition and etching of layers, cutting and welding, waste treatment, cleaning of detrimental gases, light generation and spectrochemical analysis. In this thesis different microwave induced plasmas (MIPs) are investigated with respect to the latter application.

The technique of atomic emission spectroscopy (AES) has become very popular during the last 20 years, especially for the elemental analysis of aqueous samples. The plasma is used to evaporate and atomize the sample and excite elements present in the sample. The emission that is generated by the spontaneous decay of excited levels provides information on these elements. Typical detection limits of AES when a so-called inductively coupled plasma is used as excitation source are around 1 ppb for most elements (1 ppb  $\approx$  1 ng/ml).

By applying different plasma sources (i.e. the "torche à injection axiale", the microwave plasma torch, the Beenakker cavity, the surfatron and the guide-surfatron) a large variety of plasma conditions is obtained. With various spectroscopic studies more insight is obtained in plasma processes related to spectrochemical analysis.

It is found that many MIPs have a high tolerance to the introduction of molecular gases. Accordingly, the "torche à injection axiale" has been used successfully for the on-line monitoring of the flow of metals in combustion gases in the secondary combustion chamber of AVR-Chemie, a large hazardous waste incinerator in the Netherlands. The potential of this torch for measurements under extremely rough experimental conditions, for which generally commercially available laboratory equipment is not suited, has been clearly demonstrated. A large variety of elements (like zinc, lead, sodium and magnesium) could be easily detected quasi-simultaneously.

In general, emission spectra of the studied microwave induced plasmas are dominated by emission of diatomic molecules that are generated in the plasma itself ( $C_2$ , CN, NO, OH, NH). Since interference with these molecular bands can disturb the detection of element lines, dissociation and association processes have been studied. Results of this investigation can also be used to find out whether it is possible to analyze molecules with plasmas. For this purpose experiments with different molecular gases have been performed. It is found that at atmospheric pressure 3-body association processes play an important role. Moreover, it is concluded that in free expanding torches molecular emission bands are inevitable as a result of air entrainment. At reduced pressure ( $\sim$ 1-10 mbar) the importance of 3-body processes is limited. However, it is found that in this pressure regime association at the wall of the discharge tube is important (which is a process with two atoms or molecules and the wall as a substitute for the third body). Although, unlike for the atmospheric discharges, under some conditions diatomic dissociation products are observed when 3-atomic molecules are injected (CO emission after  $CO_2$  injection), no conditions are found in which originally injected molecules are observed in emission (except for nitrogen). Moreover, since matrix effects are readily observed, i.e. changes in the concentration of a certain element/molecule affect the

emission of another element/molecule, it can be concluded that the analysis of molecular gas mixtures with plasmas will be very complex.

Excitation balances and transport properties in free expanding plasma torches have been studied by means of so-called interruption experiments, in which the power of the microwave generator is momentarily interrupted (typically 60  $\mu$ s). In the active part of the plasma it is found that the injection of molecular gases has a large influence on the responses of emission lines to power interruption. Significant changes are observed, even for less than 1% of molecular gas injection. The agreement of the measurements in the recombining plasma zone with an established relationship between the intensity decay time of some element lines and the decay time for the gas temperature, suggests that in this zone the corresponding radiative levels are populated by thermal excitation. From the fast decay times of line intensities that result from electron excitation, information is obtained on diffusion and convection losses. Moreover, the axial gas flow velocity is determined from the propagation of a disturbance that is created in the active part of the plasma.

Finally, density profiles of the argon metastable  $4s^3P_2$  level have been determined in free expanding plasmas via diode laser absorption. The populations of the 4s levels constitute a decisive factor for the step-wise excitation and ionization of argon. Moreover, these levels can be responsible for Penning ionization of other elements. It is found that the  $4s^3P_2$  density is maximal in the active part of the plasma, where the plasma has a hollow cone-like structure. Abel-inversion has shown that the distribution of the  $4s^3P_2$  profile is less steep in this region than that of the electron density. The  $4s^3P_2$  density points towards an electron temperature of 1.3 eV, which is significantly less as determined with Thomson scattering (2.0 eV) but is in rather well agreement with the temperature that can be calculated from the particle balance (1.1 eV). Experiments with molecular gas injection have established that molecules quench the population of the  $4s^3P_2$  level. The broadening and the shift of central frequency of the absorption profile have been used to study trends in plasma parameters (such as gas and electron temperature and electron density).

## Samenvatting

Plasma's hebben inmiddels een niet meer weg te denken positie verworven in diverse industriële processen en laboratoriumtoepassingen. Enkele bekende voorbeelden zijn het deponeren en etsen van lagen, snijden en lassen, afvalverwerking, reiniging van schadelijke gassen en spectrochemische analyse. In dit proefschrift worden verschillende microgolf-geïnduceerde plasma's (MIPs) onderzocht met het oog op toepassingen in de laatste categorie. Atomaire emissie spectroscopie (AES) is een techniek die de afgelopen 20 jaar een enorme vlucht heeft genomen en is vooral gangbaar voor elementanalyse van waterige oplossingen. Hiertoe wordt een plasma gebruikt om de vloeistof te verdampen, moleculen te dissociëren en aanwezige elementen te exciteren. De straling die wordt gegenereerd door spontane de-excitatie van aangeslagen toestanden geeft informatie over aanwezige elementen. Typische detectielimieten van AES, die met behulp van zogenaamde inductief gekoppelde plasma's (ICPs) bereikt worden, liggen voor de meeste elementen rond het ppb niveau ( $1 \text{ ppb} \equiv 1 \text{ ng/ml}$ ).

Met de gebruikte plasmabronnen (de "torche à injection axiale", de "microwave plasma torch", de Beenakker trilholte, het "surfatron" en de "guide-surfatron") is een grote variëteit aan plasmacondities verkregen. Door middel van diverse spectroscopische studies is getracht meer inzicht te verkrijgen in processen die gerelateerd zijn aan spectrochemisch onderzoek.

Het is gebleken dat MIPs doorgaans goed bestendig zijn tegen de introductie van moleculaire gassen. De "torche à injection axiale" is dan ook succesvol gebruikt voor het monitoren van de concentraties van metalen in verbrandingsgassen in de nabrandkamer van een chemisch afvalverbrander bij AVR-Chemie. Het grote potentieel van deze toorts voor metingen onder extreem ruige condities, waar commercieel verkrijgbare laboratorium-apparatuur doorgaans niet op berekend is, is duidelijk aangetoond. Elementen die in relatief hoge concentraties aanwezig waren, zoals zink, lood, natrium en magnesium konden uitstekend worden gedetecteerd.

Emissie spectra afkomstig van de bestudeerde MIPs blijken vaak gedomineerd te worden door straling van twee-atomige moleculen die in het plasma zelf gecreëerd zijn ( $\text{C}_2$ , CN, NO, OH, NH). Aangezien deze banden kunnen interfereren met elementlijnen is onderzocht welke dissociatie- en associatieprocessen zich afspelen. Resultaten van dit onderzoek kunnen tevens inzicht verschaffen in de mogelijkheden van het detecteren van moleculen met behulp van plasma's. Hiertoe zijn experimenten met verschillende moleculaire gassen verricht. Bij atmosferische plasma's is gebleken dat 3-deeltjes volume associatie een belangrijke oorzaak voor de waargenomen spectra is. Bovendien zorgt inmenging van lucht ervoor dat moleculaire banden niet te voorkomen zijn in vrij expanderende plasma's. Bij lage druk plasma's ( $\sim 1\text{-}10 \text{ mbar}$ ) is de invloed van 3-deeltjes associatie gering. Echter, in dit regiem blijken associatieprocessen voornamelijk plaats te vinden aan de wand van de ontladingsbuis (een proces met twee atomen of moleculen waarbij de wand de rol van het derde deeltje overneemt). Hoewel, in tegenstelling tot bij atmosferische druk, onder bepaalde condities emissie van 2-atomaire dissociatie-producten van geïnjecteerde 3-atomaire gassen is geobserveerd (CO emissie na  $\text{CO}_2$  injectie), zijn geen condities gevonden waarin emissie van

het geïnjecteerde molecuul zelf is waargenomen (op moleculair stikstof na). Omdat bovendien matrixeffecten optreden (wat inhoudt dat concentratieveranderingen van een element of molecuul de emissie van een ander element of molecuul beïnvloedt), is moleculdetectie met behulp van plasma's een zeer complexe zaak.

Met behulp van zogenaamde interruptiemetingen (waarbij het uitgangsvermogen van de microgolfgenerator kortstondig onderbroken wordt, typisch gedurende 60  $\mu$ s) is onderzoek verricht naar excitatie balansen en transport eigenschappen in vrij expanderende argon toortsen. In het actieve gebied van het plasma blijkt de introductie van moleculaire gassen grote invloed te hebben op de respons van emissielijnen op vermogensinterrupties. Grote verschillen zijn reeds waargenomen bij de injectie van minder dan 1% moleculaire gassen. De overeenkomst tussen de vervaltijden van enkele emissielijnen zoals die gemeten zijn in het recombinerend deel van het plasma en de vervaltijden die afgeleid zijn van de vervaltijd van de gastemperatuur, suggereert dat in deze zone de desbetreffende aangeslagen niveaus thermisch worden geëxciteerd. Uit het snelle verval van de emissielijnen die het gevolg zijn van elektron-excitatie is inzicht verkregen in diffusie en convectieverliezen. Bovendien is de axiale gassnelheid bepaald uit de voortplanting van een verstoring die bij de interruptie aan het actieve deel van het plasma wordt opgelegd.

Tenslotte zijn met behulp van een diode laser absorptiemetingen verricht aan de bezetting van het metastabiele argon  $4s^3P_2$  niveau in vrij expanderende plasma's. De bezettingen van de  $4s$  niveaus vormen een dominante factor in ladderexcitatie en stapsgewijze ionisatie van argon. Bovendien kunnen deze niveaus zorgen voor de Penning ionisatie van andere elementen. De absorptiemetingen hebben aangetoond dat de  $4s^3P_2$  dichtheid maximaal is in het actieve gebied, waar het plasma de vorm heeft van een holle kegel. Abel-inversie heeft echter aangetoond dat het  $4s^3P_2$  profiel minder scherp is dan dat van de elektronendichtheid. De  $4s^3P_2$  dichtheid duidt op een elektrontemperatuur van 1.3 eV, wat significant minder is dan de temperatuur gevonden met Thomson verstrooiing (2.0 eV) maar vergelijkbaar is met de temperatuur die volgt uit de deeltjesbalans. Het is gebleken dat de bezetting van het  $4s^3P_2$  niveau sterk wordt verminderd door introductie van moleculen. De verbreding en de verschuiving van de centrale frequentie van het absorptieprofiel zijn gebruikt om trends in plasma parameters (zoals de gas- en elektrontemperatuur en de elektronendichtheid) te bestuderen.

## Dankwoord

Dit proefschrift zou nooit stand hebben kunnen komen zonder de hulp van vele anderen. Bij deze wil ik dan ook iedereen bedanken die zijn of haar steentje heeft bijgedragen.

Allereerst wil ik hierbij dagelijks begeleider en tevens copromotor Joost van der Mullen noemen. Aan zijn niet aflatende inzet en grote toewijding is het te danken dat er via diverse instanties steeds weer financiering werd verkregen om het aanvankelijke AIO-2 project tot een promotie te verlengen. Bovendien heb ik al die tijd erg prettig met Joost samengewerkt en veel profijt gehad van zijn inzichten in de plasmafysica. De inspirerende discussies met eerste promotor Daan Schram zijn eveneens van groot belang geweest voor het tot stand komen van dit proefschrift. Ook de bijdrage van Jeroen Jonkers is erg belangrijk geweest. De gezamenlijke experimenten en gesprekken hebben veel inzichten verschaft en bovendien heeft hij dit proefschrift kritisch doorgenomen. Verder wil ik alle collegae van ETP bedanken. Zonder de anderen te kort te willen doen wil ik met name Marco van de Sande vermelden, met wie ik veel heb samengewerkt en die eveneens dit proefschrift onder de loep heeft genomen. Mijn dank gaat ook uit naar Jeanne Loonen voor haar administratieve hulp en naar de commissieleden Bram Veefkind en Wijnand Rutgers die met allerlei suggesties eveneens hebben bijgedragen tot de definitieve vorm van dit werk. De discussies met Ton Boekkooi hebben me veel geleerd over projectmatig werken.

Van groot belang was de inbreng van de verschillende stagiairs, afstudeerders/sters en tijdelijke medewerkers (in chronologische volgorde): Niels Melman, Robert Tas, Karine Letourneur, Frank de Groote en Ivo Thomas.

Bij experimenteel onderzoek is een goede technische ondersteuning onontbeerlijk. De hulp van Ries van de Sande, Herman de Jong en Bertus Hüsken was dan ook essentieel voor het slagen van de experimenten. Ook Bert van Lierop, die meer dan eens te hulp schoot, dient hierbij niet onvermeld te blijven. De ondersteuning van de medewerk(st)ers van de werkplaats is eveneens cruciaal geweest. Hierbij wil ik in het bijzonder Ginny ter Plegt noemen, die de experimentele opstelling grotendeels vervaardigd heeft.

Gedurende de eerste fase van het promotieonderzoek is gewerkt aan een systeem om bij AVR-Chemie (te Rozenburg) verbrandingsgassen “on-line” te monitoren. Van dit bedrijf wil ik met name Wisse van de Guchte en Joep Verwoerd bedanken voor hun steun tijdens de metingen. Twan Hendriks van Philips CFT heeft me in staat gesteld diverse plasmabronnen door te meten met een network analyzer bij CFT.

De contacten met buitenlandse universiteiten hebben veel nieuwe inzichten verschaft. Zo hebben de bezoeken aan de groep van tweede promotor prof. Broekaert (Universität Dortmund) me veel geleerd over analytische chemie, terwijl de stage die ik heb verricht binnen de groep van prof. Moisan (Université de Montréal) me veel heeft bijgebracht over microgolf plasma's. Voortvloeiend uit mijn afstudeerproject, is er veel samengewerkt met de groep “Física Aplicada” van de Universidad de Córdoba. Hiervan wil ik in het bijzonder Mari-Carmen Quintero, Antonio Sola, Antonio Gamero en Antonio Rodero noemen.

Tenslotte wil ik “het thuisfront” bedanken: mijn ouders, familie, vrienden en “last but not least” Marga, zonder wie dit proefschrift nooit geworden was wat het nu is.

**Curriculum vitae**

- 21 augustus 1970 Geboren te Kessel (L),
- 13 juni 1988 Diploma Atheneum,  
Bouwens van der Boije College te Helden-Panningen,
- 31 augustus 1994 Doctoraal examen Technische Natuurkunde,  
Faculteit der Technische Natuurkunde,  
Technische Universiteit Eindhoven,
- 11 juni 1997 Diploma ontwerpersopleiding “Fysische Instrumentatie”,  
Stan Ackermans Instituut,  
Technische Universiteit Eindhoven,
- 1 juni 1997 – 1 september 1999 Promotieonderzoek in de werkgroep  
“Evenwicht en Transport in Plasma’s”,  
vakgroep Deeltjesfysica,  
Faculteit der Technische Natuurkunde,  
Technische Universiteit Eindhoven.



*Spectrum on cover: C<sub>2</sub> Swan System*

# STELLINGEN

behorende bij het proefschrift

## **Atomic and Molecular Excitation Processes in Microwave Induced Plasmas**

*A Spectroscopic study*

**Eric Timmermans**

Eindhoven, 19 oktober 1999

## I

De grote variëteit aan plasmacondities die met behulp van door microgolven geïnduceerde plasma's verkregen kan worden, maakt deze plasma's uitermate geschikt voor het onderzoeken van moleculaire processen.

*(dit proefschrift)*

## II

Door het optreden van dissociatie en associatie van moleculen, zowel bij hoge als bij lage druk, gaat de samenstelling van de aan het plasma toegevoerde gassen vaak verloren.

*(dit proefschrift)*

## III

Ofschoon een door een microgolftoorts geproduceerd argonplasma een relatief grote belasting van moleculaire gassen kan weerstaan, leidt de introductie van een veel kleinere hoeveelheid van deze gassen reeds tot grote veranderingen in de plasmakinetica.

*(dit proefschrift)*

## IV

Door de drang om detectielimieten in elementanalyse steeds verder te verbeteren wordt relatief weinig kleinschalige, robuuste of goedkope apparatuur ontwikkeld.

## V

Veel bedrijven voegen het woord "environmental" toe aan hun bedrijfs- of productnaam zonder dat duidelijk gemaakt wordt wat hun relatie met het milieu is.

## VI

Bij een uitbreiding of aanpassing van een analysetechniek dient overwogen te worden een geheel nieuwe term in te voeren. Het gebruikelijke aanbrengen van toevoegingen leidt veelal tot onhandelbaar lange benamingen.

## VII

Het verbod op het gebruik van levende aasvissen zou effectiever worden nageleefd, indien ook het gebruik van dode aasvissen zou worden verboden.

## VIII

Door reeds ruim voor het hoogtepunt van een gedeeltelijke zonsverduistering de straatverlichting te ontsteken, zoals in veel gemeenten is gebeurd tijdens de verduistering van augustus jongstleden, draagt de overheid ertoe bij dat de verwachting van de bevolking te hoog gespannen is.

## IX

Actieborden die waarschuwen tegen gevaarlijk weggebruik, zijn langs sommige wegen dermate talrijk en complex dat deze op zichzelf een gevaar voor de weggebruiker vormen.

## X

Ofschoon de liefde niet tastbaar is, is zij duidelijk voelbaar aanwezig.